LBL-7054

SEISMOLOGICAL INVESTIGATIONS IN GEOTHERMAL REGIONS

Ernest Luther Majer
(Ph. D. thesis)

May 1978

Prepared for the U. S. Department of Energy
under Contract W-7405-ENG-48

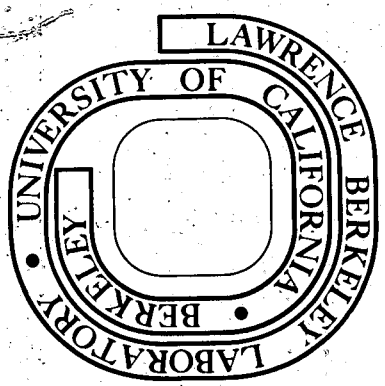

LBL-7054

DISCLAIMER

SEISMOLOGICAL INVESTIGATIONS IN GEOTHERMAL REGIONS

by

Ernest Luther Majer
(Ph.D. Thesis)

Lawrence Berkeley Laboratory
University of California
Berkeley, California 94720

and

Department of Geology and Geophysics
University of California
Berkeley, California 94720

Prepared for the U.S. Department of Energy
under Contract W-7405-ENG-48

SEISMOLOGICAL INVESTIGATIONS IN GEOTHERMAL REGIONS

by

Ernest Luther Majer

Abstract

Seismological methods, including studies of microearthquakes, P- and S-wave velocities and P-wave attenuation are investigated as tools for the exploration and delineation of geothermal resources. Seismograms from explosions and microearthquakes are examined for changes in frequency content and relative arrival times across a known geothermal area, The Geysers, California and a potential geothermal region, Grass Valley, Nevada. Microearthquakes within the two regions are examined for evidence of spatial variations in radiated P- and S-waves. Additional information concerning Basin and Range structure is provided by regional refraction studies. Detailed structural analysis in Grass Valley is obtained by commercial reflection and refraction work. Heat flow modeling, consistent with structure inferred by seismological techniques, is used to discriminate between conductive and convective heat flow anomalies in Grass Valley.

Concentrated observations in Grass Valley around Leach Hot Springs revealed moderate microearthquake

activity on a trend crossing the southern end of the valley, with occasional swarms in the area of high heat flow, (4-6 hfu) at the north end of the 1915 Pleasant Valley earthquake (mag = 7.5) fault trace. In the context of Basin and Range tectonics and seismicity, the Grass Valley microearthquakes are not anomalous in spatial or temporal occurrence. Studies of source properties obtained from P-wave spectral characteristics are inconclusive in so far as defining a unique geothermal earthquake. Refraction and reflection studies indicate normal faulting, with major faults bounding the valley and controlling spring activity. Heat flow models indicate small anomalies (3-5 hfu) may be conductive rather than convective in origin, controlled by basement topography. Fluid flow is required to account for the heat flow anomaly associated with Leach Hot Springs and that in the southern part of Grass Valley. Modeling also revealed that shallow (2-3 km), moderate temperature (200°C) hot water reservoirs can be present without large surface heat flow anomalies (7-8 hfu).

Regional refraction studies show high apparent P_n velocity (8.1 km/sec) northward, indicating either crustal thinning or crustal velocity increase northward in northern Nevada, assuming true P_n velocity is near 7.8 km/sec. Regional heat flow modeling suggests upper mantle hot spots or plumes could account for the northern Nevada high heat flow (>2.5 hfu).

Studies in The Geysers steam field reveal significant velocity and attenuation anomalies associated with the production zone. V_p/V_s data from Wadati diagrams indicate lower Poisson's Ratios in the field than in surrounding areas. P-wave velocity and attenuation data indicate a shallow high velocity - high Q zone, (1-2 km) overlying a lower velocity - lower Q region. Fault plane solutions are largely consistent with right lateral strike-slip movement and NE-SW compression. Microearthquake spatial distribution and source parameters from P- and S-wave spectral characteristics suggest a close relationship to the high gradients in pressure and temperature bounding the steam reservoir. A b-value of 1.1 ± 0.1 is possibly slightly anomalous compared to the 0.83 ± 0.04 regional value. b-values depend critically on the magnitude scale utilized. Although additional data are required, the microearthquake activity implies an association with steam withdrawal. Recommendations are given for the application of seismological techniques in the context of reservoir exploration and/or monitoring.

With proper sampling in space and time, P- and S-wave velocity and attenuation data can detect and delineate significant anomalies associated with the static properties of a geothermal resource. Microearthquake data are useful for monitoring the dynamic strain

relief processes associated with fluid movement, temperature and pressure gradients in geothermal environments. Refinement of the techniques presented in this study, and the addition of future case histories, should make seismological methods significant elements in the exploration and delineation of geothermal resources.

ACKNOWLEDGMENTS

My greatest debt of gratitude is to my family, without whose support I would never have completed my schooling.

I am indebted to my advisor, Thomas McEvilly for his guidance, understanding, insight, and support through the years. His enthusiastic and generous help has been indispensable. I wish also to thank Frank Morrison and his almost infinite capacity of advising students.

I am grateful to Chi Wang for his comments and suggestions on this work.

Throughout the course of this investigation I have had many valuable discussions, particularly with Steve Dickman, Brian Stump, Paul Okubo, Marcelo Lippmann Oleh Weres, Lane Johnson, and my fellow students and friends.

Without the technical support of Lawrence Berkeley Laboratory and the University of California Seismographic Station, this work would never have been undertaken. Of particular mention are, Russell Sell, Halvard Andersson, Eugene Binnall and the many field assistants.

I would like to thank Pat Hood and Mary Ann Radigonda without whose patience and help this work would never have been typed.

This work was supported by the Department of Energy through University of California, Lawrence Berkeley Laboratory.

I would also like to thank Richard Dondanville, Dennis McMurdie and the Union Oil Company for access to The Geysers.

TABLE OF CONTENTS

		Page
ACKNOWLEDGMENTS		i.
CHAPTER		
1	INTRODUCTION	1.
2	THE PHYSICAL BASIS FOR THE APPLICATION OF SEISMOLOGICAL TECHNIQUES TO THE EXPLORATION AND DELINEATION OF GEOTHERMAL RESOURCES	5.
	2.1 Definition of a Geothermal Resource	5.
	2.2 Microearthquakes	6.
	2.2.1 Experimental Design	10.
	2.3 Wave Propagation	11.
	2.3.1 Velocity	11.
	2.3.2 Attenuation	14.
	2.3.3 Experimental Design	17.
	2.4 System Specifications	18.
	2.5 Conclusions	26.
3	SEISMOLOGICAL INVESTIGATIONS OF A VAPOR DOMINATED RESERVOIR - THE GEYSERS, CALIFORNIA	27.
	3.1 Introduction	27.
	3.2 Geological Setting	29.
	3.3 Reservoir Properties	35.
	3.4 Explosion Data	39.
	3.4.1 P-Wave Velocities	40.
	3.4.2 Attenuation	45.
	3.5 Microearthquake Data	55.
	3.5.1 Locations	55.
	3.5.2 Mechanisms	61.
	3.5.3 Magnitudes	63.
	3.5.4 Velocities	68.
	3.5.5 Source Parameters	73.

Table of Contents--continued

		Page
3.6	Interpretation	87.
3.6.1	Summary of Observations	87.
3.6.2	Microearthquakes	89.
3.6.3	Velocities	98.
3.6.4	Attenuation	100.
3.7	Conclusions	103.
4	SEISMOLOGICAL INVESTIGATIONS IN A HIGH HEAT FLOW REGION - NORTHERN NEVADA	107.
4.1	Introduction	107.
4.2	Geological Setting	107.
4.3	Microearthquake Data	109.
4.4	Explosion Data	122.
4.4.1	P-Wave Velocities	122.
4.4.2	Attenuation Data	129.
4.5	Refraction and Reflection Data	135.
4.6	Regional Refraction Data	136.
4.7	Interpretation	154.
4.7.1	Microearthquake Occurrence	154.
4.7.2	Microearthquake Source Parameters	163.
4.7.3	Velocity and Attenuation	164.
4.7.4	Reflection Profiles	167.
4.7.5	Regional Refraction Study	177.
4.7.6	Heat Flow Modeling	180.
4.8	Conclusions	205.
5	SUMMARY, CONCLUSIONS, AND RECOMMENDATIONS	208.
5.1	Summary of Objectives and Methods	208.
5.2	Conclusions	209.
5.3	Recommendations and Future Studies	213.

Table of Contents--continued

	Page
5.3.1 Exploration----------	213.
5.3.2 Reservoir Monitoring ------	215.
5.3.3 Future Studies and Development----------	216.
REFERENCES----------	218.

CHAPTER 1

INTRODUCTION

The increasing importance of locating additional and alternative energy sources motivates the search for a basic understanding of the environments and conditions in which these resources occur. In the case of geothermal energy, the conditions are geologically complex, with the resource occurring in varied states (vapor, liquid-vapor, liquid) and in diffuse or disseminated form. Because of these unusual properties, conventional seismological methods are not easily or profitably applied to geothermal exploration.

Previous to the initiation of this study in 1973, few results of a comprehensive seismological investigation in a geothermal area had been published. The most common study associated microearthquakes and geothermal activity, (Lange and Westphal, 1969; Ward and Bjornsson, 1971; Conant, 1972; Hamilton and Muffler, 1972; Hochstein and Hunt, 1972; Ward, 1972) dealing mainly with the spatial relationship between occurrence (or non-occurrence) of microearthquakes and geothermal regions. These studies were concerned with the location of faults that could possibly serve as conduits in which hot fluids or steam could exist. It was also thought that microearthquakes might reflect the presence of material that had been weakened by geothermal activity. A second exploration

method used early in geothermal studies was based on the premise that geothermal reservoirs were characterized by detectable emanation of seismic waves, apparent as seismic "ground noise". Other seismological studies in high heat flow or potential geothermal regions dealt with the presence of magma chambers associated with volcanic regions, (Matumoto and Ward, 1967; Matumoto, 1971). Although studies of this nature were more comprehensive, they were concerned with the size and source of magma chambers and/or the prediction of volcanic eruptions, rather than the location of a geothermal resource. However, few studies if any, gathered all possible seismological data and interpreted it in terms of the physical properties and processes in a geothermal reservoir. Therefore, premature judgements were made in selecting exploratory wells, which almost always resulted in poor returns. For this reason the seismological methods, particularly noise surveys, were not considered of prime importance in geothermal exploration.

This study seeks to assess the utility of a complete seismological data set for locating and estimating the extent of geothermal resources. To contribute significantly to a comprehensive exploration program, information must be contributed that is either unobtainable or inefficiently obtained by other techniques. The data must also be interpretable in terms of the basic physics and properties of the resource. The desired parameters in

this case are porosity, permeability, heat content and state of the pore fluid. If these properties are not directly detectable, what related characteristics are evident in the seismological data? If existing techniques and equipment are inadequate, can new methods and instrumentation be developed? Finally, in considering several different environments of known or potential geothermal resources, this study will contribute to the almost non-existent file of case histories on geothermal areas.

The impetus for the study was provided by a large scale program to evaluate and develop geological, geochemical, and geophysical techniques for geothermal exploration sponsored by the Atomic Energy Commission (later Energy Research and Development Administration and now the Department of Energy). Ideally, the study would be conducted in a region of known geothermal potential that had not yet been disturbed by production. However, such constraints as land access, logistics and government participation narrowed the possibilities to the high heat flow regions on Bureau of Reclamation land. The most attractive possibility available was the Battle Mountain heat flow high in north central Nevada.

Although no confirmatory drilling was done based on the work in northern Nevada, the seismological techniques and experience gained were applied to a producing geo-

thermal reservoir, The Geysers in northern California. Chapter Two of this study deals with the seismological manifestations and basic properties of a geothermal resource. Presented in Chapters Three and Four are the results, interpretation and conclusions of the work carried out at The Geysers and northern Nevada. Because The Geysers is a known geothermal resource, the results of that study are presented first. The Nevada work is then presented and discussed in terms of the findings at The Geysers with possible implications relating to geothermal resources in northern Nevada. Finally, Chapter Five is the overall conclusion regarding the utility of seismological methods for reservoir exploration and management.

CHAPTER 2

THE PHYSICAL BASIS FOR THE APPLICATION OF SEISMOLOGICAL TECHNIQUES TO THE EXPLORATION AND DELINEATION OF GEOTHERMAL RESOURCES

2.1 Definition of a Geothermal Resource

Random drilling deep enough into the earth would produce adequate heat for a geothermal resource. However, this heat must be in an accessable and usable form. This implies ample porosity and permeability to maintain the correct balance between a heat source and a working fluid. The volume and state of this working fluid must be large enough to justify the effort to find and exploit it. Ideally, dry steam would be the product. However, hot water and water-vapor systems are more common. Although the above criteria on heat content and volume may have been met, the working fluid must not be in a form that is corrosive or high in dissolved solids. Therefore, a geothermal resource or reservoir will be defined as a region within the earth that has sufficient porosity, permeability, heat content, water content, volume and accessability with the water in such a state that it can be exploited profitably.

The parameters affecting seismological phenomena in a geothermal environment can be divided into two categories, static and dynamic. Static properties are

porosity, permeability, temperature, pressure, density, thermal conductivity and state of the pore content. Dynamic properties include fluid movement, phase changes, stress release, thermal expansion and hydrothermal alteration, or physical and chemical processes that may be affecting the static properties. Basically, there are 3 different seismological circumstances of interest, microearthquakes, wave propagation and "noise" generation. Although the three processes are probably interrelated in their origin, only the latter subject is not dealt with in this study. The method of noise analysis has been treated by Liaw (1977), as part of this same overall study in northern Nevada.

2.2 Microearthquakes

To understand fully the relation between microearthquakes and a geothermal environment, many different factors must be considered. A crucial question to answer is: are the microearthquakes observed in geothermal areas unique with respect to earthquakes in non-geothermal regions? That is, does such a phenomenon as a "geothermal earthquake" exist? If so, a useful exploration tool would be provided. If not, then possibly the environment in which these events are occurring may provide an indication to causes of all earthquakes.

The basic mechanism of an earthquake is a sudden loss of cohesion or strength of a material. The factors

controlling failure are: rock type, confining pressure temperature, amount and manner of directed stress, solubility of the material, time and rate of strain (Spencer, 1969). Although all these factors are closely interrelated, the most obvious characteristic to examine in geothermal regions is the temperature. Though not always consistent, the effect of increasing temperature is to lower the brittle-ductile transition pressure, (Griggs, Turner and Heard, 1960). Increasing temperature may tend to decrease the rate of microearthquakes (McNally, 1976). However, only at temperatures in excess of 400^{o}C does this effect begin to dominate. At these temperatures the motion on a fault becomes stable gliding rather than a series of discrete, rapid slips or "stick-slip" (Stesky, 1977). Therefore, in a region that is anomalously hot, microearthquakes may be expected to be absent or to exist only at shallower depths. An increase in temperature also tends to increase the fault angle with respect to the principal stress direction (Handin, 1966). In a region that is under relatively uniform stress, a hot area may be indicated by anomalous fault plane solutions compared to the cooler surrounding areas.

Increased temperature may have a secondary effect by influencing the content of the pores. If the temperature is high enough, steam, rather than water, may be present. A common failure criteria is the Coulomb re-

lation, $\tau = \tau_o + \sigma_n' \tan \phi$, where τ, the total shearing resistance offered by an isotropic material to failure, is proportional to the effective normal stress σ_n', the difference between the actual normal stress σ_n, and the pore pressure σ_p; i.e., $\sigma_n' = \sigma_n - \sigma_p$. If the pores contain steam, which is highly compressible, σ_p is small; thus σ_n' is larger than in an adjacent area where the pores are filled with water and σ_p is large. Therefore, τ would be expected to be higher in a steam filled region, thus resulting in fewer earthquakes compared to an adjacent region. This assumes, of course, that all other parameters remain constant, which is not the case.

The parameter most likely to be affected by a geothermal environment would be the rock type. The high temperatures and hydrothermal activity undoubtedly alter the rocks within the reservoir. Muffler and White (1969) reported extensive metamorphism associated with the Salton Sea geothermal system. The high temperatures ($360^{\circ}C$) and pressures (500-1000 bars) in the Salton Sea region combine to produce a brine containing over 250,000 ppm dissolved solids. Although this is an extreme case, similar dissolution of solids in other geothermal environments is probably occurring. A possible mechanical effect is to weaken the rocks in certain regions and possibly strengthen the rocks where the hydrothermal solution cools and deposits its dissolved solids. Along with hydrothermal activity, such factors as differential

expansion due to larger temperature gradients, weakening from dehydration (Heard and Ruby, 1965; Raleigh and Paterson, 1965), erosion, and hydrolytic weakening of quartz (Griggs, 1967) may all lower the failure criteria of the material, thus encouraging seismicity.

In a convective geothermal system the temperature gradients in the zone of convection are not as large as the temperature gradients on the edges of the reservoir. If the reservoir is a vapor dominated resource, pore pressure may also remain relatively constant within the steam zone, especially compared to a hydrostatic gradient. However, the pressure differential between the outside and inside of the reservoir would vary considerably from the top to the bottom. These pressure differentials may be evident in the stress drops or available stresses for an earthquake. If there is a systematic variation in the magnitude of microearthquakes with depth, or in relation to steam zones, such a differential pressure effect may be responsible.

Unfortunately, geothermal reservoirs are not describable in steady-state terms, especially if the resource is being exploited. Continual fluid movement, phase-changes, and heat transfer will change the state of the reservoir. If microearthquake activity is related closely to these processes, then the seismicity will also be in continual state of flux. Microearthquake activity may indicate the balance between the withdrawal

of fluids and the recharge of fluids from the surrounding water supply. Volumetric changes occur when the fluid is withdrawn, and, because of finite permeability, the recharge is not instantaneous. McGarr (1976) has shown that for volume changes due to mining operations, there is a close relationship between the volumetric moment due to seismic failure and the amount of rock removed. Although rock is not being removed in the geothermal case (other than the amount by dissolution), compaction would be expected to occur with possible failure consistent with the direction of the maximum principal stress. If more fluid is being withdrawn than replaced by ground water recharge or reinjection, an increase in microearthquake activity could be expected. Also, as this occurs and pore pressure drops, a steam zone may develop if ample heat is available. Therefore, rather than an exploratory tool, microearthquake monitoring may prove useful for determining areas of recharge and depletion within a producing reservoir.

2.2.1 Experimental Design

To conclude firmly that there exists such a phenomenon as the unique geothermal earthquake, several necessary data sets are required: accurate hyopcenter determination of all events, with sufficient azmuithal coverage to determine unambiguously faulting mechanisms, and spectral data with adequate dynamic range ($\geq 10^3$) and

bandwidth (10^2 Hz) to record several orders of magnitude earthquakes for determination of spectral long period level, corner frequency and high frequency roll off. Finally, a multiple component recording is needed for the analysis of S- and P-wave data. With these data meaningful comparisons with similar data in non-geothermal environments can be made.

2.3 Wave Propagation

It is not the purpose of this section to summarize all the properties of wave propagation. However, it is the intent to investigate the effect of the anomalous characteristics of a geothermal reservoir on the propagation of P- and S-waves. Two basic properties of these waves will be examined, velocity and attenuation. The rapidly time varying characteristics of a geothermal reservoir are not evident as effects on velocity and attenuation as much as they are in microearthquake occurrence. It is then the average static reservoir properties which are reflected in wave propagation characteristics.

2.3.1 Velocity

The principal factors that influence velocity are: water content, porosity, crack content, temperature, metamorphism, confining pressure, and rock type. Within a geothermal region all of these factors are probably

anomalous.

Nur and Simmons (1969) report that the P-wave velocity may easily increase by 20% if a dry rock is saturated with water. White (1975), also found a 20% increase in P-wave velocity with partial saturation, and noted no change in the S-wave velocity. Toksoz, Cheng and Timur (1976) also report that saturation has a greater effect on P-wave velocities than on S-waves. In a gas filled environment, considering only water saturation, the P-wave is thus expected to be delayed with respect to surrounding areas. Because the S-wave is not affected as much by pore water content, Poisson's Ratio should decrease. If the geothermal reservoir is not gas or vapor dominated, then there should be no change in the velocities due to pore water content alone.

Although a geothermal resource may not be anomalous with respect to water content, it may be anomalous with respect to porosity or crack content. In a geothermal reservoir the crack content is probably higher than in surrounding areas, with increased crack aspect ratios likely. Both of these effects reduce the P-wave velocity and only mildly affect the S-wave velocity (Toksoz, Cheng and Timur, 1976). Again, the effect is to delay the P-wave and decrease Poisson's Ratio.

Confining pressure, on the other hand, increases the velocities of both P- and S-waves, (Nur and Simmons, 1969; Toksoz, Cheng and Timur, 1976). The velocities increase

rapidly at first loading, due to crack or pore closure, and approach an asymptotic behavior beyond 3 kilobar for typical crustal rocks. The P-wave velocities are increased further when the rock is water saturated. The shear-wave however, is little affected by water saturation. For a geothermal reservoir, the effect of confining pressure on velocity may be noted only in vapor dominated regions. In such a case, because of the lack of pore water, the effective normal stress may be higher than in surrounding areas, thus causing an increase in P-wave velocity. However, the higher porosity and crack content may compensate for the increased confining pressure, resulting in little or no velocity change.

Other than causing steam, thus influencing pore water content, temperature effects on velocity would be small at the values typical of most geothermal environments ($<400^{\circ}C$) (Murase and McBirney, 1973). At temperatures above $800^{\circ}C$, the velocities of both P- and S-waves decrease with temperature. Further, in the case of a liquid, such as a magma chamber, only P-waves will be transmitted.

Rock type and degree of metamorphism may well be the most important factors controlling the velocity of seismic waves in geothermal areas. Extensive hydrothermal alteration, deposition of dissolved material and densification will all occur in geothermal environments. In most cases, metamorphism and induration will increase the

velocity of both P- and S-waves. Lin (1977) found that metamorphism of Franciscan Graywacke could increase the P-wave velocity significantly at pressures less than 4 kilobars (depths less than 10 kilometers). If deposition of silica or carbonates is occurring in sediments around a geothermal resource, a P-wave velocity increase is expected due to increased bulk and shear moduli, although the density is also increasing. On the other hand, hydrothermal dissolution of material, within the reservoir, may conceivably influence the bulk and shear moduli such that the P- and S-wave velocities would decrease.

All of the above factors depend for detectability upon the wavelength of the seismic wave and the extent of the anomalous region. Furthermore, without the availability of independent data it may be impossible to determine which physical conditions dominate in an anomaly. Also, it is possible that all effects may be present but in a combination such that the total result is an insignificant velocity change. For additional resolution, velocity data should be complemented by attenuation characteristics.

2.3.2 Attenuation

The same factors that influence velocity will also influence the attenuation characteristics of the medium. However, in general, the Q (reciprocal of specific attenuation) of expected reservoir materials varies over

a broader range (10-500) than does velocity (4-6), thus providing an added sensitive measurement of rock characteristics. Depending upon the frequency of the wave and the pore water content, the mechanism of attenuation may vary. At seismic exploration frequencies (1-100 Hz), the dominant mechanism appears to be grain boundary friction (Johnson and Toksoz, 1977), although elastic geometrical effects, such as scattering, may play a secondary role.

As for velocity, water saturation plays a dominant role. As the crack surfaces become wet the rock will tend to "soften" from chemical interaction with the intergranular material, thus increasing attenuation of both P- and S-waves (Johnson and Toksoz, 1977). In a dry steam environment, where little water is present, one would expect less attenuation, or higher Q values. If a rock is altered in such a manner that the intergranular material becomes less effective in "softening", attenuation would be reduced. This could be expected in highly metamorphosed or hydrothermally altered regions.

In addition to pore content, the confining pressure will influence the attenuation characteristics. As pressure increases, cracks close, thus reducing the number of cracks available for frictional loss, which will in turn reduce attenuation. In a low pressure region, where steam may exist, the differential or confining pressure will be greater and attenuation less than

for a hydrostatically equilibrated pressure region. However, the number of cracks in such low pressure reservoir may be much greater, thus offsetting the differential pressure effect, as in the case of velocity.

To date, the main body of experimental work on wave propagation at high temperature and pressure has been in seismic velocities rather than in attenuation analysis. If grain boundary friction is adopted as the dominant attenuation factor, then rock type and metamorphism should also be reflected in Q_P and Q_S. Attenuation should decrease with increasing metamorphism and induration. In a geothermal region where both phenomena occur, attenuation should thus be reduced locally. Most geothermal regions, however, are geologically complex, with a variety of structural units. Though one rock type may have been metamorphosed, with reduced attenuation, another may have been affected such that attenuation is increased.

At intermediate values, temperature does not influence attenuation significantly. At higher temperatures, when partial melting occurs, the P- and S-waves are greatly attenuated (Walsh, 1968). Unless very hot material is close to the surface, attenuation is not a good indication of shallow temperature. However, as for velocity suspected deep heat sources or magma chambers may be delineated by mapping lateral variations in apparent attenuation.

Similar interpretational difficulties thus arise in

the search for attenuation as for velocity anomalies. Offsetting changes in physical properties may reduce detectability of anomalous characteristics. Such ambiguity may be resolved partially by the use of independent data though uncertainties will still exist. It is desired to develop the ability to distinguish between a change in rock type from one area to another and a change in rock properties, such as porosity, pore water content and permeability.

2.3.3 Experimental Design

As for microearthquake recording, ample dynamic range (10^4) and bandwidth (10^2 Hz) are desirable to detect and map subtle velocity and attenuation variations. Conventional refraction studies can provide data on structures controlling water flow. Local explosions and earthquakes can serve as sources for P- and S-waves. Because of the high frequency nature (5-50 Hz) and shallow propagation paths (0-5 km) associated with small, nearby sources, these sources could be useful for detailed structural analysis. Station placement should be as close as 100 meters, and rarely more than 1 km for recording local and regional sources. P-wave investigations from regional and teleseismic events (1-10 Hz) can provide information on broader and deeper structural trends and rock properties. In the western United States, the use of nuclear explosions from the Nevada test site

can provide precise data on crustal structure and attenuation changes, with information on heat sources due to crustal thinning.

2.4 System Specifications

The requirements of accurate timing (±0.005 sec) for Fourier analysis and relative arrival time measurement, along with the dynamic range used, data must be in either digital or in a readily digitizable form. For the early microearthquake work in Nevada, Sprengnether Model MEQ 800 smoked paper recorders with 4.5 Hz Geospace GSC-8D geophones (0.7 damping, 76 volts/m/sec coil constant, 1350 ohms) were used. The system response is shown in Figure 2-1. The best timing accuracy between stations for these smoked paper recorders was 50 milliseconds.

Although crude amplitude analyses can be made with the smoked paper records, the high frequency nature of the waves obscure phases and makes timing difficult. In addition, no spectral analyses can be performed on the data. For these reasons a 12 channel telemetered - FM analog tape recorder system was built. The system components and specifications are listed in Table 2-1. Typical out-station and central recording site configurations are shown in Figures 2-2 and 2-3, respectively. The overall system response at 72 dB amplifier gain is shown in Figure 2-4. The majority of data collection was done with single component stations; however, the capa-

Figure 2-1

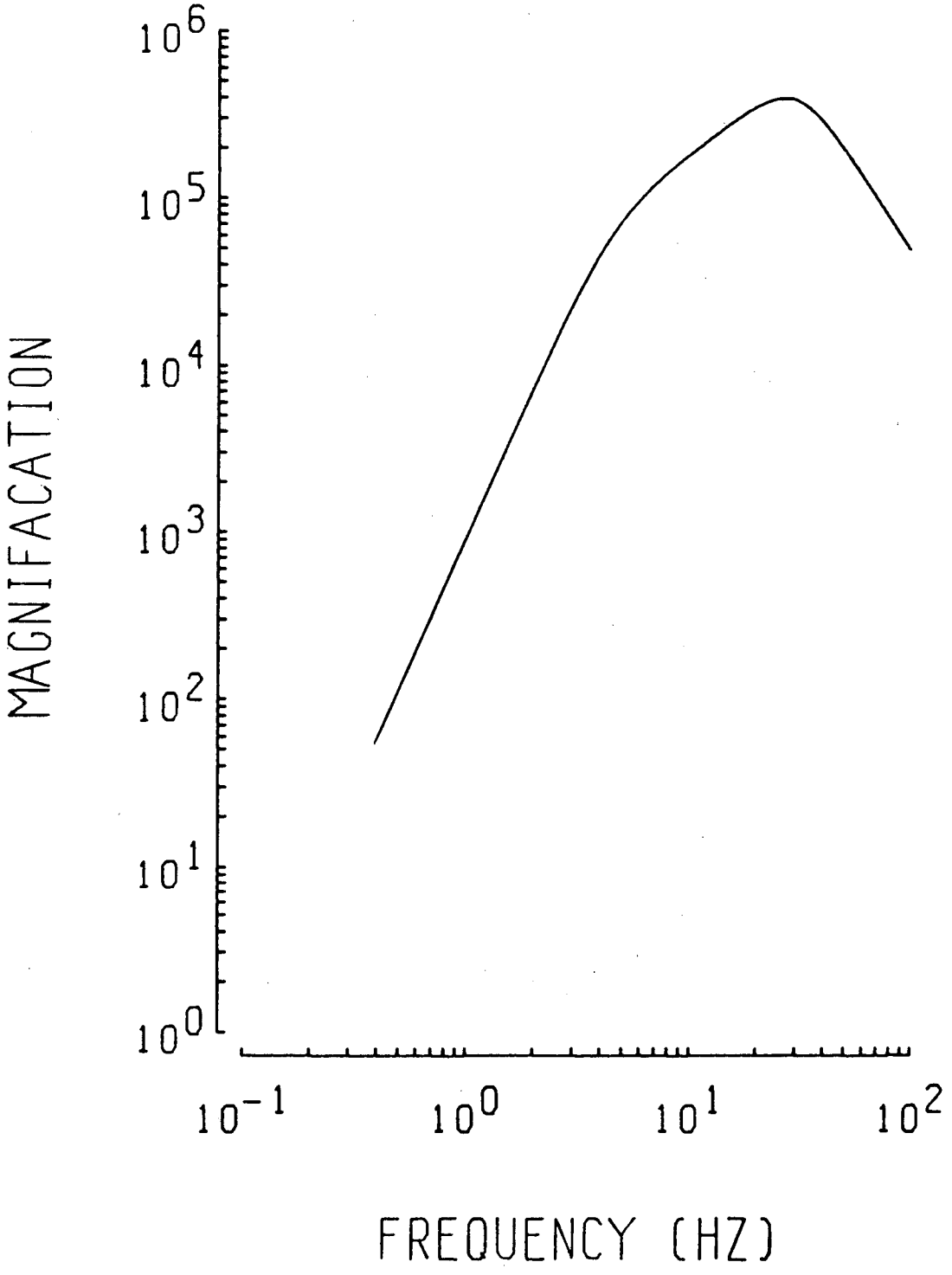

Magnification of MEQ-800 with 4.5 Hz GSC 8D geophone,
gain = 102 dB high filter = 30 Hz low filter = 0.2 Hz

Table 2-1

System Components and Specifications

I. Central Recording Site

(A) 14 channel Geotech tape recorder

12 channels data
1 channel time code
1 channel flutter compensation
DC-80 Hz response
0.24 ips
4 days per tape
25 watts at 12VDC

(B) 12 Sprengnether FM Discriminators

(4) 680 Hz ± 250 Hz
(4) 1360 Hz ± 250 Hz
(4) 2380 Hz ± 250 Hz

(C) Power Supply ± 12VDC, Two systems for alternate use

6 70 amp-hrs automobile batteries each system

System power for > 4 days

(D) Time code generator (IRIG-C) and Time code receivers (WWV & WWVB)

(E) Two-wheeled trailer

(F) 12 radio receivers and antennas

II. Out-Station Equipment

(A) 12 Sprengnether Amplifiers (± 12VDC)

0.1 Hz to 70 Hz
Filters

A Low 0.1 Hz to 10 Hz
B High 10 Hz to 70 Hz

Gain: 60-120 dB in 6dB steps

Table 2-1 (continued)

(B) 12 Sprengnether Voltage Controlled Oscillators (± 12VDC)

(4) 680 Hz ± 250 Hz
(4) 1360 Hz ± 250 Hz
(4) 2380 Hz ± 250 Hz

(C) Geophones

12 4.5 Hz Vertical
6 4.5 Hz Horizontal

(D) Power: ± 12VDC from two 70 amp-hrs automobile batteries

(E) 6 multiplexors (± 12VDC)

(F) 12 radio transmitters (24VDC) 100 mw, 164-172 MHz

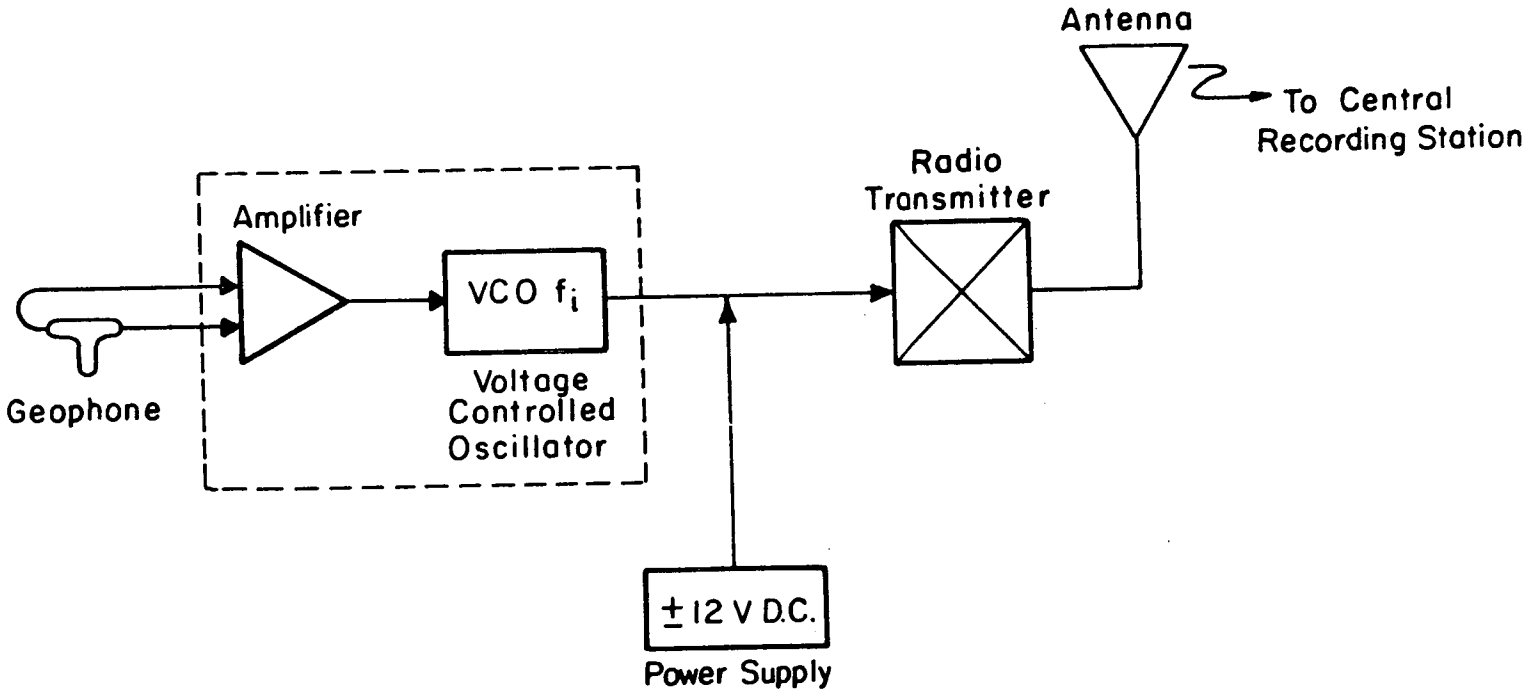

XBL 778-5997

Figure 2-2

Out-station components with a typical operating configuration

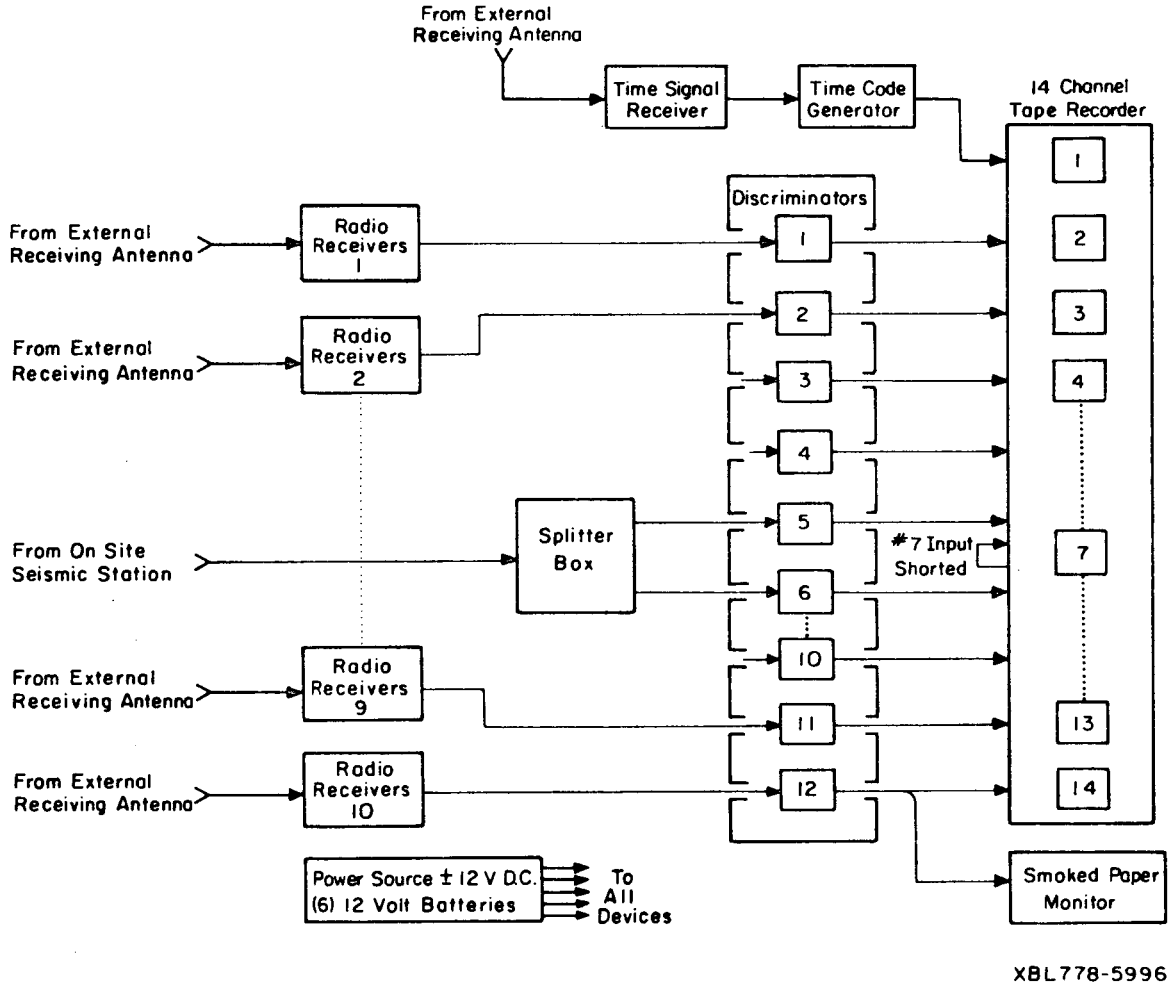

Figure 2-3

Central site telemetry system and associated components

Figure 2-4

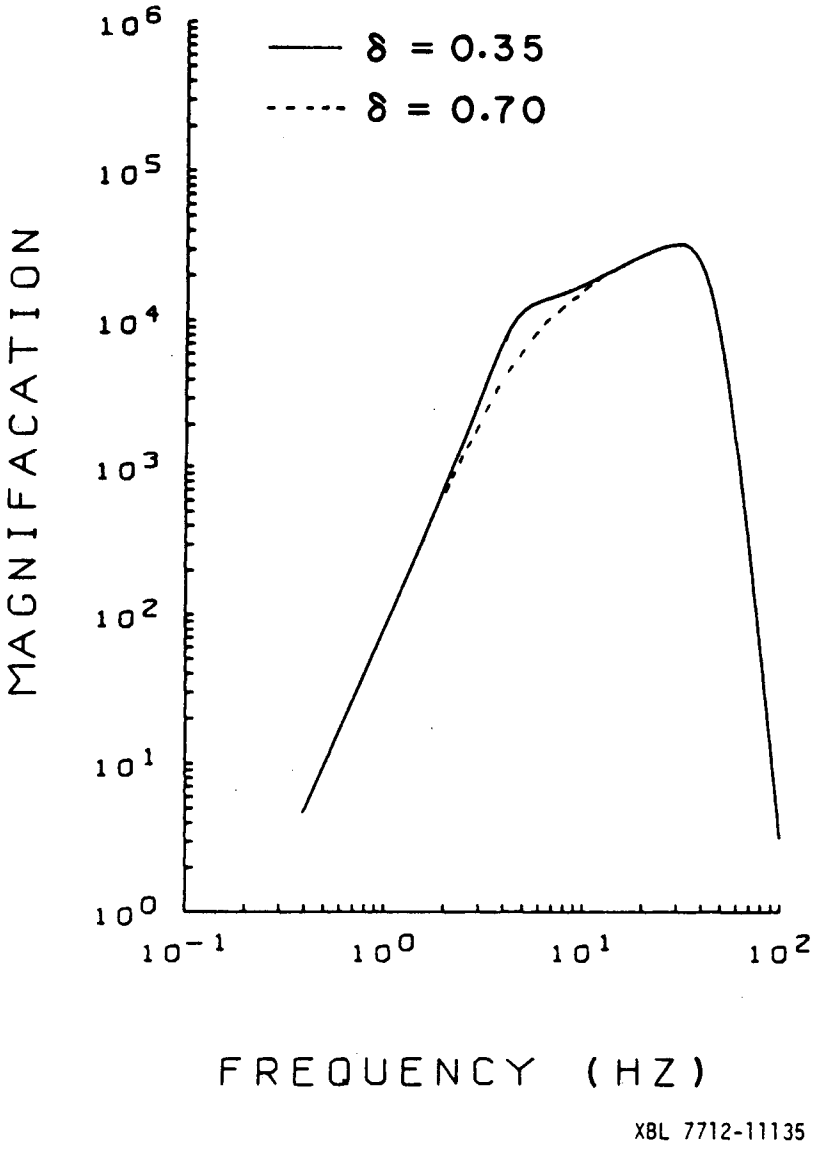

Displacement sensitivity of telemetry system with HS-1 4.5 Hz geophone, at two damping values. Gain of amplifier = 72 dB.

bility exists to multiplex 3-component data. Each station also can be used as a relay with a maximum of 9 multiplexed signals. The dynamic range of the system was 40 dB (peak basis) when initially deployed; however, due to tape recorder noise the signal-to-noise ratio deteriorated to 34 dB after six months of use. Except for geophones, all components remained the same throughout both studies, at The Geysers and in Nevada. For acquisition of attenuation data, a set of 12 closely matched Geospace HS-1 4.5 Hz vertical geophones were used (coil constant 55 volts/m/sec, 0.35 damping, 3400 ohms coil resistance) in Nevada and at The Geysers. For microearthquake data in Nevada, the Geospace GSC-8D geophones were used.

From the above specifications, it is apparent that the previous requirements on dynamic range (10^4) and bandwidth (10^2) were not met. However, a single component triggered digital cassette, 12-bit, recorder was used first with a 4.5 Hz vertical, then with a horizontal GSC-8D geophone, at The Geysers. The improvement in data quality is apparent by observing the signal-to-noise ratio in Figure 3-13. It is unfortunate that the rest of the data used in this study are not of such quality; however, useful and meaningful results were obtained with the FM tape system.

2.5 Conclusions

Because of the complexity of most geothermal systems, the estimation of porosity, permeability, water content and heat content can only be attempted with a suite of data types. Microearthquake data are useful in determining the dynamic behavior of the reservoir. Data on wave propagation characteristics can aid in determining the static reservoir properties. However, since each geothermal region seems unique, a complete study of methodology is required to determine each area's characteristics. Although only indirect properties are measured by seismological methods (arrival times and amplitudes, with attendant velocity and attenuation values), the capability to record data with sufficient bandwidth, dynamic range and accuracy will, it is hoped, allow us to infer specific reservoir properties of interest, assuming relatively straightforward physical models.

CHAPTER 3

SEISMOLOGICAL INVESTIGATIONS OF A VAPOR-DOMINATED RESERVOIR - THE GEYSERS, CALIFORNIA

3.1 Introduction

At the present time, The Geysers geothermal reservoir produces more power than any other geothermal field in the world. Although the exact boundaries of the resource are not known, the planned production will soon exceed the output of a modern conventional nuclear power plant. To be of practical interest in the exploration for geothermal resources, seismological methods must be capable of detecting a resource the size and quality of The Geysers, and preferably smaller resources. In addition to method evaluation, a comprehensive study of the seismological properties associated with the known characteristics of the reservoir may aid in determining the extent of the production zone. If successful, the geothermal potential of other geologically similar high heat flow areas could possibly be determined by applying the methods and experienced gained at The Geysers.

This study was prompted by the planned detonations of two explosive sources, 8 and 18 km west of the geothermal field (see Figure 3-1) for an unrelated U.S. Geological Survey (USGS) refraction study. In addition to the two explosions, seventy microearthquakes were recorded during the 20-24 September 1976 study. Based

Figure 3-1

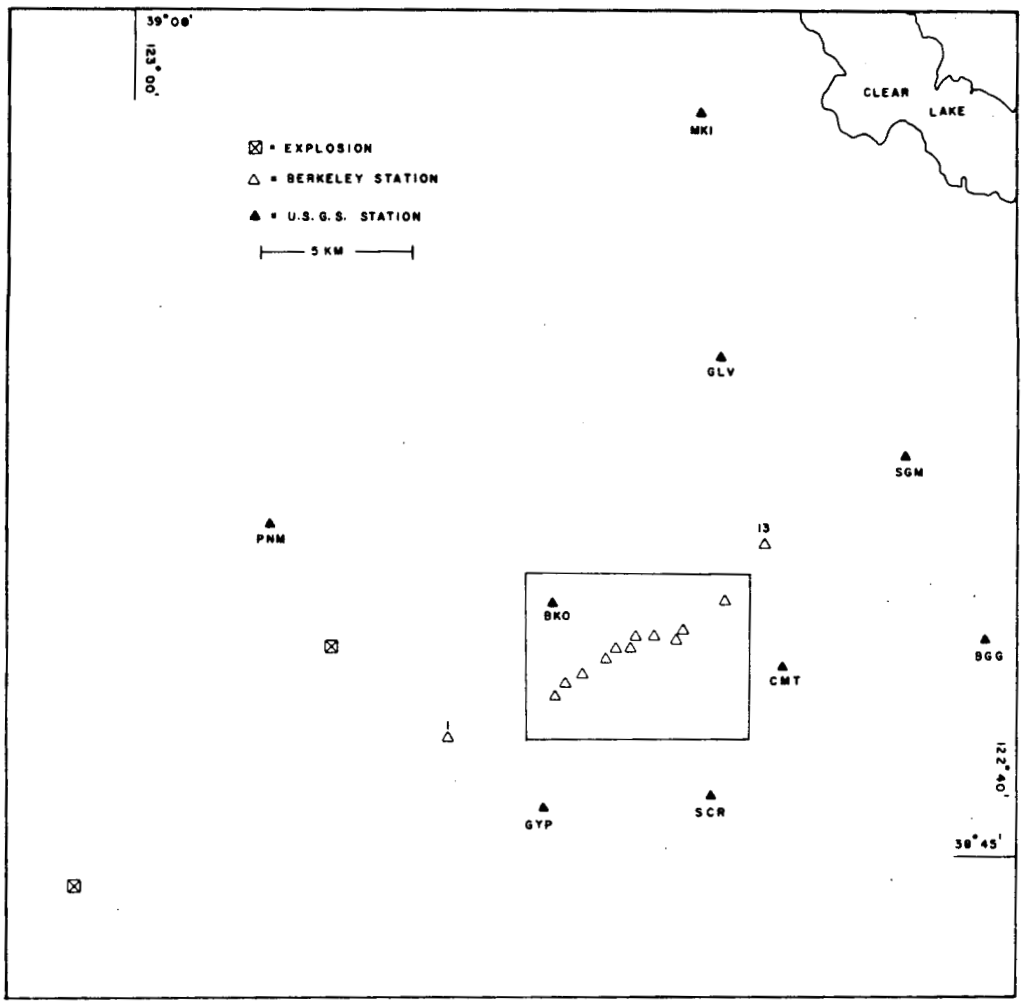

Permanent (USGS) seismographic stations in The Geysers - Clear Lake area, and temporary (Berkeley) station array in the geothermal field. Box indicates area in subsequent maps. Refraction explosion locations are shown.

on the results of the 1976 study, to obtain additional wide dynamic range information on magnitudes and source properties of microearthquakes, a single channel 12-bit triggered digital cassette recorder and smoked-paper recorder were set out near Station 7 in the steam field July 22-25 and August 2-8, 1977. A total of 340 events were recorded on the smoked-paper recorder. The digital recorder malfunctioned during the July 22-25 period, but 101 events were recorded using a horizontal geophone and 54 events were recorded with vertical geophone during the August 2-8 period.

The linear array of the September 1976 study was placed through the producing steamfield perpendicular to strike of the major geologic trends in the region, as shown in Figure 3-1. Station 1 and the USGS station SGM served as reference stations to the west and east, respectively, of the present production zone which extends from station 2 through station 12. The thirteenth station, east of the producing field, was a model MEQ-800 portable smoked-paper recorder. Conventional short-period USGS stations in the area provided additional arrival times and first motion data. The locations of the temporary stations are given in Table 3-1.

3.2 Geological Setting

The following is a discussion the dominant lithologies

Table 3-1

Locations of Temporary Berkeley Stations

	Latitude (N)	Longitude (W)	Elevation (m)
1	38°47.124'	122°52.692	746
2	47.847'	50.258	736
3	48.100'	50.109	567
4	48.210'	49.845	476
5	48.483'	49.296	552
6	48.653'	49.000	692
7	48.669'	48.639	731
8	48.840'	48.532	889
9	48.891'	48.193	950
10	48.788'	47.735	988
11	49.045'	47.456	882
12	49.474'	46.639	721
13	50.578'	45.662	1,050

and structural trends in The Geysers. For a more detailed discussion, the reader is referred to McLaughlin and Stanley (1975) and McLaughlin (1977) from which this outline was obtained.

The Geysers steam field is located in the Mayacmas mountain of Northern California. The Basement complex of this coastal range consists of Late Mesozoic and Early Tertiary Franciscan assemblages of volcanic-sedimentary sequences. The ophiolite complex beneath the Great Valley sequence may represent rocks originally emplaced east of the Franciscan assemblage. The Franciscan assemblage has been interpreted to be high pressure, low temperature metamorphic terrain, with the deformation and metamorphism related to subduction zone processes, whereas the contemporaneous Great Valley sequence has been altered only mildly.

The Great Valley sequence now overlies Franciscan rocks of equivalent age along a zone of regional thrust faults. It is hypothesized that as subduction ceased, the relative motion between the continental and oceanic plates was accommodated by transform motion, with the dominant mechanism of faulting becoming strike-slip, resulting in the present-day San Andreas system. This sequence of events is evident in The Geysers region by a northwest-trending fault pattern with at least two senses of displacement. The oldest being imbricate northeast-

southeast and southwest dipping high to low angle thrust faulting separating tectonic slabs in the Franciscan. The younger type of motion, steeply-dipping northwest-trending faults with vertical and strike-slip components, is commonly superimposed on the earlier thrust faulting.

The most abundant assemblage in the region is the Franciscan, consisting of graywacke and minor shale, with shale being more prevalent in the structurally higher, most deformed parts of the assemblage. Greenstones (altered intrusive and extrusive igneous rocks) also occur in the structurally higher parts of the assemblage. Serpentinite is present along the faults and within highly sheared zones of the Franciscan. Although Franciscan assemblages range in age from Late Jurassic to Early Tertiary in other parts of California, they are considered to be no younger than Cretaceous in The Geysers region.

In addition to the Franciscan assemblage, ophiolitic rocks are present below Mount St. Helena to the southeast, between Geyser Peak and Black Mountain to the southwest and along the north side of Cobb and Collayomi Valleys to the northeast. Still less abundant in The Geyser region are strata of the Great Valley sequence which are probably correlative to the Knoxville Formation. Considerable thicknesses of the Knoxville Formation are present in the Clear Lake area to the north.

In The Geysers steam field upper Jurassic and Cretaceous rocks of the Franciscan assemblage form the

core of a southeastward plunging antiform which has been cut by the previously mentioned fault pattern of thrust faults superimposed by strike-slip faulting. McLaughlin and Stanley (1975) divide the rocks within this antiform into three structural units. Unit one, which dominates much of the known steam zone, is the lowest structural unit, composed of a relatively intact flysch-like sequence of graywackes and shale, compressed onto tight southeast-trending folds. Unit two, overlying unit one north of the Mercuryville fault zone and south of the Geyser Peak fault zone, is highly deformed, lithologically hetero-generous, and locally chaotic. Unit two consists of relatively undeformed slabs composed of subordinate well-bedded graywacke, with shake, conglomerate and basaltic volcanic rocks and chert. Unit 3, which overlies unit 2 is truncated by the southeastward extension of The Geyser Peak and Mercuryville fault zone in the southern part of the area. Lithologically, unit 3 is very similar to unit 2, except the rocks in unit 3 are texturally distinct. Figure 3-2 shows the relative position of units 1-3 and several cross sections through The Geysers area with possible interpretations of the relative positions of the structural units.

Undoubtably, the structure and fault patterns play an important role in the permeability, porosity and the occurrence of microearthquakes. The extent to which the

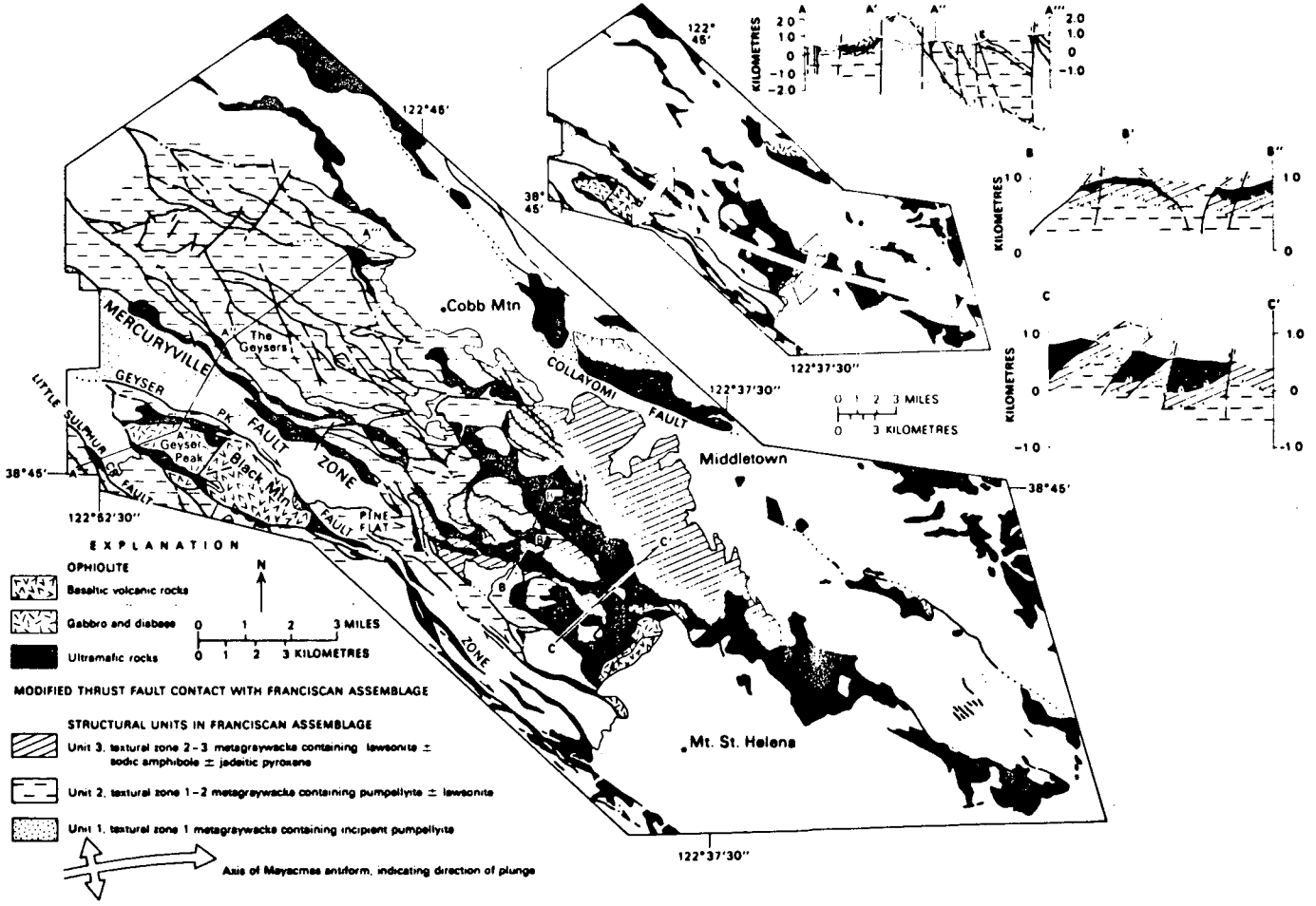

Major structural units in The Geysers Region (McLaughlin & Stanley, 1975).

Figure 3-2

geothermal resource influences the spatial and temporal distribution, as well as the source mechanisms of the microearthquakes and wave propagation, will be discussed in the following sections. However, the observed anomalies in velocity and attenuation could be due to the alternation of structural units discussed above.

The heat source that is responsible for the steam field may be related to the recent volcanism in the region. The Clear Lake volcanics become progressively younger as one proceeds north from Mount St. Helena, with the youngest ages occurring near Clear Lake (Donnelly, 1977). Although the volcanics in The Geysers area are not the youngest observed, the complex faulting and hydrology of the region may be obscurring the true location of the heat source or hot waters supplying The Geysers steam field.

3.3 Reservoir Properties

It is hoped the characteristics of earthquake genesis and wave propagation reflect the steam reservoir properties. The Geysers geothermal field is a vapor dominated reservoir, as opposed to a hot water or brine system characteristic of the Basin and Range or Salton Sea regions. The temperature and pressure of the vapor region is fairly constant, ranging within a few degrees of 240°C at 30 to 40 bars (Weres, et al., 1977).

An unusual characteristic of the reservoir is that it is not at hydrostatic pressure, but much below. The

observed pressures are much less than expected hydrostatic pressures at the depths involved (2-3 km). Several hypotheses have been advanced to explain the pressure differential. In one, an "incrustation seal" has formed on the edge of the reservoir, preventing any pressure equilization from the surrounding ground water (White, et al., 1971). The model proposes that minerals such as calcite and anhydrite, which have solubilities that decrease with increasing temperature, have precipitated from the cooler ground water upon entering the geothermal zone, thus reducing the permeability at that point. A second model proposes reservoir permeability such that the relatively viscous water, as compared to steam, cannot flow rapidly enough into the low pressure steam zone to equalize pressure. This implies an expanding reservoir, if the withdrawal rate were high enough and the heat source adequate, to convert incoming water to steam. A third explanation calls upon "traps" of steam, similar to gas traps found in oil producing regions, sealed from surrounding waters.

As previously stated, the dominant rock type in The Geysers reservoir is Franciscan graywacke (McLaughlin and Stanley, 1975), which is initially impermeable and non-porous, but extensively sheared and fractured such that its porosity and permeability is sufficient to provide the existing reservoir. Drill cuttings have shown evidence of secondary porosity due to hydrothermal

dissolution of minerals (Weres, et al., 1977). Often in place of these minerals is a "sand" or alteration product of the minerals. In successful steam wells, "geothermal sand" is often encountered above the steam zones, (Joe Lafleur, personal communication, 1977). The steam-water interface is probably not smooth but irregular, reflecting different porosities and capillary effects. The actual amount of economic steam in the reservoir will depend upon the rock type, porosity, permeability, water content and available heat. A rock with low permeability and porosity will surrender less steam per ^{o}C than a highly permeable and porous rock.

An important characteristic of The Geysers reservoir is that it seems to be a maximum enthalpy system. In a saturated steam, the enthalpy (heat content) has a maximum value of 2,804 kj/kg at 234^{o}C and 30 bars. The enthalpy of the steam entering the different units at The Geysers is very near this value (Weres, et al., 1977). Why the enthalpy of the steam is at this particular value is not entirely clear. However, other steam reservoirs, Lardarello, Italy and Kawah Kamojang, Indonesia also exhibit, to some degree, the maximum enthalpy phenomenon (Weres, et al., 1977).

Natural leakage, commercial production and inter-connected reservoirs are several mechanisms proposed to explain the maximum enthalpy phenomenon at The Geysers. This implies that the steam flowing toward the bottom of

the wells begins as saturated steam at some temperature above 234°C and is expanded isoenthalpically to below 30 bars under conditions which cause the water to condense out of it. For example, an initially water-saturated reservoir isolated from other parts of the reservoir would, due to commercial production or leakage, eventually boil dry at some temperature below 234°C and at a pressure below 30 bars, depending on the permeability and initial temperature. On the other hand, if there were an unlimited amount of steam available from other parts of the reservoir, the temperature and pressure would stabilize at the maximum enthalpy point. As production continued, the 234°C zone would spread and new wells drilled might also encounter the maximum enthalpy phenomenon. The actual case is doubtless between unlimited steam and zero steam, which would account for deviation from the maximum enthalpy point.

The state of the reservoir before commercial production began is not entirely clear. Weres, et al., (1977) hypothesized that there was a shallow initial vapor zone in the region of units 1 and 2, but as production increased the "deep water table" was boiled down by two or more km to the present 2.5 km. This "cracked sponge model" hypothesizes that the water is boiled rapidly out from the cracks which are innerconnected; however, there is still a large amount of water left behind in the body of the

sponge or in the fine pore structure of the rock, which could serve as a water supply to the steam reservoir. White et al. (1971) suggested a system which was initially water saturated, but with the introduction of a potent heat source, a hot water convection system was initiated. Eventually, near-surface temperatures and pressures allowed the onset of boiling and because of limited recharge and permeability, the hot water system turned into a vapor-dominated system. An important aspect of White's model, from a seismological point of view, is the recharge area. Because of limited permeability due to the incrustation seal, there would be large pressure gradients near the margins. This high pressure would provide large pressure gradients between the reservoir, which is much below the hydrostatic pressure, and the boundary of the reservoir which is possibly above hydrostatic. As production increased, the vapor front would advance, thus exposing new regions to pressure differentials. The front would stop advancing when either the heat sources was insufficient to cause boiling or the permeability increased such that the recharge and discharge rates balanced.

3.4 Explosion Data

3.4.1 P-Wave Velocities

A fundamental question in this study is whether the presence of the geothermal reservoir is evident in the velocity of porpagation of P-waves. A regional reference travel-time curve, shown in Figure 3-3, with velocities of 4.49 ± 0.10 km/sec and 4.98 ± 0.09 km/sec, was constructed from USGS station readings for both explosions, omitting, however, stations in The Geysers and Clear Lake areas. An attempt was made to fit the data with a velocity model of the form $v = v_o + kz$, with v_o = 2.0, 2.5, 3.0, 3.5 km/sec and k = 0.4, 0.5, 0.6, 0.7; however, the best fit was a layered model. These values can then be compared, for velocity anomalies, to the regional travel-time curve. Explosion arrival times are given in Table 3-2. The travel-time data in Figure 3-3 indicate that only the upper two to three kilometers of the crust are sampled by the first arrivals from the explosions. It was hoped that by recording several regional earthquakes or teleseismic events the deep structure could also be studied. Unfortunately, no such events were recorded during the five-day field period.

Figure 3-4 presents reduced travel-times for the temporary stations with respect to the regional data in Figure 3-3. Times are corrected for elevation differences with respect to Station 4 using 4.0 km/sec. Also shown are the reduced times for the USGS stations

Figure 3-3

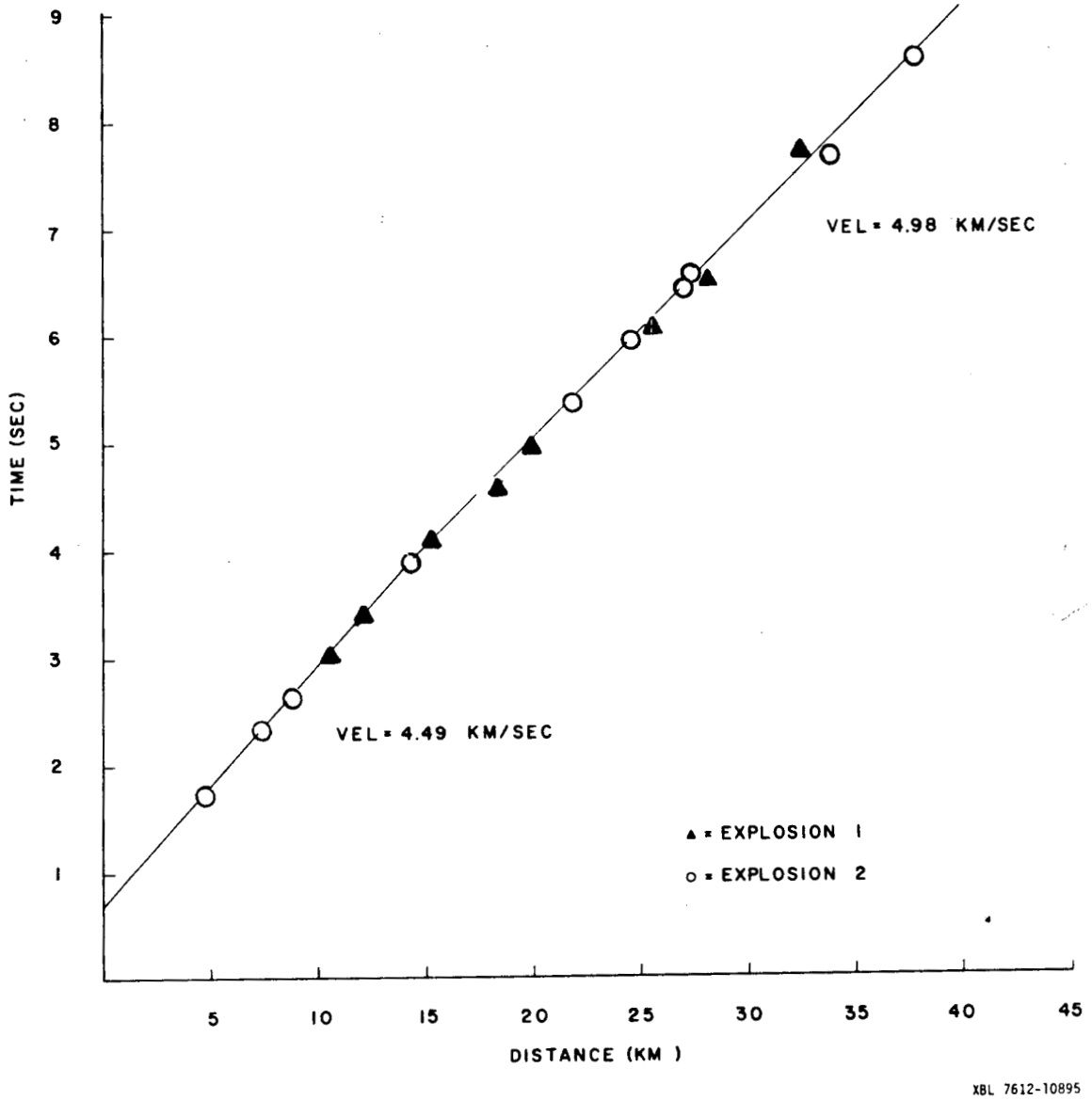

Regional travel-times for stations outside known geothermal area, based on the two explosions.

Table 3-2

Explosion Data and Arrival Times

	Time (UTC)	Location
#1	1235 00.58 Day 266	38°43.50'N 123°01.44'W
#2	1235 00.64 Day 268	38°48.60'N 122°55.62'W

USGS Stations	Arrival Time of #1 (UTC)	Arrival Time of #2 (UTC)
*BKO	1235 05.05 ± 0.05 sec.	1235 02.43 ± 0.05 sec.
BGG	07.22	05.21
ALX	05.75	04.50
CMT	05.95	03.88
CVD	01.82	03.00
*DRY	04.92	06.65
*FTR	06.08	08.50
AAF	10.15	11.10
*GYP	04.51	02.85
*HLS	07.82	06.20
*HOC	05.00	--
HOG	--	07.85
*HLB	07.82	05.90
GLV	06.95	04.41
MKI	08.30	05.65
*MOF	03.10	05.46
*MCL	03.40	04.56
*MWS	07.65	07.60
SCR	05.38	03.58
SGM	07.60	05.10
*SNO	06.60	06.55
*SKG	01.36	04.05
*PNM	04.30	01.80

* Station used for velocity model.

Berkeley Stations	Arrival Time of #1 (UTC)	Arrival Time of #2 (UTC)
1	1235 04.170 ± .005 sec.	1235 01.890 ± .005 sec.
2	04.857	02.540
3	04.863	02.535
4	04.900	02.580
5	05.185	02.750
6	05.200	02.840
7	05.263	02.935
8	05.327	02.990
9	05.396	03.070
10	05.478	03.200
11	05.564	03.270
12	05.883	03.610
13	--	03.816

Figure 3-4

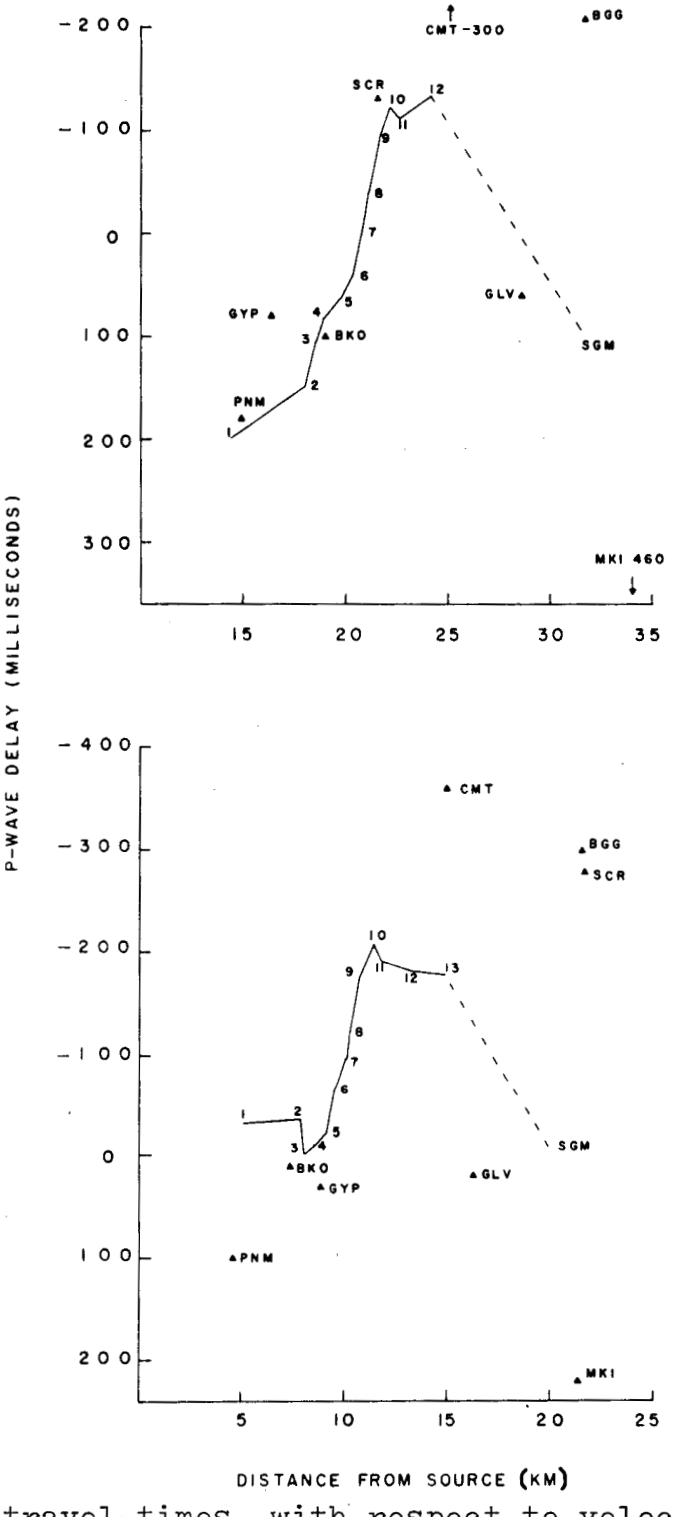

Reduced travel-times, with respect to velocities shown in Figure 2, for stations within The Geysers-Clear Lake area, for both explosions. Temporary stations are numbered, USGS stations are shown by name.

in Figure 3-1 which were not used in deriving the regional curve. Along the temporary station array, early arrivals with relative P-wave advances of up to 200 milliseconds are seen commencing around Station 5 and continuing to the end of the temporary linear array at Station 13. Station SGM to the northeast of the producing field appears normal. USGS Stations SCR, CMT and BGG are also early, i.e., fast with respect to the regional reference model. Stations GYP, BKO and GLV, like SGM, appear normal, regionally. Station MKI, near Clear Lake, is especially late, PNM is somewhat so. The general tendency seems to be that times in the production zone and southeast of it are early, and as one proceeds northeastward toward Clear Lake the times become regionally normal, then significantly delayed. This general pattern holds for both the near and far explosions. Closer inspection of data from the far explosion reveals that, even though the shape of the curve is the same as that for the near source, the times from the far explosion have been shifted down or delayed by nearly 100 milliseconds with respect to the regional travel-time reference. This effect is seen at all distances, PNM to MKI, and may represent regionally low velocity material west of Station 1.

3.4.2 Attenuation

In addition to possible anomalous velocity, it was desired to know if the production zone affected the amplitude and waveform of the P-wave. Figure 3-5 shows seismograms from the far explosion plotted in relative time and distance and at equal gains. It is evident from visual inspection of the first two or three cycles of the P-wave that the waves are attenuated less within the production zone than at Station 1, five kilometers west of the production zone.

Two approaches were taken to estimate the attenuation effect at the different sites. The first approach is an adaptation of a technique developed by Teng (1968) for analysis of teleseismic data. The ratio of the spectrum of the P-wave at each station to an arbitrary reference station is used to obtain the differential attenuation. Assumptions are that Q is frequency-independent over the particular frequency band used. The attenuation operator can be expressed as:

$$\exp\left[-\pi f \int_{\text{path}} \frac{ds}{QC}\right]$$

Figure 3-5

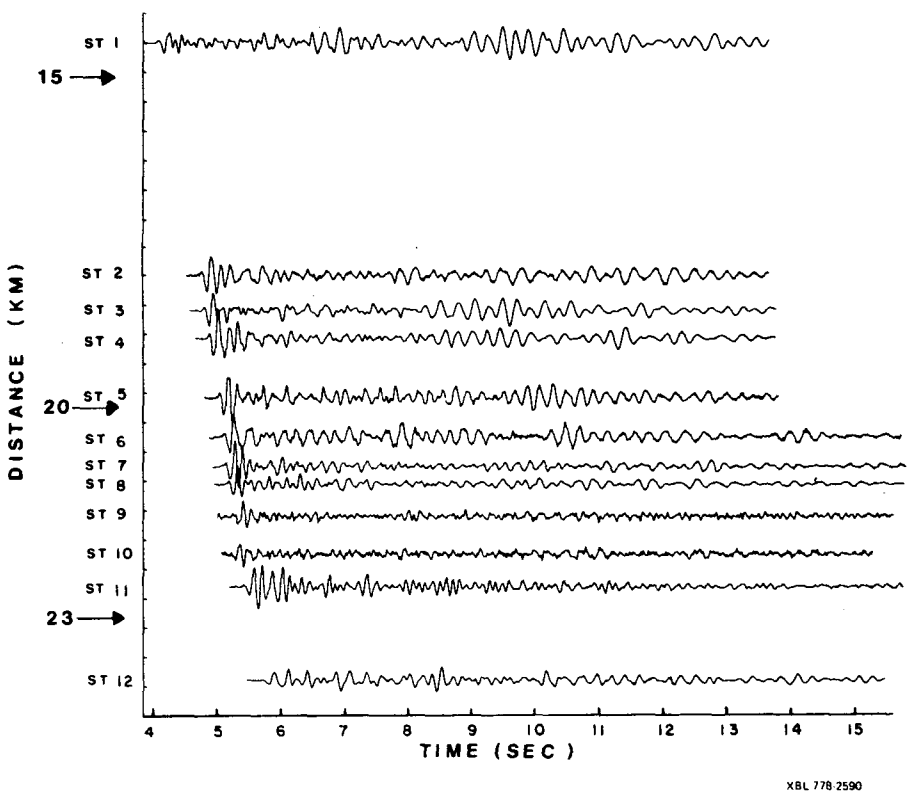

Seismograms from the far explosion, plotted at equal gains and at relative distances.

where s = path length

Q^{-1} = intrinsic attenuation = $\frac{2\pi \Delta E}{E}$

$\frac{\Delta E}{E}$ = fraction of strain energy dissipated per cycle

C = wave velocity

The path of integration is taken along the ray path. The log of the spectral ratio, reduced ratio, of the P-wave at two different points will be a linear function of frequency with the slope of the spectral ratio, $-\pi \delta t/Q$, where δt is the travel-time difference between the two stations. The resulting attenuation, assumed constant, applies to the differential ray path. In practice, one corrects for differences in instrument response and radiation pattern or any frequency dependent effects which differ at the two stations and then fits a straight line to the resulting reduced spectral ratio.

An implicit assumption in this method is that the path to the first point is common to the second path. This implies a negative slope to the spectral ratio, with zero slope for infinite Q; i.e., no attenuation. In practice, positive slopes can be obtained if the path to the first point contains a segment of low Q medium not common to the second path. Widely differing near-surface transfer functions at the two sites can also produce strange effects in the reduced spectral ratio. To minimize such effects often it is necessary to use a

smoothed average spectrum as reference in forming ratios.

The procedure used in this study was as follows: The seismograms from each site for the distant explosion were anti-alias filtered and digitized at 200 samples/sec. The digitized data were then plotted for comparison checks with the analog data to select the proper P-wave intervals. The 0.65 sec P-wave data windows were tapered with a 20% cosine taper, average signal level was removed, and zeros were added to a total of 2^{10} points. The data were then transformed with a Fast Fourier Transform and corrected for instrument response. Spectra were smoothed with a moving 10-point window. The reduced spectral ratios were than computed and plotted.

The P-wave forms along with individual displacement spectra are shown in the first two columns of Figure 3-6. The spectra are not corrected for geometrical spreading. The individual spectra show that, within the production zone, the high frequency components are less attenuated. At stations 1 and 12, the spectra have no definite high frequency corner. However, stations in the field, e.g., 7 and 8, have well-developed corners at approximately 10 Hz suggesting higher Q beneath the production zone.

The third column in Figure 3-6 shows reduced ratios with respect to an average spectrum. Initially, spectral ratios were obtained using station 1 as reference.

Figure 3-6

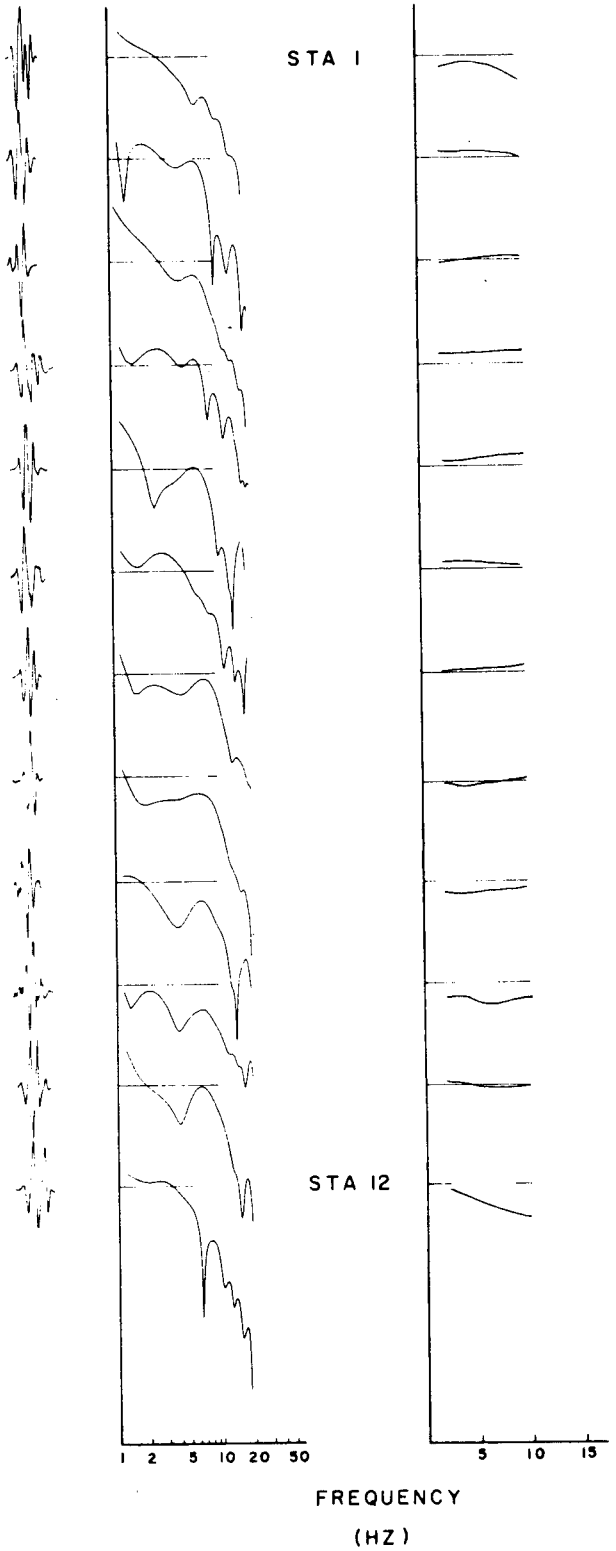

P-wave signals, spectra, and spectral ratios with respect to smoothed reference spectrum (see text).

Examples are shown in Figure 3-7. Signal-to-noise ratios are maximum in the 2-10 Hz range. In an attempt to reduce the large variations in the ratios, an alternate reference spectrum was sought. The first cycle of the P-wave was analyzed, these spectra were then smoothed and averaged using all the stations. The resulting average was used as the reference spectrum. Reduced spectral ratios (between 1 and 10 Hz) with respect to this average spectrum are given in the third column of Figure 3-6. These ratios resemble straight lines. A positive slope to the line means a higher Q than average, a negative slope means a lower Q. Considering the entire 1-10 Hz span, stations 1, 2, 6, and 12 have negative slopes while all other sites have positive slopes, roughly indicating lower Q at the edges and outside of the field than inside the production zone. Further attempts to use the slopes in Figure 3-6 for inversion to obtain Q structure would be beyond the quality of the data. It would have been better had several stations been outside of the steam field, and their average spectrum used as reference. The frequency range 3-10 Hz is also susceptible to effects of very shallow structure, rendering difficult the estimation of meaningful spectra. In general, if the data are of high enough quality in bandwidth and dynamic range, if there are several reference stations outside the zone of interest, and if the target is large enough, then this

Figure 3-7

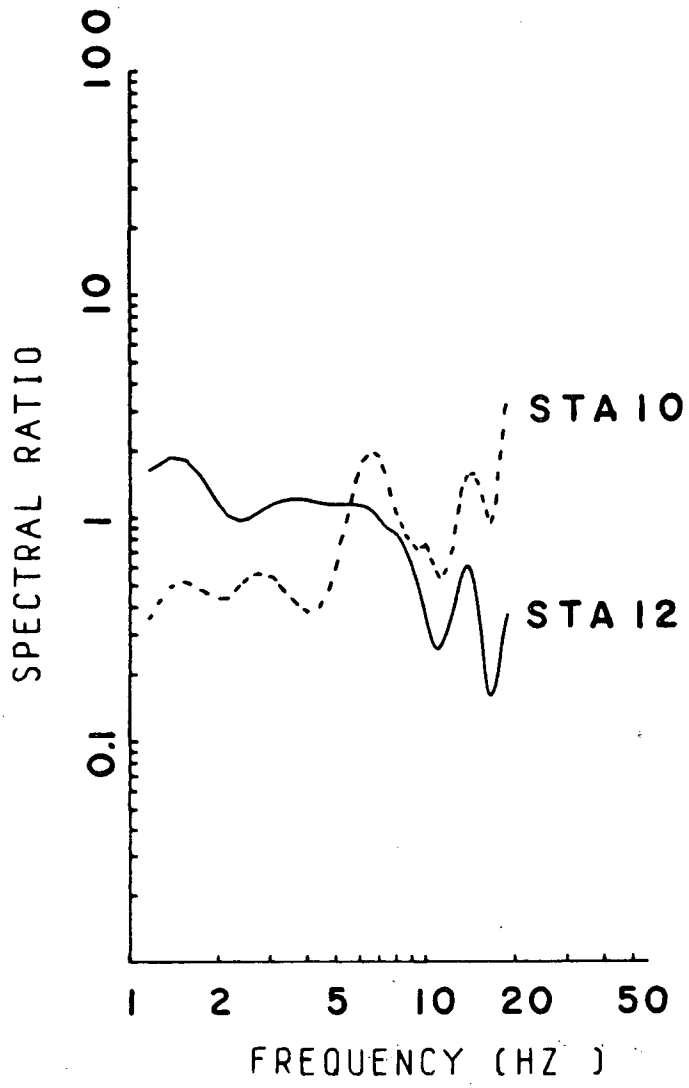

Example, spectral ratios with respect to station 1 spectrum, unsmoothed, as reference.

method can probably be used successfully. The effectiveness might also be raised if longer periods are available, though the effects become small on the scale of this experiment.

A second attempt was made to localize the Q effect by considering only the amplitude of the first half cycle of the P-wave at each station and to specify more precisely the differential ray paths by using both explosions. A velocity model as shown in Figure 3-8 was selected to specify the ray paths and velocities along the ray paths.

The procedure is to select a reference station, r, with amplitude A_r, and correct for the vertical part of the path to station r, assuming a value Q_r. There can then be calculated, based on the model, a value Q_i corresponding to the horizontal propagation path from the reference station to station i and the near-vertical propagation under i. The resulting Q_i value will depend on the Q_r assumed immediately beneath the reference station, and it will contain information on the entire path from beneath the reference station to the surface at station i. Results for Q_r values of 30, 45 and 60 for station 2 as reference are given in Table 3-3 for both explosions. A maximum value of 250 was assigned to Q_i, because the fractional change in amplitude of the wave for higher values of Q cannot be measured over the distances involved. The Q_i values for Q_r = 60 are shown

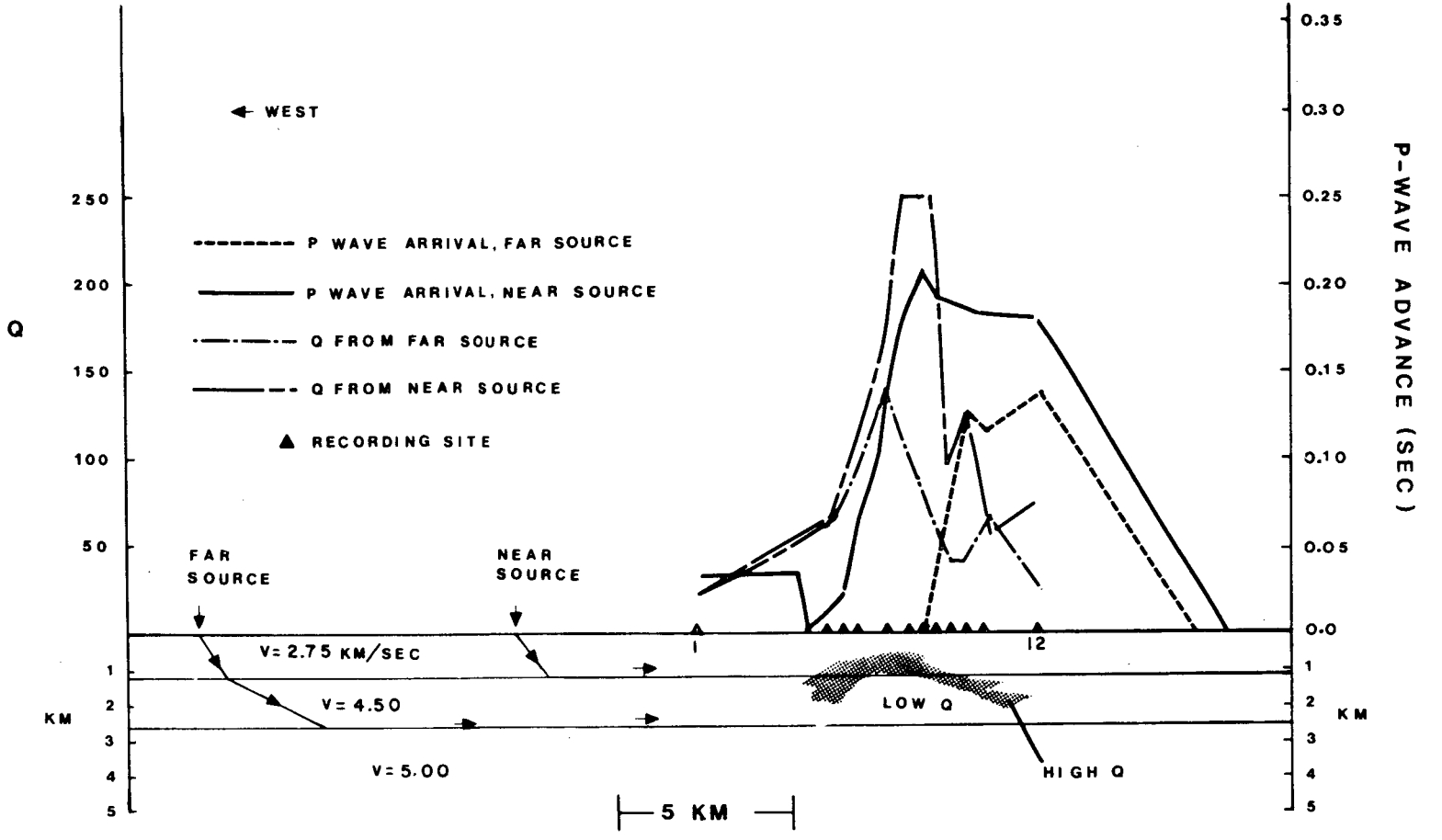

Figure 3-8

Composite model for Q estimation, showing P-wave travel-time resuduals and Q_i through the production zone, for both explosions. Zone of inferred high Q and high velocity is shaded. Q_r is assumed to be 60.

Table 3-3

Average Attenuation Values, Q_i, for various Q_r.

Far Source

Station	$Q_r = 30$	$Q_r = 45$	$Q_r = 60$
1	14	17	19
2	30	45	60
3	33	52	71
4	38	63	94
5	48	86	142
6	44	71	102
7	41	63	86
8	34	47	58
9	28	36	43
10	30	37	44
11	40	56	70
12	19	23	25

Near Source

Station	$Q_r = 30$	$Q_r = 45$	$Q_r = 60$
1	10	12	13
2	30	45	60
3	32	51	67
4	-	-	-
5	-	-	-
6	75	189	250
7	164	250	250
8	92	250	250
9	50	76	94
10	62	100	132
11	34	42	47
12	51	66	75

in Figure 3-8.

For both explosions the apparent Q increases throughout the field then decreases again by station 12, for all Q_r. This is the same general pattern seen in the spectral ratios. The apparent Q values within the field are higher for the shallower penetrating waves from the near source than for the deeper penetrating waves from the far source. Although the apparent Q values are higher than regional values for the distant explosion, they include the effect of the shallow high Q zone as well as the effect of a deeper Q. Also, because the Q values are similar for both near and far explosions at station 1, a zone of lower Q beneath the high Q zone in the production area is indicated. Q values in the steam field thus appear high with respect to regional values at shallow depth (<1 km), decreasing at greater depths (3 km). It is not clear whether the Q values decrease below regional values at depth. Data consistent with high Q in the field come from the study of the corner frequencies of microearthquakes, discussed in the following section.

3.5 Microearthquake Data

3.5.1 Locations

During the five days of recording, seventy earthquakes were observed in the monitored signals from

stations 1, 7 and 12. There were no local events recorded by the USGS stations PNM, BKO, SGN, CMT, SCR, BGG and GYP that were not recorded by the temporary stations. However, there were 12 events recorded by the temporary stations that were recorded only by the two USGS stations closest to the production zone, BKO and CMT, indicating that the microearthquakes are confined to the general area of the steam field. The high rate of seismicity is apparently an ongoing phenomenon. Hamilton and Muffler (1972) recorded 53 events in three weeks with epicenters in the same general area. Lange and Westphal (1969) recorded 19 "small" earthquakes throughout the production zone during a four day observation period. In a later survey, July 22-25 and August 2-8, 1977, 340 events with S-P times less than 1 second were recorded near station 7.

Hypocenters were estimated using a simple velocity model of two layers over a halfspace, with velocities of 4, 5 and 6 km/sec, and layer thickness of 1 and 5 km, respectively. This model was obtained by locating several large events in the center of the array, using different velocities consistent with the explosion data; the model giving the smallest standard error in depth was selected as best. Events with clear arrivals on at least five temporary stations and three USGS stations were processed for locations. Forty of the fifty-eight events processed are plotted in Figure 3-9 and listed in Table 3-4. These events could be located with

Figure 3-9

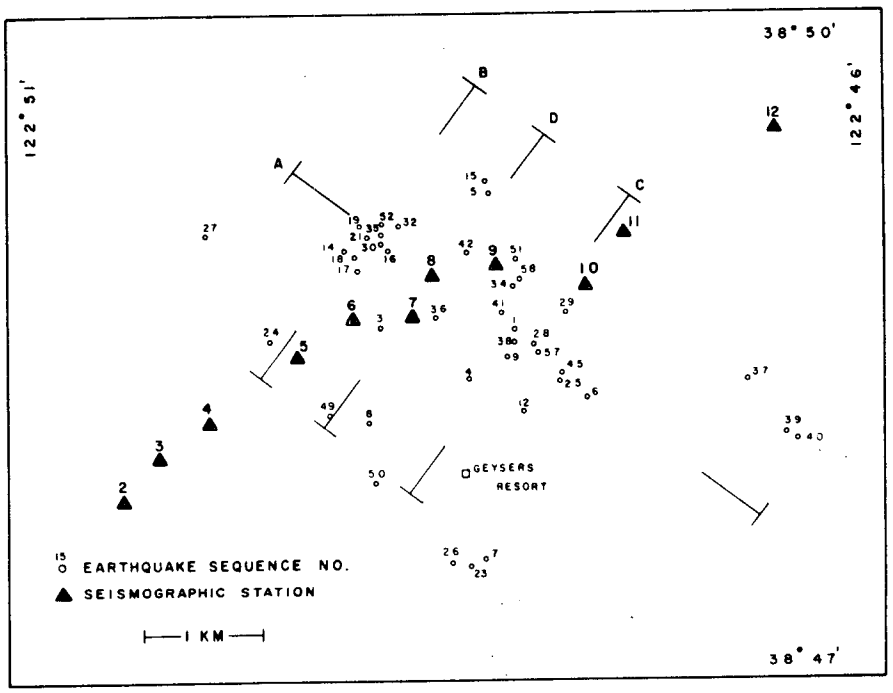

Epicenters, with sequence numbers (see Table 4), for well-located microearthquakes recorded 20-24 September, 1976. Sections in Figure 9 are indicated.

Table 3-4

Microearthquake Locations

Sequence Number	M_{CB}	M_{CL}	Latitude	Longitude	Depth (km)	S.E. of Epicenter (km)
1			38°48.54'N	122°48.06'W	0.71	.02
2	0.6	0.1				
3	0.4	-0.5	48.58'	48.86'	1.19	.07
4			48.35'	48.37'	2.79	.01
5	0.2	-1.0	49.18'	48.26'	0.84	.05
6	0.4	-0.6	48.32'	47.70'	1.41	.03
7	0.7	0.2	47.57'	48.25'	4.40	.07
8	0.2	-1.0	48.17'	48.93'	0.90	.10
9	0.7	0.2	48.46'	48.16'	0.75	.07
10	0.1	-1.3				
11	0.5	-0.4				
12	0.8	0.5				
13	0.4	-0.6				
14	0.1	-1.3	48.94'	49.06'	1.43	.07
15	0.4	-0.6	49.24'	48.25'	1.74	.03
16	0.4	-0.5	48.86'	48.82'	1.58	.05
17	0.3	-0.7	48.84'	48.94'	1.49	.08
18	0.3	-0.9	48.89'	49.04'	1.30	.07
19	0.3	-0.9	49.06	48.95'	1.41	.04
20	0.3	-0.7				
21	0.3	-0.8	48.98'	48.95'	1.54	.03
22	0.2	-1.2				
23	0.3	-0.7	47.57'	48.34'	3.0	.05
24	0.3	-0.9	48.53'	49.50'	1.11	.01
25	0.6	0.1	48.36'	47.86'	4.14	.05
26	0.4	-0.5	47.56'	48.50'	3.0	.06
27	0.4	-0.4	49.01'	49.84'	0.67	.09
28	0.7	0.3	48.51'	47.97'	3.55	.05
29	0.9	0.9	48.66'	47.80'	3.76	.05
30	0.8	0.8	48.97'	48.86'	1.25	.03
32	0.3	-0.8	49.05'	48.74'	0.60	.03
33	0.4	-0.6				
34	0.7	0.1	48.78'	48.10'	1.64	.04
35	0.5	-0.2	48.63'	48.55'	3.70	.08
36			49.01'	48.84'	1.38	.04
37			48.37'	46.74'	3.77	.09
38	0.3	-0.8	48.50'	48.16'	2.86	.10
39	0.4	-0.4	48.11'	46.54	1.64	.07
40	0.6	0	48.09'	46.49'	0.52	.10
41	0.3	-0.7	48.65	48.18'	3.18	.03
42	0.7	0.2	48.93'	48.34'	3.75	.06
44	0.5	-0.3				
45	1.0	1.2	48.39'	47.81'	3.05	.05
46	0.5	-0.3				
47	0.2	-1.1				
48	0.3	-0.9				
49	0.4	-0.6	48.21'	49.17'	1.92	.04
50	0.7	0.3	47.90'	48.92'	0.40	.05
51	0.5	-0.1	48.88'	48.09'	3.50	.05
52	0.5	-0.1	49.01	48.97'	0.98	.07
53	0.4	-0.5				
57			48.48'	47.95'	3.59	.04
58	0.5	-0.3	48.80'	48.06'	4.01	.07

standard errors less than 0.1 km in epicenters. S-waves were not used in locating the events, but S-wave arrival times were used to estimate Poisson's Ratio, as discussed later.

Figure 3-10 presents the microearthquakes hypocenters projected onto the vertical sections shown in Figure 3-9. The spatial distribution of foci is diffuse, with no well-defined throughgoing faults. Focal depths are less than 5 km, with a notable absence of foci in the depth range of 2 to 3 km. Seismicity is also low in the field north and northeast of The Geysers Resort, the area first exploited for steam production. The wells in this area are shallow (several hundred meters) compared to more recent wells, which extend to nearly 3 km. In general, the production zone throughout the field is between two and three km in depth (Richard Dondanville, oral communication, 1977). Most of the larger events, e.g., 28, 29, 45, occurred in an area northeast of The Geysers Resort. During the later field study, July 22-25, August 2-8, 1977, a magnitude 2.3 shock was recorded in this same general area.

The temporal distribution of events is also of interest. While clusters of events are seen, there is no indication of systematic migration through the field. For example, events 36, 37, 38, 39 and 40 occurred within a two hour period, but in three separated areas. There were not apparent instances of foreshock activity

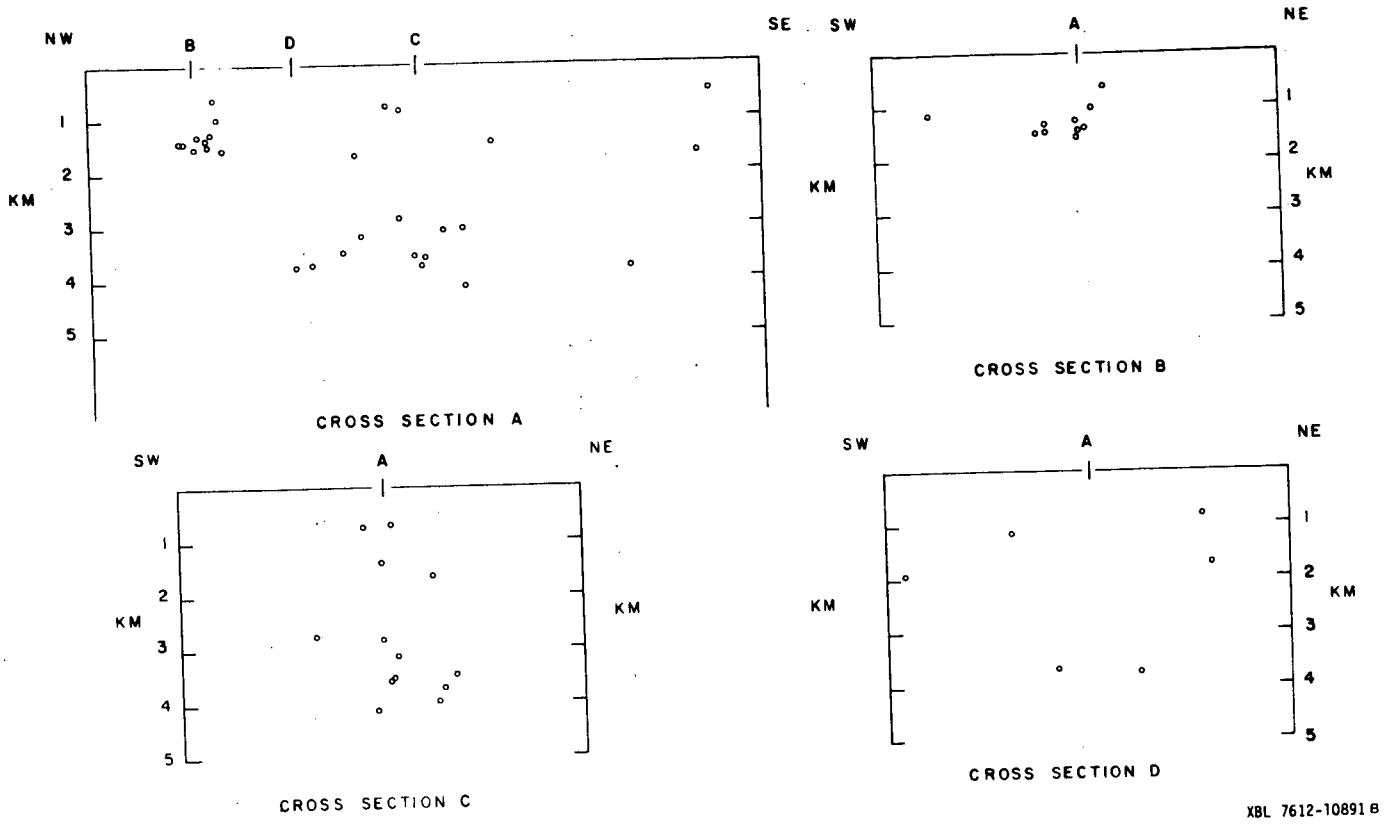

Figure 3-10

Cross sections of hypocenters through the steam production zone. Section lines are shown in Figure 8.

followed by a main shock, nor of clear aftershock sequences. There were no long aseismic periods; rather the activity seems to progress at a more or less constant rate.

3.5.2 Mechanisms

P-wave polarities were used in focal mechanism studies. Because complete asimuthal coverage was not often obtained, there is some ambiguity in the details of fault plane solutions. For this reason, only the better constrained solutions are shown on the regional fault map in Figure 3-11. Plotted are the principal stress axes, which are mainly compressional in the northeast-southwest direction, consistent with strike-slip faulting on near vertical, north-south trending faults, typical of regional Coast Range tectonics east of the San Andreas fault. The major fault zones in the Clear Lake volcanics to the northeast are the Collayomi and Konocti Bay fault zones, which are at least 18-21 km long, respectively, and show both right-lateral and vertical movement. The Collayomi trends northwest and the Konocti Bay trends north-northwest, consistent with the regional San Andreas trend. Donnelly (1977) states that many of the small ($<$1 km lengths) normal faults trending northeast and northwest at Clear Lake are probably due to crustal adjustments from the extrusion of magma in the region. In The Geysers region, the

Figure 3-11

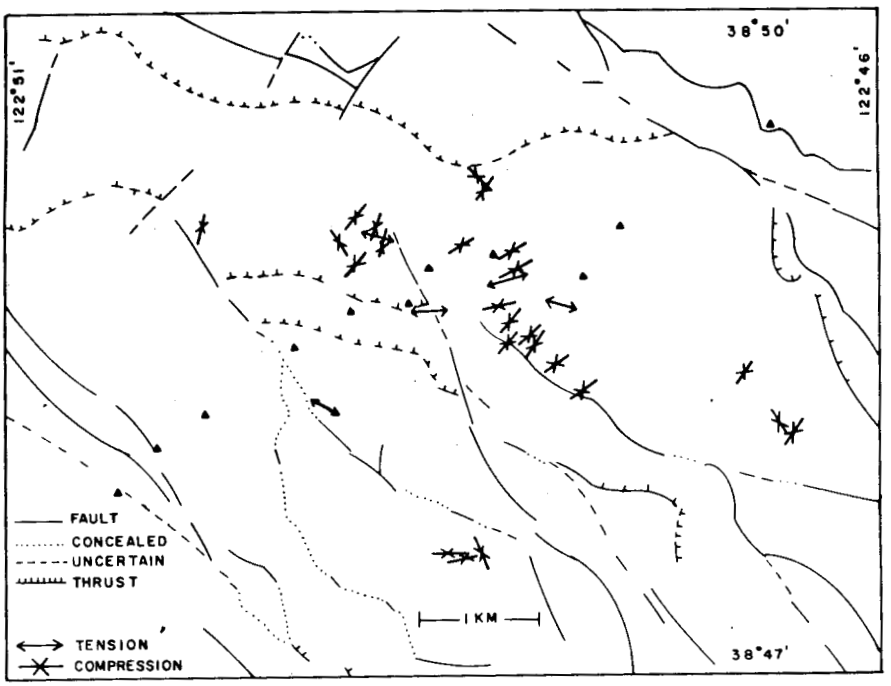

Horizontal projections of principal stress axes from fault-plane solutions. Either compression or tension axis is given, whichever is near-horizontal. Faults adapted from McLaughlin, 1974.

northwest-southeast structural grain is due to the prevailing fault pattern which consists of imbricate northeast-, southeast-, and southwest-dipping high- to low-angle faults. These reverse faults are cut by later strike-slip faults, reflecting the tectonic evolution of the area (McLaughlin and Stanley, 1975). Some thrust faulting is indicated in the fault plane solutions. Permeability may be controlled by both thrust faulting and strike-slip faulting.

3.5.3 Magnitudes

Microearthquake magnitudes were obtained by averaging coda durations for events recorded at stations 5, 7, 9 and 12. These magnitudes are intended to be equivalent to the local Richter magnitude, M_L. Two different formulae were used for magnitude determination. In the first, $M_{CL} = -0.87 + 2 \log_{10} (T)$ where T is the average coda length from the four stations. The amplitude threshold taken for coda length was obtained by observing the same events on the USGS Develocorder systems which have peak magnifications around 15 Hz. This relation, after Lee et al. (1972) was developed for central California earthquakes. The second formula $M_{CB} = -.28 + 0.71 \log_{10} (T)$ was obtained by Bakun and Lindh (1977) for earthquakes with coda lengths less than 30 seconds in the 1975 Oroville, California sequence, recorded by similar systems used for M_{CL}. If no magnitude

is given in Table 3-4, at least one of the four stations did not have sufficient quality data to obtain coda length.

Figure 3-12 presents the distributions obtained for the two different formulae, b-values of 0.81± .03 and 2.3 ± 0.15 were found using the M_{CL} and M_{CB} formulae, respectively. A regional b-value of 0.83 ± .04 was calculated for 73 events, $2.8 \leq M_L \leq 4.8$, occurring with a 50 km radius of The Geysers between 1934 and 1973. C. Bufe (personal communication, 1977) has obtained a b-value of 1.2 for events in The Geysers area with M_{CL} magnitudes between 1 and 3. The M_{CL} derived b-value of 0.8 implies the occurrence of two $M_{CL}=3$ events per year, and a $M_{CL}=4$ shock every three years. However, this rate of occurrence of larger events has not been observed, indicating either some natural magnitude limiting process in operation, or that the local b-value is higher than the 0.8 regional value, or that the rate of seismicity is higher now than in recent decades. $Log_{10}(N) = 2.4-2.3\ M_{CB}$ predicts one $M_{CB}=3$ event every 600 years and 121,000 years between $M_{CB}=4$ earthquakes. While b = 2.3 is high, as b-values go, a value greater than 1 is consistent with the absence of larger events in the area.

The application to The Geysers of coda magnitude formulae developed for other regions is a questionable step if occurrence data are then compared to data for

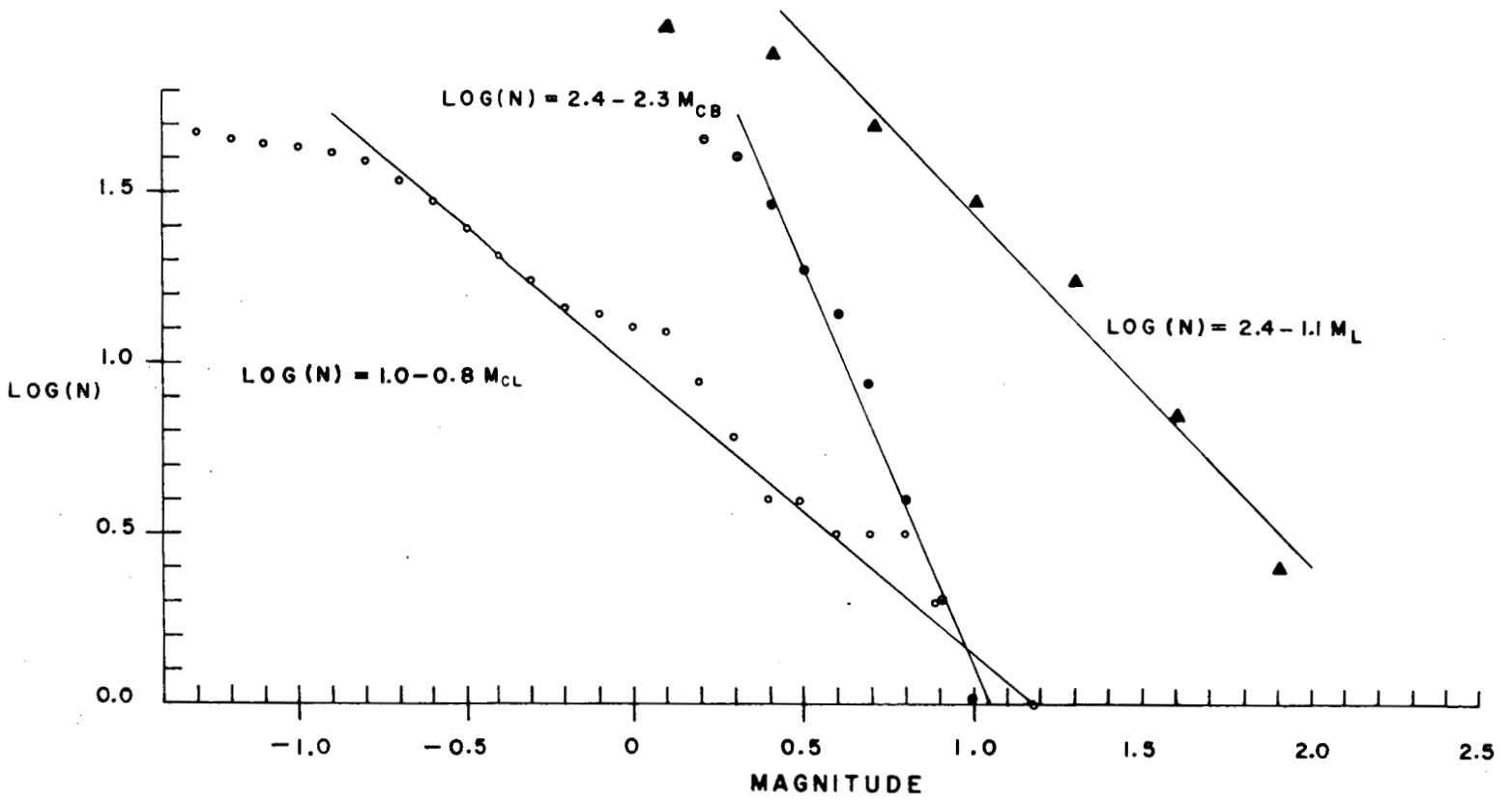

Figure 3-12

Microearthquake occurrence data based on different magnitude formulae. M_{CL} and M_{CB} are coda-length magnitudes for the same 1976 data set (4 days). M_L is equivalent Wood-Anderson magnitude for the August, 1977 data set (3 days).

different regions. Coda lengths for several large events and the two explosions varied widely from one USGS station to the next, depending on distance and azimuth. Thus, although the same measurement used routinely by USGS was attempted, it suffered from the unusual variability of earthquake characteristics at The Geysers. The same near-station properties that affect the amplitude of the P-wave will affect the measured coda length. Attenuation is anomalous in The Geysers; thus our magnitudes and resulting b-values may be meaningless for comparisons to other regions. It is important, but unfortunately difficult, to know if there exists a unique geothermal earthquake, with occurrence properties different from normal tectonic events.

Becuase the coda magnitudes were not satisfactory, an attempt was made to obtain Wood-Anderson magnitudes (M_L) using data from a single-component 12-bit triggered digital cassette recorder and a 4.5 Hz horizontal geophone, set out near station 7 during August 5-8, 1977. 101 events with S-P times less than 1 second were recorded during the 3-day period. The events were recorded at a sample rate of 200/sec. The digitized time series were transformed, the instrument response removed, and the resulting spectra of the horizontal ground displacement were conditioned by the Wood-Anderson instrument response

$$\frac{-s^2}{s^2 + 2\delta\omega_n s + \omega_n{}^2}$$

where $s = i\omega$

δ = damping factor = 0.8

ω_n = natural frequency of Wood-Anderson, $\frac{2\pi}{0.8}$ rad/sec

To avoid noise-induced peaks in the spectra at low and high frequencies a window was applied to the data between 3 and 40 Hz. The equivalent Wood-Anderson spectra were then inverted to the time domain and the resulting synthetic Wood-Anderson seismograms were read for magnitude M_L in the conventional manner.

To check the method, events from other areas with known magnitudes and existing Wood-Anderson records were processed in the manner described. Several events from the Briones Hills, California swarm of January 1977 recorded on the Berkeley magnetic tape system were used. Good agreement was found between magnitudes. Waveforms differed, but the Wood-Anderson records and short period horizontal records used for obtaining the synthetic Wood-Anderson records were not written at the same site in Berkeley.

It was felt that the large sample which was used in this study would minimize the fact that only one station with one horizontal component was used. Ninety-

eight events were processed for Wood-Anderson magnitudes, resulting in a magnitude range of 0 to 1.8, with a b-value of 1.1 ± 0.1. This b-value is between the two coda b-values of 0.8 and 2.3. The magnitude 3.7 earthquake near Cobb Mountain on September 22, 1977, indicates that the 2.3 b-value is too high, if this event is from the population of events in the production zone. This is not clear but the shock did occur on the edge of the hypothesized steam zone (Goff et al., 1977). As production of steam continues and the hydrology is altered, it may well be that the b-values are changing with time. At any rate, the best estimate b-value for The Geysers field earthquakes, based on conventional M_L magnitude, is somewhat greater than unity, implying a process producing a higher proportion of small magnitude events than characteristic of regional seismicity.

3.5.4 Velocities

P- to S-wave velocity ratios (V_p/V_s) may be estimated using the Wadati diagram, where S-P time is plotted versus the P-wave arrival time at many different stations for a single event, assuming the same (V_p/V_s) along all propagation paths. The slope of the line through the points is k-1 (where $K = V_p/V_s$). From K, Poisson's Ratio, σ, may be calculated

$$\sigma = \frac{(K^2-2)}{2(K^2-1)}$$

This method, which gives an average σ along the paths between the stations and the event, does not require knowledge of the origin time of the earthquake. However, it does require a relatively large number of good S-wave arrivals to obtain a reliable slope. Because horizontal geophones were not used throughout this study, the number of sharp S-wave radings was limited for any particular event. Therefore, it was elected to use multiple events and single stations as an alternative method for estimating K-1. This method required a knowledge of the origin time. However, because the events were located using P times only and the standard errors were small, it was felt that errors in the origin times would not obscure any significant lateral variation in σ. The method gives a value of Poisson's Ratio along the path to the station for each source, relative to the P-wave velocity used in locating the earthquake. An average σ was obtained for each station by using multiple sources. Stations 1, 5, 7 and 12 were selected for analysis and the events used are listed in Table 3-5. K-1 was determined by a least squares fit to the data points. Results are shown in Figure 3-13. Because the P-0 times did not vary over a wide range at stations 1, 7 and 12, the values were weighed to pass through the origin. However, the values at station 5 were weighed at the point P-0 = 0.0 and S-P = 0.1 sec, because the

Table 3-5

Events Used for Poisson's Ratio Estimation

STATION 1	STATION 5	STATION 7	STATION 12
27	3	12	3
28	5	14	5
29	7	24	14
42	15	25	16
σ = 0.37	19	34	17
	23	39	18
7	24	40	21
49	45	51	22
50	50	58	23
σ = 0.32	σ = 0.15 ± 0.05	σ = 0.21 ± 0.03	30
			35
			36
			37
			39
			40
			52
			σ = 0.24 ± 0.05

Figure 3-13

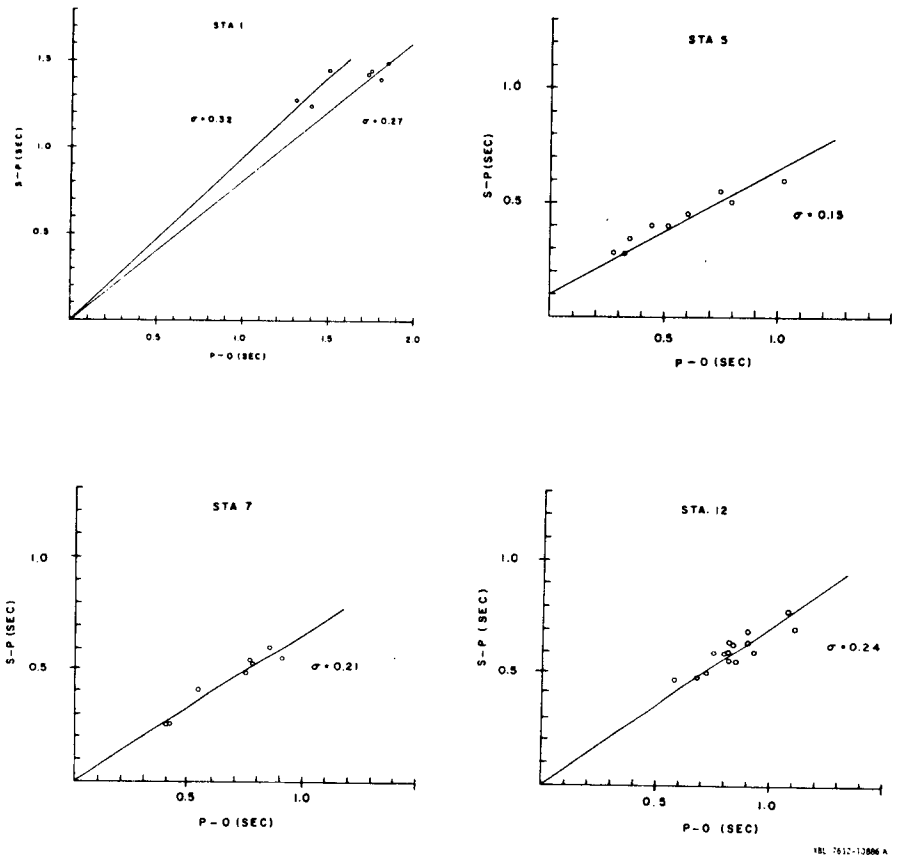

Wadati diagrams for four stations, using multiple events and assumed origin times.

residual travel times were consistently between -0.1 and -0.2 (early) for station 5, while the residuals average zero at the other stations. When no weighing at P-0 = 0 is used, σ is (0.02 ± .04), (0.21 ± 0.07) and (0.15 ± .13) at stations 5, 7 and 12, respectively. The data for station 1 are inadequate because of the small range of P-0 times. However, extrapolating to the origin, two different values of σ are obtained at station 1; σ = 0.32 is found using events outside of the field and travel paths not passing through the production zone, σ = 0.27 is obtained for events in the center of the field so that part of the path is through the production zone. For travel paths completely within the field, stations 5, 7 and 12, the Poisson's Ratios are lower. Although the data set is limited, the general tendency is for Poisson's Ratio to be less in the production zone than outside of it. Combs and Rostein (1975), obtained a low Poisson Ratio, σ = 0.15, at Coso Hot Springs using the same technique.

Because we know the P-wave velocity is higher than regional within the field, the lower Poisson's Ratio implies anomalously high values of the shear modulus within the reservoir. Such a characteristic may be related to the vapor domination.

3.5.5 Source Parameters

Spectral characteristics of selected events were examined in the search for anomalous features in The Geysers microearthquakes. A difficulty with this approach is the lack of comparative data on the spectral characteristics of microearthquakes in other areas. Douglas et el. (1970) and Douglas and Ryall (1972) have studied Basin and Range events and concluded that scaling laws accepted for large events seem to apply for earthquakes as small as magnitude 1. Because a comparison was desired to other central California areas, Brune's (1970) widely used source model for S-waves, extended to P-waves, was applied. The parameters of interest are the seismic moment $M_o = 4\pi R\rho v^3 \Omega_o$, the stress drop $\Delta\sigma = (7/16)M_o/r^3$, fault slip $u = M_o/\pi\rho v_s^2 r^2$, and source radius $r = 2.34\ v/f_o 2\pi$, where R = distance from source to receiver, ρ = density (2.67 g/cc), Ω_o = long period displacement spectral level, f_o = corner frequency and v = velocity of material (4.5 km/sec for v_p, 2.6 km/sec for v_s). Such effects as attenuation, complex propagation path, site response and radiation patterns will affect the spectra, as will the source parameters. If spectra are averaged for many events or stations, these effects will tend to decrease. The approach is no more than a rough estimate, but it provides a basis for comparing earthquakes. In this study the only correction made was for instrument response, and source parameters

were averaged over several stations.

Fourteen events were selected on the basis of magnitude and location within the field. Figure 3-14 shows typical data for P-wave signals recorded analog FM and digitally, and an S-wave recorded digitally. Spectra are shown for the indicated data windows. The events recorded on the FM magnetic tape system were filtered at 50 Hz and digitized at a rate of 200 samples/sec. While the length of P-wave signal used varied with event it was kept constant from station to station for a particular event. Table 3-6 lists the results. In some cases one event was examined at several different locations to determine the effect of propagation path and azimuth. Corner frequency, f_o, was picked by using Q-corrected templates of the function

$$\left[1 + (f/f_o)^{2\delta}\right]^{-1/2} \exp(-\pi f t/Q)$$

for t = 0.5, 1.0, 1.5 sec, Q = 40, 80, 120, 250, 700, = 3, 5, 7 and f_o = 15, 20, 25, 30, 35, 40, 45, 50, 60 Hz. The procedure was to pick the long period level, then fit each spectrum for f_o, Q, and high frequency roll-off, δ. Also listed in Table 3-6 are the results for events recorded on the digital recorder, with both vertical and horizontal geophones. As can be seen in Figure 3-14, showing typical spectra of signals and background noise, the dynamic range is much greater for

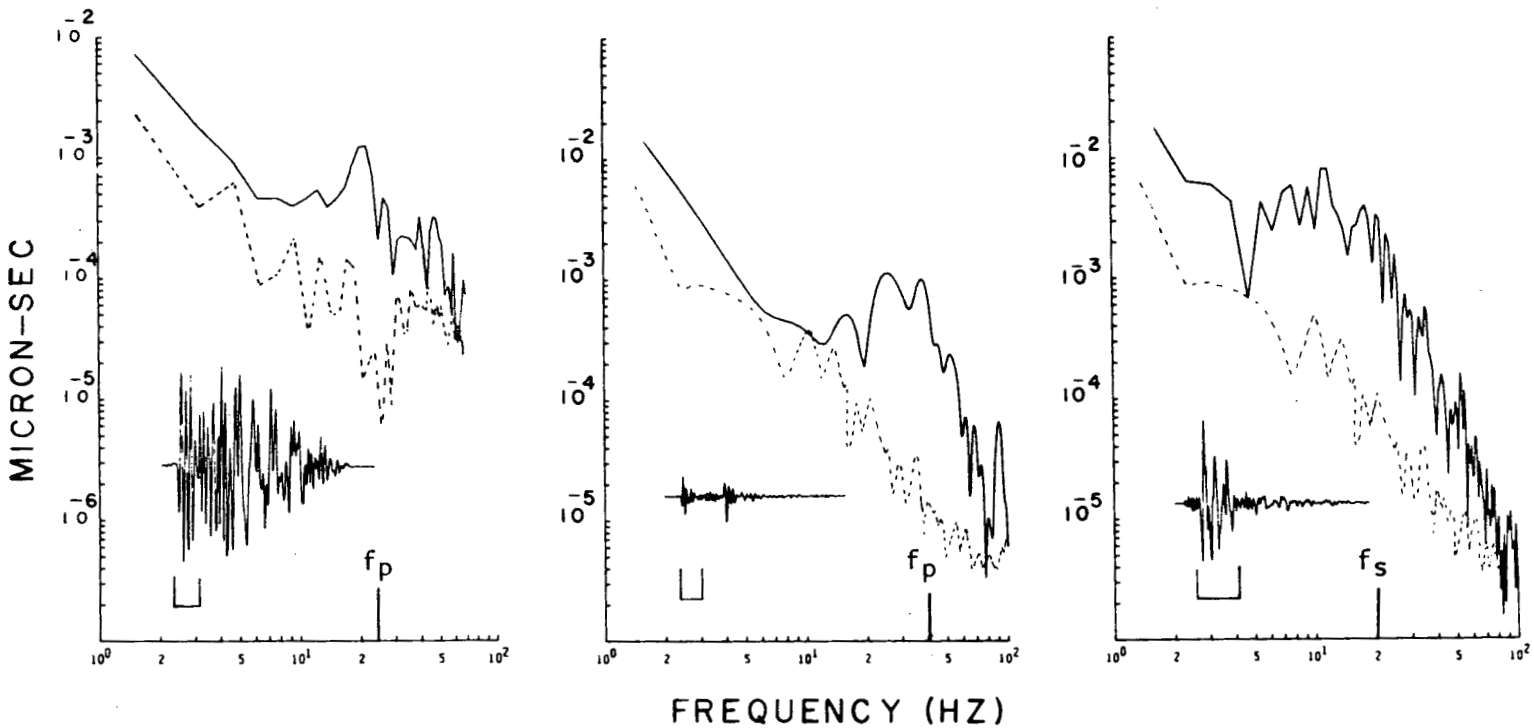

Figure 3-14

Typical displacement spectra used in source studies. On left is P-wave recorded on FM tape system, center is P-wave recorded on digital system, and right is S-wave recorded digitally. FM signal is shown at higher gain than other two. Corner frequencies and data windows are indicated. Note the higher quality data obtained with the digital system.

Table 3-6

a) P-wave Spectral Parameters (Analog FM System)

Event	STA	R (km)	M_o (dyne-cm)	Q	f_o (Hz)	δ	Depth (km)	Δσ (bar)	u (cm)	r (m)
3	7	1.3	1.2×10^{17}	250						
3	11	2.5	1.7×10^{17}	120	25	5	1.2	0.23	2.02×10^{-3}	66
3	12	3.8	1.9×10^{17}	80						
37	7	4.7	1.3×10^{17}	250						
37	3	6.3	3.8×10^{17}		25	3	3.8	0.25	2.27×10^{-3}	66
37	11	4.1	1.5×10^{17}	250						
37	12	4.3	1.3×10^{16}	120						
39	7	3.6	6.4×10^{16}	250						
39	3	5.1	6.1×10^{16}	120	35	3	1.6	0.13	9.32×10^{-3}	47
39	11	2.7	1.6×10^{16}	80						
39	12	3.0	1.3×10^{16}	40						
42	7	3.8	3.4×10^{17}	250						
42	3	3.9	4.1×10^{17}	120						
42	11	4.0	3.5×10^{17}	120	25	5	3.8	0.48	4.32×10^{-3}	66
42	12	4.6	2.7×10^{17}	80						
42	1	8.0	2.6×10^{17}	60						
41	7	3.3	7.8×10^{16}	250						
41	3	4.1	4.8×10^{16}	120	30	3	3.2	0.14	1.01×10^{-3}	55
41	11	3.5	4.6×10^{16}	120						
41	12	4.2	3.7×10^{16}	40						
51	7	3.6	1.4×10^{17}	250						
51	3	4.5	1.7×10^{17}	120						
51	11	3.6	1.5×10^{17}	120	35	5	3.5	0.63	3.46×10^{-3}	47
51	12	4.2	1.3×10^{17}	40						
51	1	8.2	9.7×10^{16}	40						
7	7	4.8	2.0×10^{17}	250	30	7	4.4	0.52	3.89×10^{-3}	55
15	7	2.1	7.9×10^{16}	250	50	5	1.7	0.96	4.27×10^{-3}	33
17	7	1.6	1.0×10^{17}	250	30	7	1.5	0.26	1.94×10^{-3}	55

Table 3-6a
(continued)

Event	STA	R (km)	M_o (dyne-cm)	Q	f_o (Hz)	δ	Depth (km)	Δσ (bar)	u (cm)	r (m)
18	7	1.5	7.9×10^{16}	250	35	3	1.3	0.33	2.11×10^{-3}	47
28	7	3.7	4.0×10^{17}	250	25	5	3.6	0.61	5.41×10^{-3}	66
34	7	1.8	1.3×10^{17}	250	35	5	1.6	0.54	1.75×10^{-3}	47
38	7	3.0	1.0×10^{17}	250	25	7	2.9	0.15	1.35×10^{-3}	66
58	7	4.1	3.2×10^{17}	250	25	5	4.0	0.49	4.32×10^{-3}	66

b) P-Wave Spectral Parameters (Digital System)

$\bar{R}$ = 4.0 km STATION = 7

M_o (dyne-cm)	f_o (Hz)	Δσ (bar)	u (cm)	r (m)
1.6×10^{17}	40	1.02	5.6×10^{-3}	41
3.7×10^{16}	40	0.23	1.3×10^{-3}	41
2.1×10^{17}	20	0.17	1.8×10^{-3}	82
2.1×10^{17}	20	0.17	1.8×10^{-3}	82
1.6×10^{17}	25	0.24	2.2×10^{-3}	66
2.6×10^{16}	35	0.19	6.9×10^{-4}	47
8.5×10^{16}	40	0.54	2.9×10^{-3}	41
6.3×10^{16}	40	0.40	2.2×10^{-3}	41
8.5×10^{16}	35	0.36	2.3×10^{-3}	47
2.4×10^{16}	40	0.15	8.4×10^{-4}	41
5.3×10^{16}	40	0.33	1.9×10^{-3}	41

Table 3-6 (continued)

c) S-Wave spectral Parameters (Digital System)

$\bar{R}$ = 4.0 km STATION = 7

M_L	M_o (dyne-cm)	f_o (Hz)	$\Delta\sigma$ (bar)	u (cm)	r (m)
0.6	4.1×10^{16}	25	3.0×10^{-1}	4.8×10^{-3}	38
0.3	1.2×10^{16}	25	9.2×10^{-2}	1.4×10^{-3}	38
0.9	7.1×10^{16}	25	5.4×10^{-1}	8.4×10^{-3}	38
0.5	2.0×10^{16}	25	1.5×10^{-1}	2.4×10^{-3}	38
0.4	1.6×10^{16}	25	1.2×10^{-1}	1.9×10^{-3}	38
1.6	1.2×10^{18}	35	2.5×10^{1}	2.8×10^{-1}	27
1.6	4.1×10^{17}	20	1.5×10^{0}	3.1×10^{-2}	48
0.9	6.1×10^{16}	25	4.6×10^{-1}	7.2×10^{-3}	38
0.4	2.0×10^{16}	25	1.5×10^{-1}	2.4×10^{-3}	38
0.5	2.0×10^{16}	30	2.6×10^{-1}	3.4×10^{-3}	32
1.4	3.0×10^{17}	25	2.3×10^{0}	3.6×10^{-2}	38
0.8	1.2×10^{17}	15	2.0×10^{-1}	5.2×10^{-3}	64
1.1	1.8×10^{17}	25	1.3×10^{0}	2.1×10^{-2}	38
0.4	3.0×10^{16}	25	2.3×10^{-1}	3.6×10^{-3}	38
0.3	1.4×10^{16}	20	5.5×10^{-2}	1.0×10^{-3}	48
0.2	1.8×10^{16}	25	1.3×10^{-1}	2.1×10^{-3}	38
0.6	6.1×10^{16}	20	2.3×10^{-1}	4.6×10^{-3}	48
1.1	1.2×10^{17}	25	9.2×10^{-1}	1.4×10^{-2}	38
0.3	2.0×10^{16}	25	1.5×10^{-1}	2.4×10^{-3}	38
0.0	2.4×10^{15}	15	4.0×10^{-3}	1.0×10^{-4}	64
0.3	1.8×10^{16}	20	7.1×10^{-2}	1.4×10^{-3}	48

Table 3-6 (continued)

M_L	M_o	f_o	$\Delta\sigma$	u	r
1.4	3.0×10^{17}	20	1.1×10^{0}	2.3×10^{-2}	48
0.5	3.2×10^{16}	25	2.4×10^{-1}	3.8×10^{-3}	38
0.6	4.1×10^{16}	25	3.0×10^{-1}	4.8×10^{-3}	38
0.4	2.0×10^{16}	20	7.9×10^{-2}	1.5×10^{-3}	48
0.6	6.1×10^{16}	15	1.0×10^{-1}	2.6×10^{-3}	64
0.4	4.1×10^{16}	20	1.5×10^{-1}	3.1×10^{-3}	48
1.1	4.1×10^{17}	15	6.6×10^{-1}	1.7×10^{-2}	64
0.4	3.0×10^{16}	25	2.3×10^{-1}	3.6×10^{-3}	38
1.3	3.0×10^{17}	15	5.0×10^{-1}	1.3×10^{-2}	64
1.2	1.8×10^{17}	20	7.1×10^{-1}	1.4×10^{-2}	48
0.2	1.2×10^{16}	20	4.7×10^{-2}	9.3×10^{-4}	48
0.1	9.2×10^{15}	20	3.5×10^{-2}	6.9×10^{-4}	48
1.7	1.2×10^{18}	15	2.0×10^{0}	5.2×10^{-2}	64
0.4	3.0×10^{16}	25	2.3×10^{-1}	3.6×10^{-3}	38
0.6	4.1×10^{16}	30	5.3×10^{-1}	6.9×10^{-3}	32
1.4	2.4×10^{17}	20	9.4×10^{-1}	1.8×10^{-2}	48
0.5	4.1×10^{16}	25	3.0×10^{-1}	4.8×10^{-3}	38
0.6	4.1×10^{16}	20	1.5×10^{-1}	3.1×10^{-3}	48
0.2	1.6×10^{16}	30	2.1×10^{-1}	2.8×10^{-3}	32
0.3	1.8×10^{16}	25	1.3×10^{-1}	2.1×10^{-3}	38
0.5	3.0×10^{16}	25	2.3×10^{-1}	3.6×10^{-3}	38
0.5	1.6×10^{17}	20	6.3×10^{-1}	1.2×10^{-2}	48
0.4	1.8×10^{16}	25	1.3×10^{-1}	2.1×10^{-3}	38
0.1	1.4×10^{16}	25	1.0×10^{-1}	1.7×10^{-3}	38

Table 3-6 (continued)

M_L	M_o	f_o	$\Delta\sigma$	u	r
0.5	5.1×10^{16}	25	3.8×10^{-1}	6.0×10^{-3}	38
0.6	7.1×10^{16}	25	5.4×10^{-1}	8.4×10^{-3}	38
1.0	1.8×10^{17}	20	7.1×10^{-1}	1.4×10^{-2}	48
0.2	5.1×10^{15}	35	1.0×10^{-1}	1.1×10^{-3}	27
0.7	8.1×10^{16}	25	6.1×10^{-1}	9.7×10^{-3}	38
0.3	1.5×10^{16}	30	2.0×10^{-1}	2.6×10^{-3}	32
1.2	2.0×10^{17}	15	3.3×10^{-1}	8.7×10^{-3}	64
0.4	1.6×10^{16}	25	1.2×10^{-1}	1.9×10^{-3}	38
0.4	1.4×10^{16}	30	1.8×10^{-1}	2.4×10^{-3}	32
1.8	1.6×10^{18}	10	7.9×10^{-1}	3.1×10^{-2}	96
0.3	1.4×10^{16}	25	1.0×10^{-1}	1.7×10^{-3}	38
0.3	1.4×10^{16}	25	1.0×10^{-1}	1.7×10^{-3}	38
0.7	7.1×10^{16}	25	5.4×10^{-1}	8.4×10^{-3}	38
0.7	1.0×10^{17}	15	1.6×10^{-1}	4.3×10^{-3}	64
0.3	1.8×10^{16}	25	1.3×10^{-1}	2.1×10^{-3}	38
0.7	5.1×10^{16}	25	3.8×10^{-1}	6.0×10^{-3}	38
0.5	3.0×10^{16}	30	4.0×10^{-1}	5.2×10^{-3}	32
0.2	1.0×10^{16}	25	7.7×10^{-2}	1.2×10^{-3}	38
0.5	3.0×10^{16}	15	5.0×10^{-2}	1.3×10^{-3}	64
0.6	3.0×10^{16}	25	2.3×10^{-1}	3.6×10^{-3}	38
0.5	5.1×10^{16}	15	8.3×10^{-2}	2.1×10^{-3}	64
0.4	3.2×10^{16}	30	4.2×10^{-1}	5.5×10^{-3}	32
0.9	1.8×10^{18}	15	3.0×10^{-1}	7.8×10^{-3}	64
1.8	1.2×10^{18}	25	9.2×10^{0}	1.4×10^{-1}	38
1.1	1.6×10^{17}	25	1.2×10^{0}	1.9×10^{-2}	38

Table 3-6 (continued)

M_L	M_o	f_o	$\Delta\sigma$	u	r
.8	6.1×10^{16}	25	4.6×10^{-1}	7.2×10^{-3}	38
1.0	1.4×10^{17}	20	5.5×10^{-1}	1.0×10^{-2}	48
0.8	1.2×10^{17}	15	2.0×10^{-1}	5.2×10^{-3}	64
0.1	8.1×10^{15}	30	1.0×10^{01}	1.4×10^{-3}	32
0.8	1.2×10^{17}	20	3.9×10^{-1}	7.7×10^{-3}	48
1.3	3.0×10^{17}	25	2.3×10^{0}	3.6×10^{-2}	38
1.5	5.1×10^{17}	20	1.9×10^{0}	3.8×10^{-2}	48
0.9	1.2×10^{17}	20	4.7×10^{-1}	9.3×10^{-3}	48
1.3	2.0×10^{17}	15	3.3×10^{-1}	8.7×10^{-3}	64
0.7	1.0×10^{17}	20	3.9×10^{-1}	7.7×10^{-3}	48
1.2	3.0×10^{17}	20	1.1×10^{0}	2.3×10^{-2}	48
1.0	1.4×10^{17}	20	5.5×10^{-1}	1.0×10^{-2}	48
1.2	2.0×10^{17}	20	7.9×10^{-1}	1.5×10^{-2}	48
0.4	1.6×10^{16}	25	1.2×10^{-1}	1.9×10^{-3}	38
0.9	1.0×10^{17}	20	3.9×10^{-1}	7.7×10^{-3}	48
0.0	4.1×10^{15}	35	8.4×10^{-2}	9.5×10^{-4}	27
1.7	1.0×10^{18}	15	1.6×10^{0}	4.3×10^{-2}	64
0.8	8.1×10^{16}	25	6.1×10^{-1}	9.7×10^{-3}	38
0.7	8.1×10^{16}	26	6.1×10^{-1}	9.7×10^{-3}	38
0.6	5.1×10^{16}	15	8.3×10^{-2}	2.1×10^{-3}	64
0.2	7.1×10^{15}	20	2.7×10^{-2}	5.4×10^{-4}	48
0.1	5.1×10^{15}	25	3.8×10^{-2}	6.0×10^{-4}	38
0.5	4.1×10^{16}	10	1.9×10^{-2}	7.7×10^{-4}	96
0.4	3.0×10^{16}	15	5.0×10^{-2}	1.3×10^{-3}	64
0.2	1.2×10^{16}	25	9.2×10^{-2}	1.4×10^{-3}	38

Table 3-6 (continued)

M_L	M_o	f_o	$\Delta\sigma$	u	r
0.2	8.1×10^{15}	25	6.1×10^{-2}	9.7×10^{-4}	38
0.2	1.2×10^{16}	25	9.2×10^{-2}	1.4×10^{-3}	38
0.6	5.1×10^{16}	25	3.8×10^{-1}	6.0×10^{-3}	38

the events recorded on the digital recorder than on the FM analog tape system.

Figure 3-15 is a plot of moment versus magnitude for M_{CL}, M_{CB} and M_L. As for b-values, the choice of magnitude alters the results significantly. The results obtained for this study are:

$$\text{Log}_{10}\ (M_o) = (17.3 \pm 0.1) + (0.8 \pm 0.3)\quad M_{CL}$$

$$\text{Log}_{10}\ (M_o) = (16.2 \pm 0.3) + (1.9 \pm 0.7)\quad M_{CB}$$

$$\text{Log}_{10}\ (M_o) = (15.9 \pm 0.03) + (1.3 \pm 0.04)\ M_L$$

Results from other central California studies of M_o versus M_L are:

Bakun and Bufe (1975), San Andreas

$$3.5 < M_L < 5$$

$$1 < M_{CL} < 3.5$$

$$\text{Log}_{10}\ (M_o) = (16.2 \pm 0.1) + (1.52 \pm 0.05)\quad M$$

Bakun and Lindh (1977), Oroville, California

$$17 < \text{Log}_{10}\ (M_o) < 25$$

$$\text{Log}_{10}\ (M_o) = (17.02 \pm 0.07) + (1.21 \pm 0.03)\quad M_L$$

Johnson and McEvilly (1974), San Andreas

$$M_L > 2$$

$$\text{Log}_{10}\ (M_o) = (17.60 \pm 0.28) + (1.16 \pm 0.06)\quad M_L$$

Figure 3-15

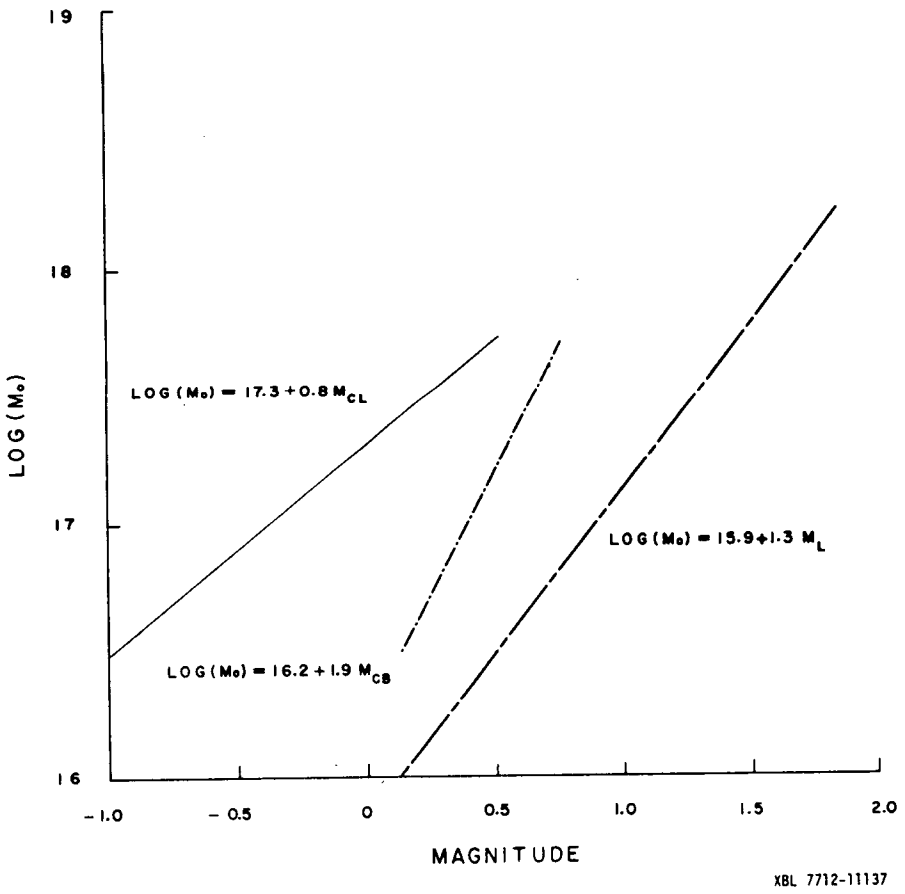

Moment - magnitude relations for Geysers microearthquakes, using the three different magnitudes. M_{CL} and M_{CB} data from Tables 4 and 6a, M_L data from Table 6c.

Thatcher and Hanks (1972), Southern California

$$\text{Log}_{10}\ (M_o) = 16.0 + 1.5\ M_L$$

Wyss and Brune (1968), Parkfield, California

$$\text{Log}_{10}\ (M_o) = 17.0 + 1.4\ M_L$$

From these results it appears that The Geysers events are only slightly unusual if the M_L magnitude is used, i.e., for a given M_L, M_o is smaller than for other relations. However, if M_{CB} or M_{CL} is used, anomalous situations exist due to the smaller and larger, respectively, ranges of magnitudes represented by the earthquake set, relative to the range on M_L. Comparing the M_o = M_{CL} relation for The Geysers with that of Bakun and Bufe (1975) above, based primarily on M_{CL} for central California earthquakes on the San Andreas fault zone, illustrates the anomaly. In view of the fact that larger events ($\geq$2.5) have occurred in the field region and that the M_L magnitudes from the equivalent Wood-Anderson seismograms produce relatively normal b-values and M_o relations, it seems that these earthquakes are not very unusual compared to other central California events in relation to moment and magnitude. Rather, the strange coda magnitude results may reflect locally anomalous propagation characteristics.

Corner frequencies are roughly independent of magnitude and moment, implying increasing stress drop

with event size if corner frequency is not controlled by Q. However, when a particular event is examined at several different stations, to maintain the same corner frequency requires varying Q. Implied Q values, relative to station 7, are given in Table 3-6a. In general, Q decreases for stations on the edge or outside of the field, consistent with Q estimates from explosion amplitudes. Table 3-6a also lists the depths of the events. It was thought that earthquakes beneath the production zone ($h > 3$ km) might exhibit lower corner frequencies (lower Q) than shallow events. Although the highest corner frequency obtained was for a shallow event ($h = 1.7$ km, $f_o = 50$ Hz), there seems to be little correlation between source depth and corner frequency. The Q distribution implied by constraining f_o to be constant at all stations for an event is generally the same as that indicated by the explosion data; i.e., high in the center of the field, decreasing towards the edges and lowest outside the major production zone. No variation with depth can be established.

As can be seen from Table 3-6 the moments are similar for the P-wave and S-wave spectra. However, as is normally observed, the high frequency content is less in the S-wave spectra than for P-waves. Because of the limited instrumentation, no events were recorded with both vertical and horizontal components so that a comparison of Q_p and Q_s could not be made. The S-wave

data recorded on the horizontal geophones were thus used only for moment and magnitude determinations and not for a regional Q_S analysis as was done for P-waves.

The majority of events had high frequency spectral slopes, δ, of 3 to 5 and sometimes 7. The corner frequency and high frequency slope depend on the source time function as well as the source dimensions. The smoother the source function the greater the high frequency roll-off. A source time function that is relatively smooth in beginning (many continuous time derivatives) and ending would produce a much more rapid roll-off than either a sharp explosion or a "chattering" or step-like rupture.

Source function rise-time information, if available in the spectrum, may be useful in determining the materials that are rupturing, the nature of rupture and the state of stress, as well as the source dimensions. Unfortunately, the effects of attenuation are extremely severe at the higher frequencies and they are almost impossible to remove accurately.

3.6 Interpretation

3.6.1 Summary of Observations

The significant points observed are:

I. Microearthquakes

(1) High level of activity $0 < M_L < 2$ at 25-30 events/day

(2) Distribution in space and time:

(a) lack of events in known steam zones

(b) lack of events in original production areas around generating units 1 and 2

(c) shallow events, < 5 km

(d) no dominant throughgoing faults defined

(e) no systematic patterns to occurrence in space a time

(f) slightly higher than normal b-value, using M_L

(3) Spectral characteristics

(a) slightly anomalous M_o versus M_L relation

(b) high corner frequencies, no relation to M_o

(c) f_o for P-waves greater than for S-waves

(d) no relation between f_o and depth

(4) Fault plane solutions consistent with regional stress

II. Velocity Data

(1) Shallow high velocity zone in production region only

(2) Deeper broad lower velocity zone extending out of production zone

(3) Low Poisson's Ratio in production zone

III. Attenuation Data

(1) Shallow high Q zone in production zone from explosions and microearthquakes

(2) Deeper lower Q zone from explosions

3.6.2 Microearthquakes

Seismologically, the significant aspects of the reservoir model are: (1) it is a maximum enthalpy system which implies limited permeability, and it is probably extensively fractured with interconnected parts; (2) it is low pressure and relatively constant temperature; (3) the recharge is limited; and, (4) it may be expanding at a rate which is controlled by porosity, permeability and net discharge.

From the concept of differential pressure, one would expect microearthquakes to occur where high pore pressures reduce the strength of the materials. The observed locations of microearthquakes are on the margins of the production zone (above and below), where the model would predict the highest pore pressures. Activity is very low, however, above and below the older production zones. This would seem to imply that the steam source recharge for the older production zone is mainly flow from the surrounding reservoir, rather from ground water recharge above and below. The temporal occurrence of microearthquakes suggests also an interconnected geothermal system. The events are random in time as well as space, and occur without regard to one another, i.e., they do not seem to migrate from one end of the field to the other. The spatial occurrence suggests no dominant throughgoing faults. On the other hand, the

primary cause of the microearthquakes may simply be due to the intense fracturing of the region with the pressure differential acting as a catalyst along a series of small faults.

The historical data are not sufficient to show that the microearthquakes are migrating with an expanding reservoir. However, the limited data available suggest the rate of seismicity is increasing. Lange and Westphal (1969) detected a rate of 4 events/day in the fall of 1968. Hamilton and Muffler (1972) recorded a rate of 2-3 events/day in the spring of 1971. Power generation rate in the fall of 1968 is not available, but it was 82 Mw when Hamilton and Muffler carried out their study. The power generation rate at the time of this study was 550 Mw or about 7 times the 1971 rate. The microearthquake activity during this study was 25-30 events/day or about ten times the rates observed in previous studies. As this study was conducted in a different manner from previous studies, and because of the short sampling times, it would be difficult to conclude firmly, solely on the basis of occurrence data, that the microearthquake activity is related to steam withdrawal.

The higher than regional b-value may indicate anomalous stress within the microearthquake region. Studies on microfracturing of rock (Scholz , 1968, Wyss, 1973) have found that b-values depend primarily

on the state of stress and to a lesser extent on the physical properties of the rock. Scholz found that in a low stress state energy was released in small events, resulting in high b-values. This was particularly true of ductile and high porosity rocks. He also noted that small magnitude events occur in material where crack closing and sliding are important, with the larger events occurring in situations where new fractures are propagating.

With respect to principal stress directions, The Geysers events are not anomalous compared to regional stresses. Almost all events exhibited strike-slip or dip-slip faulting with the principal compressive stresses in the northeast-southwest direction. It seems plausible that the direction of failure is controlled by regional stress while the rate of failure is controlled by local stress levels.

Another possible factor controlling microearthquakes may be thermally induced differential expansion between water in isolated voids and the rock matrix (Knapp and Knight, 1977). This is attractive from several points of view, the first being that earthquakes would be expected to occur where the permeability is low and the temperature gradient is high, at the edges of the reservoir. For this mechanism to apply, the fracture must coalesce simultaneously over an area of several m^2, in

order to produce an event of detectable size. Knapp and Knight calculate that, if all the pores fracture at once in a cubic meter of rock with porosity 1%, a zero magnitude event would result. This is ideal, while in reality only selected pores fracture, those with preferential orientation with respect to the maximum principal stress. The differential expansion may only act as a triggering mechanism for formation of a small fault surface. The maximum size of an event would be limited by the scale of variations in rock permeability, porosity and available heat. Such a failure model would explain an apparent upper magnitude threshold and the higher than regional b-value. Differential expansion is also consistent with the observed fault plane solutions. The model predicts that, with a sufficient increase in temperature, the effective pressure becomes equal to the strength of the rock, resulting in fracture in the direction of maximum principal stress, which in this case would cause strike-slip faulting, as observed. It thus seems the different permeabilities and porosities as well as heat content at The Geysers may be reflected in the occurrence of microearthquakes in space and time.

To associate volume changes due to fluid withdrawal with the occurrence of microearthquakes, McGarr's (1976) hypothesis between volume change and seismic moment can be applied, $\xi Mo = h\mu|\Delta V|$, McGarr theorized that the volumetric moment, approximately, $h\mu|\Delta V|$, is a measure

of the amount of seismic failure in response to shear stresses induced by volume change (where μ = shear modulus, $|\Delta V|$ = volume change). Several examples support his theory; volume changes in mining operations, volume changes due to fluid injection (Denver earthquakes), and volume changes associated with uplift, (Matsushiro, Japan). An independent estimation of ΔV at The Geysers involves the amount of fluid withdrawn, less groundwater recharge and fluid reinjection. This can be compared to the calculated ΔV from the summed moments of the observed seismicity, 1.5×10^{21} to 10^{22} dyne-cm/year, depending on the occurrence of magnitude 3 events. Solving for ΔV, the larger value (10^{22}), implies ΔV of 0.5×10^{11} cm^3/year, the total volume change necessary to accomplish the observed seismicity, assuming McGarr's model of earthquake genesis.

The volume of fluid withdrawn can be calculated from the power generation. At a capacity of 550,000 kw, using a steam rate of 10 kg/kwhr and a specific volume of water of 1.2 cm^3/g, the ΔV for 1 year is 5×10^{13} cm^3, some 10^3 times greater than the ΔV calculated from the seismicity rate. In other words, McGarr's hypothesis would predict a much higher level of seismicity if the total ΔV was consumed by seismic failure. However, the actual ΔV available for earthquake generation is much smaller due to ground water recharge and reinjection. A recharge rate equal to discharge would imply no volume

change or microearthquakes. (This may explain why seismicity does not change with withdrawal rate in a hot water dominated reservoir that is in hydrostatic equilibrium (Helgeson 1968, Combs 1976).) Recharge, however, is not instantaneous, nor would one expect the volume change from seismic failure to equal the net volume of water withdrawn. The seismicity may reflect volumetric change in the reservoir and, if so, the microearthquakes would indicate the regions of expansion of the vapor dominated zone. Temporal change in the spatial pattern of seismicity may occur too slowly to be of practical use. Cessation of events on the edge of the reservoir may indicate an equilibrium situation where the recharge rate is equal to the discharge or that the reservoir has expanded to the point where it has been extended beyond a heat source that is sufficient to produce vaporization of available water.

Whether the withdrawal of steam and associated volumetric change is the primary cause of microearthquakes in The Geysers is not certain. In an environment that is as hydrologically active as The Geysers, and because of the intimate relation between fluids and faulting (Hubbert and Ruby 1959, Nur 1973), it is difficult to believe that fluid withdrawal would not be a contricuting factor. However, only as production increases and expands to areas that are now seismically

inactive will definite evidence exist, one way or another, that the fluid withdrawal is inducing the microearthquakes. Positive correlation opens a new methodology for reservoir modeling.

Another failure mechanism which may influence microearthquake activity is "stick-slip" (Brace and Byerlee 1966) in which the motion occurs in a series of discrete rapid slips. In general, stick-slip is enhanced by high pressure or normal stresses, low temperature, the presence of strong brittle materials such as feldspars and quartz, the absence of gouge and lower surface roughness. At higher confining pressures the dominant factory controlling friction strength is effective pressure (Stesky, 1977).

In The Geysers reservoir where the temperature is high, pressure is low and brittle material is possibly absent, stick-slip would not be expected to occur. At the reservoir edges where pressures are higher, temperatures are lower, with possible embrittlement due to dehydration (Heard and Ruby, 1965; Raleigh and Paterson, 1965), one would expect stick-slip behavior more readily. The lack of deep events would, in the context of stick-slip earthquakes, imply elevated temperatures beneath the reservoir, (4-5 km).

The moment versus magnitude relation for The Geysers may be anomalous with respect to other central California

regions. Using $\text{Log}_{10} M_o = (15.9 \pm 0.03) + (1.3 \pm 0.04) M_L$ as the most reasonable relation, the zero-magnitude moment is low compared to other central California earthquakes. In terms of the seismic waves, for a given moment (low frequency relation), the amplitude used to determine the magnitude (higher frequency radiation) is larger than for other regions. This is consistent with the high Q observation, but it may indicate different source effects. It is difficult to separate source and path effects without dense station coverage.

An indication that source information may be masked by path effects is found in the differences between P-wave and S-wave corner frequencies. On the average, the P-wave corner frequencies, f_p, were around 30 Hz, and the S-wave corner frequencies, f_s, about 20 Hz. Assuming fault propagation at a finite rupture velocity controls the observed corner frequencies and that the rupture velocity is less than the S-wave velocity, then consistent observation of $f_p > f_s$ are incompatible with the fault model. In fact, if the fault can be modeled as a long, narrow crack propagating unilaterally, we should observe $f_s > f_p$ over half the radiation pattern. A plausible explanation of observation to the contrary, is the effect of attenuation along the propagation path. A value of Q_s 1/3 to 1/2 that of Q_p would be adequate to produce the observed corner frequencies. If we assume

the actual value of f_s at 40 Hz, and that it has been reduced by attenuation to 20 Hz for a travel time, t, of 1.5 seconds for the S-wave, the Q required for the reduction in f_s can be computed from $Q = t/t^*$. $f_s t^*$ of 0.5 is approximately correct for a factor of two reduction in apparent corner frequency (Johnson and McEvilly, 1974, Figure 5).

The resulting Q_s of 120 is consistent with the Q_p estimation within the field. This illustrates the extreme difficulty that exists in recovering source parameters such as stress drop or dimensions from microearthquake spectra, even at a distance of 5 km or less.

From the S-wave corner frequencies, calculated stress drops were between 0.1 and 3.0 bar. Because a large number of events at varying azimuths were analyzed, the spectral characteristics are probably representative estimates for the field. The relatively constant values of corner frequency may be indicative of path effect (Q controlled), rather than source effects (time function or dimensions). The larger moment events generally occurred deeper in the field than did smaller events. Assuming uniform detection capability with depth, the larger events would be occurring at depths where the largest pressure differences exist between hydrostatic and the reservoir. The constant corner frequencies can be interpreted as a uniform source dimension of about

50 meters. In a low pressure reservoir with constant permeability and porosity, one would expect uniform source dimensions. Elsewhere in central California, foci are distributed evenly without much correlation between depth and magnitude to depths of 10 to 12 kilometers (McNally, 1976). The fact that earthquakes in The Geysers do not occur deeper than 4 or 5 kilometers is strong evidence for close association with the geothermal system.

3.6.3 Velocities

Lower than normal Poisson's Ratios within the production zone, shown by the microearthquake data, may indicate partial saturation of reservoir rocks. Toksoz, Cheng and Timur (1976) found that the amount of gas present affected P- and S-wave velocities. Even a small amount of gas as an immiscible mixture in a brine was found to reduce the compressional wave velocity, V_p, the net effect being a reduced Poisson's Ratio. Nur and Simmons (1969) observed that V_p decreased with decreasing water saturation in low porosity rocks. Both studies would predict the observed low Poisson's Ratio for a vapor dominated reservoir.

As can be seen in Figure 3-4, there is a P-wave advance (higher velocity) throughout the production zone for shallow propagating waves from the near explosion. For deeper waves from the far explosion, the P-wave

velocity is lower, as would be expected within a vapor zone. However, the reduced P-wave velocity is observed over a broad area, much broader than the present production zone. If the presence of steam is controlling the velocity, it would seem that the reservoir is more extensive than generally thought. The true cause of the P-wave velocity variation is probably structural. A 0.3 second P-wave advance, observed in a Nevada hot springs environment, was clearly due to silica deposition in valley sediments around the hot spring (Beyer, et al., 1976). A similar explanation in terms of compositional differences may apply in The Geysers area. Iyer and Hitchcock (1975) observed P-wave delays throughout much of the Clear Lake/Geysers region and attributed it to a heat source beneath the area. The P-waves from the distant explosion may have been affected by this deeper lower velocity material. Because of the low pressures involved, it is difficult to estimate the temperatures necessary to account for a 10% to 20% velocity decrease. Birch (1975) gives velocity changes of -4×10^{-5} and -6×10^{-5} per degree C in granites and gabbros, respectively. Lin (1977) found -6×10^{-4} per degree C for graywacke at pressures greater than 4 kilobars. For lower pressures the effect would be greater, but it is difficult to extrapolate to pressures at The Geysers. Lin also found graywacke velocities at room temperature and pressure

to vary from 4.8 to 5.7 km/sec with increasing metamorphism. Murase and McBirney (1973) found that for common igneous rocks at 1 bar there was no change in seismic velocities below 600°C. The nonlinear nature of the temperature effect adds further uncertainty. Assuming the dominant material underlying The Geysers to be Franciscan Graywacke with a temperature coefficient for P-wave velocity of -1×10^{-3} /°C, then a 15% decrease in velocity at 3 km depth would imply a temperature increase from 100°C to 850°C. A similar large temperature increase would be required for igneous rocks. It is thus difficult to explain a broad low velocity zone beneath The Geysers by a temperature increase alone.

It appears effects of high temperature, degree of water saturation and the compositional change within the hydrothermal region are combined in producing the observed velocity variations. Detailed studies utilizing distant sources and near vertical propagation through sections will shed light on the regional velocity structure. Results of this study are clear, however, in the fact that the producing reservoir is characterized by detectably anomalous seismic wave velocities.

3.6.4 Attenuation

The observed attenuation differences may reflect variations in shallow structure and topography throughout the geothermal field and at reference stations. In a

finite element simulation of a 20^{o} slope, Smith (1975) found that the maximum spectral ratio enhancement was a factor of two at the peak. Data for The Geysers show a factor of 10-20 difference, with little correlation to topography. It is also well known that near-surface effects such as thick low velocity alluvium can cause amplification. The degree of enhancement is proportional to the contrast in acoustic impedance, and frequencies of the spectral peaks are roughly multiples of the travel time through the surficial layer. There is no evidence for anomalously low velocity shallow materials. For 2 km/sec, the thickness required for enhancement in the 5-10 Hz range would be 100-200 meters. More restrictive, the underlying material would have to be unreasonably high velocity for significant enhancement. Further, the instrument locations were selected to avoid obvious alluvium or landslide surfaces. It is conceivable that bizarre geometrical effects in propagation paths could produce the observed amplitudes. If the actual structure deviates greatly from the model assumed for reducing the data, the observed amplitudes could reflect focusing. However, the uniformity and spatial extent of the high-Q region argues against such mechanisms. In the formula used for Q estimation, errors in the distance or velocity would need to be an order of magnitude, which is unlikely, to explain the variations. Therefore, the most plausible

explanation for the observed amplitude variations is real differences in Q throughout the field.

Johnson et al. (1977) have shown that Q is a function of confining pressure and saturation. They found that Q (both P and S) for dry rocks is initially higher and increases much more rapidly with confining pressure than for rocks containing pore water. The effect was attributed to friction and crack closure in the material. Gardner (1964) also showed that Q, as a function of water content alone, increased as the water content decreased. In a theoretical study, White (1975) computed compressional and shear wave velocity and attenuation for partially gas saturated porous rocks. He concluded that for compressional waves the pressure gradients created by a wave traveling through a rock will cause flow of the fluid relative to the rock skeleton and result in attenuation. If the pore-rock matrix is homogenous the pressure gradients will be small and the attenuation due to fluid flow will also be small. However, if the rock has mixed saturation such as pockets of gas or partial gas saturation, then the pressure gradients are higher near the inhomogeneities and the loss of energy due to fluid flow will be significant. These effects could explain the shallow high Q zone and the deeper low Q zone at The Geysers. As postulated earlier (Weres et al., 1977), the reservoir may be characterized by a relatively shallow region

where the pores are vapor-dominated. In this region the behavior described by Johnson et al., (1977) and Gardner (1964) may prevail to produce higher Q. Deeper within the reservoir there may be sufficient water for attenuation due to the fluid-flow mechanism of White (1975), thus resulting in the lower Q values.

On the other hand, the degree of pore water saturation has opposite effects on P-wave velocity and attenuation. Our data indicate decreases with depth for both parameters within the reservoir, suggesting that water content cannot be the controlling factor for both velocity and attenuation. As for velocity, it would appear that low pressure, temperature and compositional heterogeneity may contribute, along with water content, to the anomalous attenuation. Temperature effects on attenuation at low pressures, however, can be nonlinear and unpredictable.

3.7 Conclusions

In terms of regional central California properties, The Geysers area is anomalous to some degree in terms of earthquake occurrence, source parameters seismic wave velocities, and attenuation properties of the reservoir rocks. Microearthquakes, while distributed diffusely, seem to outline the edge of the production zone. Depths are less than 5 km. Mechanisms are consistent with

NE-SW compressive stress, but no throughgoing faults are indicated. Earthquake occurrence rate suggests a slightly higher than normal b-value, or a seismicity rich in lower magnitude shocks relative to larger events. Both P- and S-wave velocities are higher than regional values in the shallow reservoir, the S-wave velocity, from the low Poisson's Ratio , more anomalous than P. Attenuation is low where velocities are high. There is indication that velocity and attenuation become less anomalous deeper in the field. The anomalous source parameters, low seismic moment for a given magnitude, may be merely a reflection of low attenuation.

It is unfortunately the case that it cannot be said whether these anomalies were present previous to production. The limited observations, along with proposed reservoir models, are consistent with a hypothesis in which the anomalous characteristics are closely related to reservoir depletion. It would be of great value to have such data for a potential geothermal field prior to exploitation.

The microearthquakes may relate to large pressure or temperature gradients, or to volume changes associated with fluid removal. If so, the distribution may delineate the boundary of the steam zone. In several reservoir models, this boundary is dynamic, driven by exploitation of the field, and the resulting seismicity offers promise for monitoring the steam zone config-

uration.

Source parameters based on high frequency radiation of P- and S-waves, such as fault propagation and dimensions, source rise time and stress drop, suffer in estimation from the high corner frequencies associated with these small events. Even at observation distances of only 5 km or less and with the high Q values seen in the field, attenuation may mask earthquake spectral details at frequencies above 20-30 Hz. Fault plane solutions, based on first motions, generally reflect response to NE-SW compression. More detailed studies may provide information on the fracture mechanisms involved at the field margins.

Anomalously high P- and S-wave velocities and attenuation characterize the production zone. Extrapolation to in-situ reservoir properties from laboratory and theoretical studies on similar rock types is difficult, thus the mechanisms for the anomalies are not clear. Pressure, temperature, vapor-domination and chemical alteration must be involved to various degrees.

Clearly the experiment shows that seismological data taken today are useful in delineating the present production zone of The Geysers. Further, the data may offer a means of monitoring the reservoir configuration and properties as it changes through exploitation. It is not clear, however, that the same situation would

have prevailed prior to major production of the field, i.e., that the same seismological measurements would have been successful at The Geysers in an exploration context.

CHAPTER 4

SEISMOLOGICAL INVESTIGATIONS IN A HIGH HEAT FLOW REGION - NORTHERN NEVADA

4.1 Introduction

Although it is doubtful that a resource the quality of The Geysers exists in Northern Nevada, there is a strong possibility of a lower grade (150°-200°C) hot water resource. Because of the large area over which such hot water resources may occur, their contribution as an alternative energy source may potentially be as great as The Geysers.

North central Nevada is characterized by high average heat flow of 3.0 hfu (10^{-6} cal/cm^2 sec) (Lachenbruch and Sass, 1977) and extensional Basin and Range tectonics (Thompson and Burke, 1974). Except for numerous small hot springs, there are no other indications as to where one would expect a usable geothermal resource to occur. There is almost no correlation between hot springs, regional heat flow and recent volcanism (Wilson and Paul, 1965). For these reasons, an efficient method is needed to delineate and evaluate the geothermal potential of Basin and Range structure.

4.2 Geological Setting

The three valleys of interest in this study, Buffalo, Grass, and Buena Vista, are graben-like structures with

the major bounding faults striking north-northeast. The basement complex is composed of Paleozoic siliceous clastic rocks and greenstones (Beyer et al., 1976). Intruded into the bedrock are Triassic and Cretaceous granites. Evidence of early overthrusting is found in the Sonoma and Tobin Ranges where Paloezoic rocks are in thrust fault contact with Triassic siliceous clastic and carbonate rocks. An idealized cross section of Grass Valley is shown in Figure 4-2.

The youngest volcanics in this region are basaltic rocks whose ages vary from 14.5 to 11.5 million years. These rocks cap the Tertiary sedimentary sequence. The conglomeratic sediments overlie a sequence of interbedded sandstone, fresh water limestone and altered tuffs. Oligocene-Miocene rhyolitic tuffaceous rocks are thought to be present at depth, although there are no surface exposures in the three regions of interest (Beyer et al. 1976).

In general, hot springs lie along the major faults bounding the valleys. The vertical displacement characteristics of these faults is indicated by recent fault scarps 10 to 15 meters high. Thompson and Burke (1974) have calculated Basin and Range horizontal extension of 100 km, implying ubiquitous faulting. The depth to which these faults extend is not known. However, if the faults are acting as conduits for the

hot water, they must extend at least several kilometers. Water temperatures of the springs are as high as 94°C at the surface. Estimates as high as 200°C are obtained by geochemical methods for water temperatures at depth (Beyer et al., 1976). Assuming an average temperature gradient of 30°C/km, the water could be circulating to depths of 6 km.

4.3 Microearthquake Data

The first step in the seismic exploration program was microearthquake monitoring in three separate areas: Buffalo Valley, Grass Valley (Leach Hot Springs) and Buena Vista Valley (Kyle Hot Springs) (Figures 4-1 and 4-3). Each valley was subjected to a 10-14 day reconnaissance study. If sufficient activity was recorded a more detailed study of 6-8 weeks was undertaken. The reconnaissance studies indicated activity was very low around Kyle Hot Springs (Buena Vista Valley, 1 event/10 days), but moderate in Grass and Buffalo Valleys (1-2 events/day). Figure 4-3 shows the general location of events (shaded regions) and the recording sites occupied. After each valley was studied individually, an array (Figure 4-3) was deployed in North Pleasant Valley to confirm that the events detected in Grass and Buffalo Valley were not the same events originating from the site of the 1915 Pleasant Valley earthquake

Figure 4-1

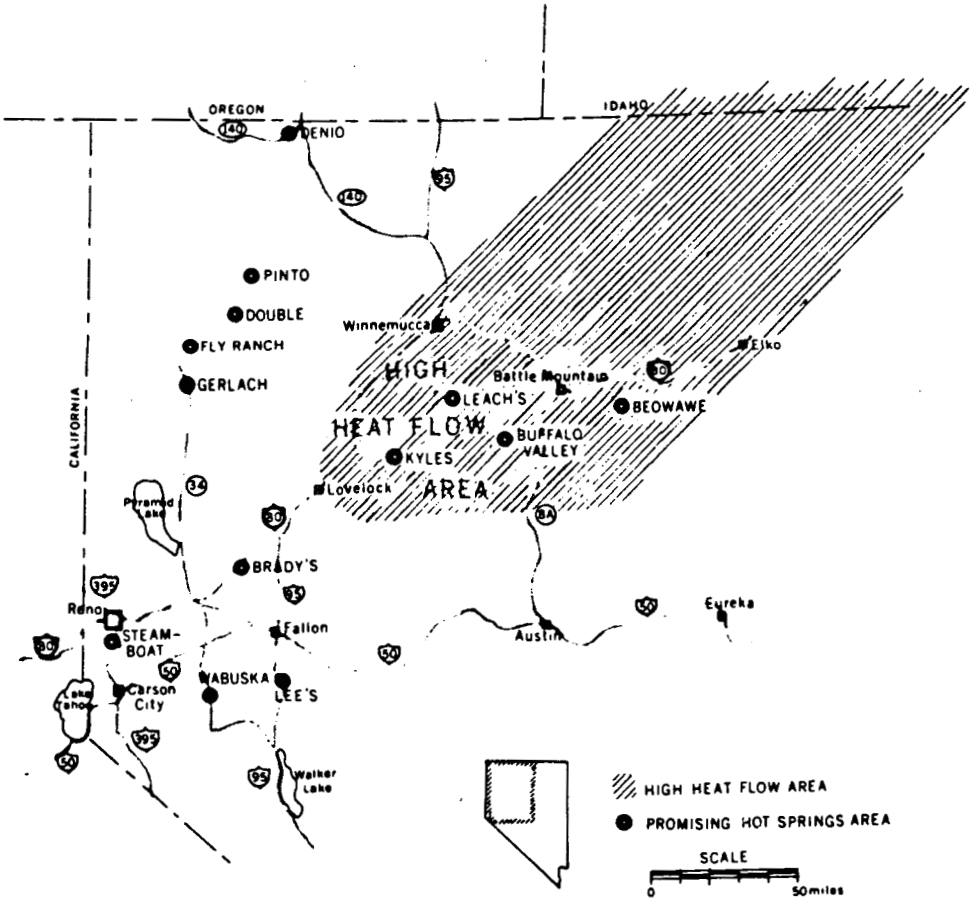

Hot Springs in Northwestern Nevada

XBL 735 676

Hot Springs in Northern Nevada. Leach, Kyle and Buffalo hot springs are the three study areas.

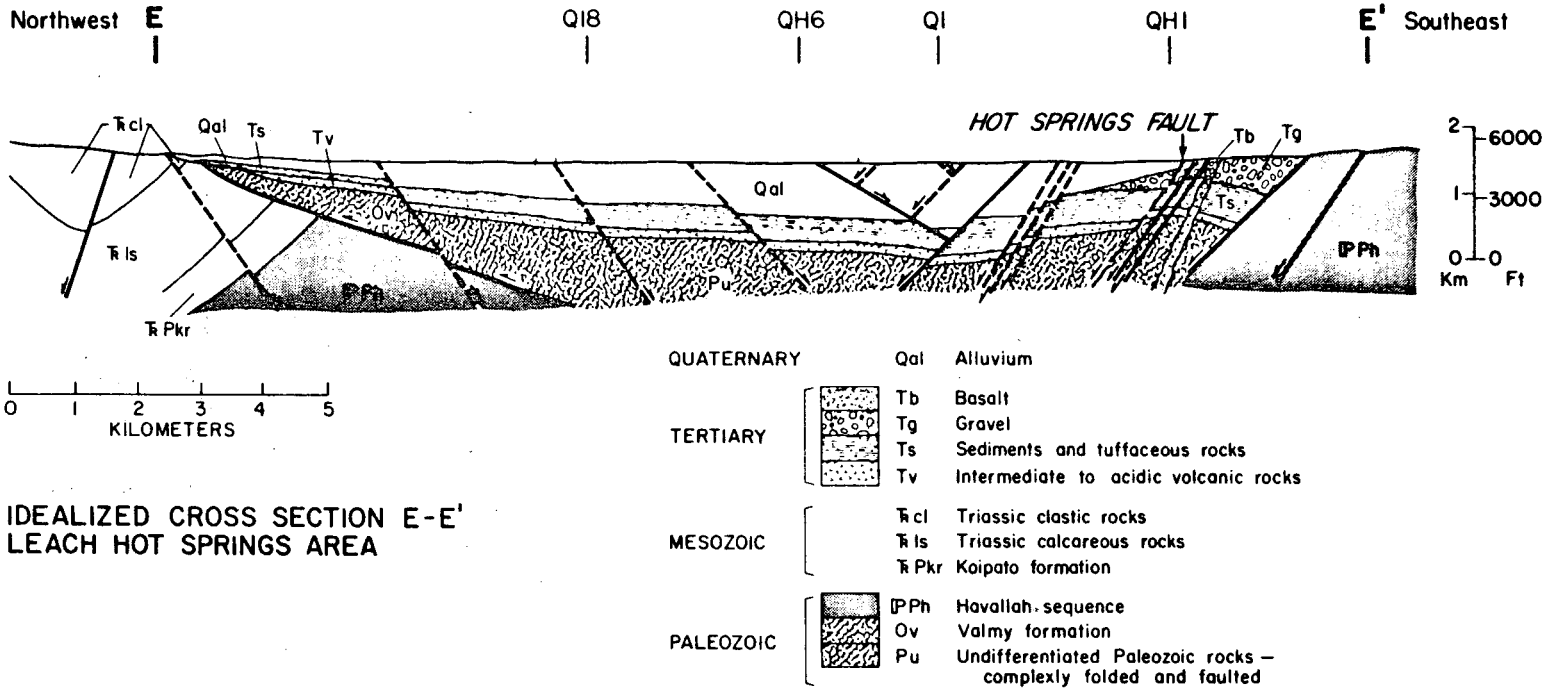

IDEALIZED CROSS SECTION E-E'
LEACH HOT SPRINGS AREA

Figure 4-2

Idealized cross section, Line E, Grass Valley (Beyer et al., 1976).

Figure 4-3

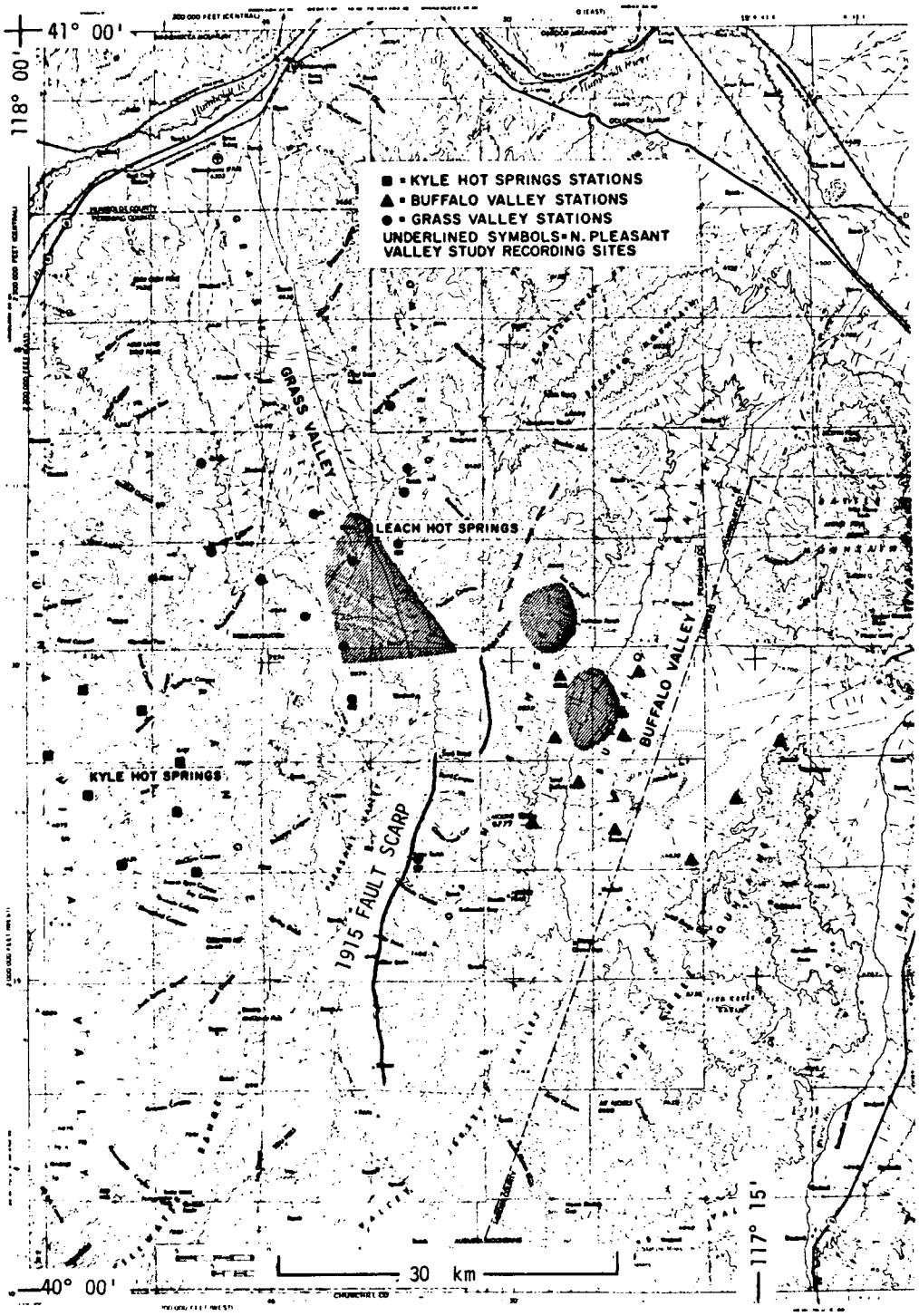

The three study areas in Figure 4-1. Cross-hatched regions are locations of microearthquakes. Symbols are locations of smoked-paper recorders. Note the fault trace of the 1915 earthquake (Mag. 7.5) and hypothesized extension, dashed line.

(magnitude 7.5). The result of this one week study was that 5 events were located at the southern end of Grass Valley, not on the fault trace of the 1915 event.

The quality of the microearthquake data was not sufficient to define accurate fault planes or fault plane solutions. However, the data were consistent with normal faulting at depths of 1 to 8 kilometers on faults bounding the valley with strikes and dips typical of Basin and Range extensional tectonics.

An 8-element analog, FM-telemetered array, later expanded to 12 elements, was set out in Grass Valley with hopes of recording seismicity associated with the hot springs activity. Because of the low power (100 milliwatts) and high frequency (163-173 MHz) of the radios, all transmitters were required to be in line of sight with the receivers. Although this did not seriously limit station locations in this study, it presents limitations in rough terrain. At each station a 4.5 Hz vertical geophone was used. Except for batteries and antennas, all components were buried to minimize temperature fluctuations and associated component drifts. When first deployed, rarely more than fifty percent of the radios functioned satisfactorily. After several months of debugging, it was concluded that the major problem was not in the basic design of the radio but in the quality of construction and components. Even at the

end of the study all 12 radios never worked simultaneously for more than 1 week. However, the microearthquake activity was traced to the southern end of Grass Valley. Events occurred at a rate of one to two per day with occasional swarm activity of 5-10 events. The events shown in Figure 4-4 occurred during two separate 6-week periods, January-February, March-April 1976. The seismicity seemed to be an on-going phenomenon and except for the occasional swarm activity, was fairly constant. During the two six week periods, approximately 100 events were recorded. The events that located with a standard error in epicenter of less than 0.10 kilometers are plotted in Figure 4-4. The model selected for locating the events was a half space with P-wave velocity of 5.5 km/sec and S-wave velocity of 3.2 km/sec, (Poisson's Ratio = 0.25). The model was chosen by locating several of the larger events in the center of the array and varying the velocity until the standard error of the depth was a minimum. Station corrections were also applied using P-wave residual information from nearby mine explosions. Although several layered models were used, the best model appears to be a half space. The depth of the events varied between two and eight kilometers with the majority of deeper events occurring at the southern end of the microearthquake cluster. Fault plane solutions (Figure 4-5) indicate normal

Figure 4-4

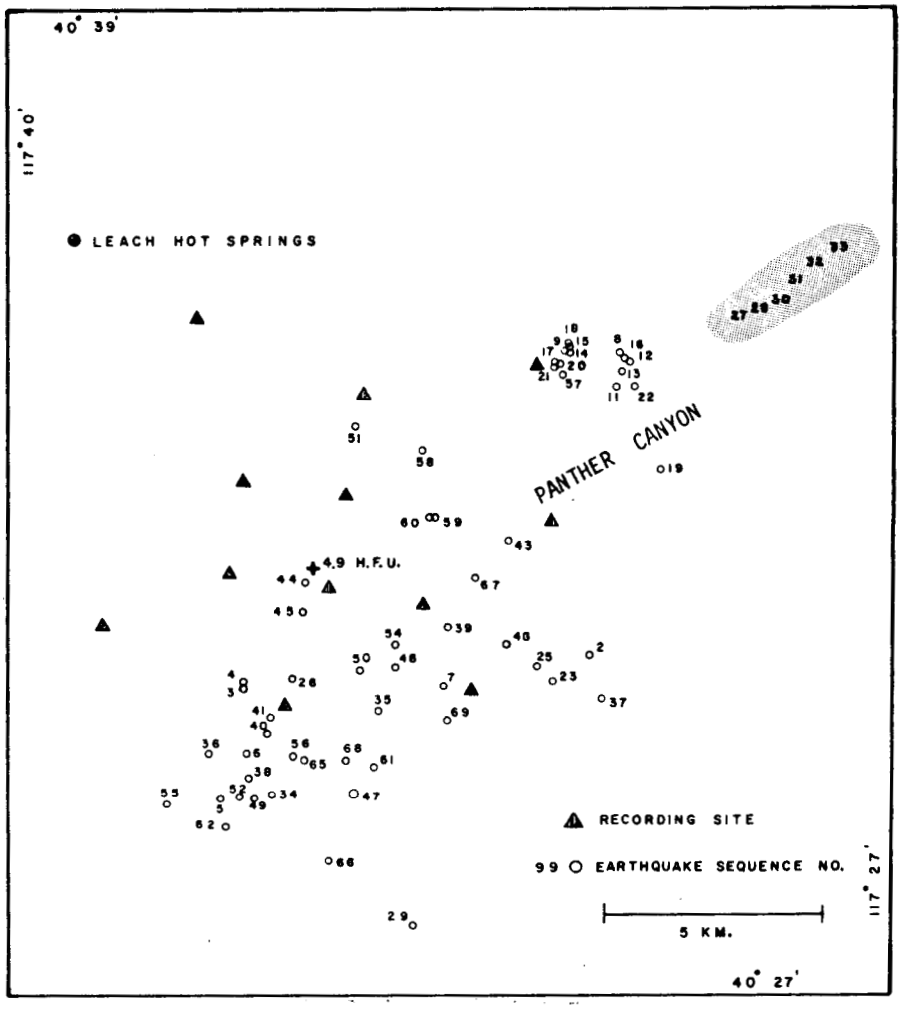

XBL 778-2594

Locations of events with standard error in epicenter of 0.10 km or less for the periods January 1 - February 15, March 15 - April 30, 1976. Events are numbered in order of occurrence. Shaded region indicates events with standard error greater than 0.10 km.

Figure 4-5

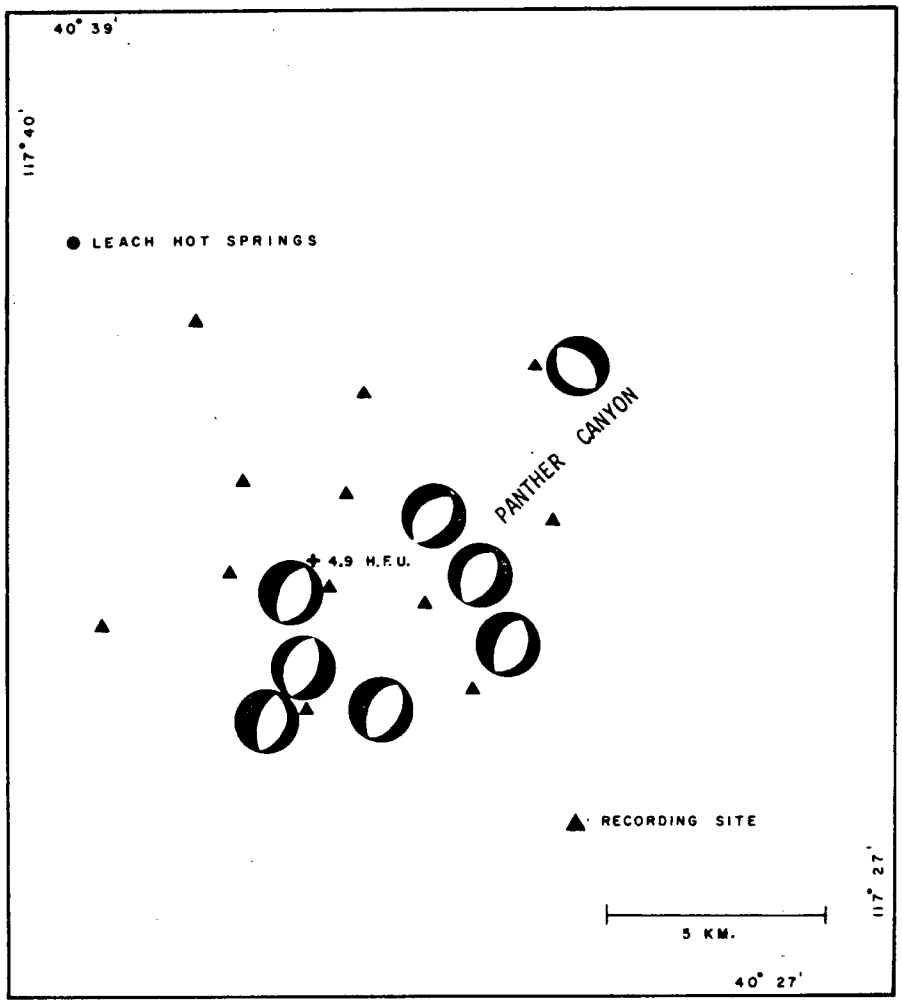

Fault plane solutions projected onto the upper hemisphere, for selected events, indicating normal faulting, with strikes in the NE-SW direction, consistent with regional tectonics. Dark area is compression.

faulting striking northeast-southwest on planes dipping between 45° and 70°, consistent with regional tectonics.

An attempt was made to determine coda magnitudes from $M_{CL} = -0.87 + 2 \log (T)$, where T is the duration of the event. Although this formula was developed by Lee et al. (1972) for central California events it is being used by the University of Nevada at Reno in magnitude determination for events in central Nevada (W. Peppin, personal communication, 1977). A coda threshold was obtained by comparing events common to stations in this study and the University of Nevada station BMN, 45 km to the east. Because of site geology and instrumentation differences, the coda magnitudes from BMN and the microearthquake array were inconsistent. Calculating a b-value from these approximately 100 events, using the M_{CL} formula, yields $b = 0.57 \pm 0.03$. Using a formula developed by Bakun and Lindh (1977) for normal faulting and coda lengths less than 30 seconds in the Oroville, California region, $M_{CB} = 0.28 + 0.71 \log (T)$, results in a b-value of 1.9 ± 0.14. Oliver et al. (1966), using trace amplitude rather than magnitude, calculated a b-value of 1 for microearthquakes occurring in the Fairview Peak, Nevada region, 125 km south-southwest of Grass Valley. Using trace amplitude for the Grass Valley events yields a b-value of 1.1 ± 0.15. Ryall et al. (1966) determined average b-values of 0.79

to 0.84 for Nevada region earthquakes between 1932 and 1961. In another microearthquake study in the Excelsior Mountains (southwest Nevada) Ryall and Priestly (1975) calculated a b-value of 1.03.

The widely varying Grass Valley b-values obtained by differing techniques may be due to site geology, or more likely to the inadequacy of the coda length technique at very close range. A more useful b-value could be obtained by recording a large number of events on horizontal geophones and converting the records to Wood-Anderson equivalents and using M_L, as was done in The Geysers section of this study. Although horizontal instruments were used in this study, they were connected in series with the vertical geophones to provide P- and S-arrivals on a single data channel. Because of the resulting uncorrectable interference effects, Wood-Anderson seismograms could not be calculated.

The number of studies dealing with spectral characteristics of microearthquakes is limited for Nevada. Table 4-1 gives results of P-wave spectral analyses for some representative events in Grass Valley. The events were selected on the basis of magnitude and azimuth. Douglas and Ryall (1972) suggested that for microearthquakes, $1<M_L<2$ near Fairview Peak, Nevada, magnitude versus moment scaling laws seemed to apply. Although they did not calculate a moment versus magnitude relation,

Table 4-1

P-Wave Spectral Properties

EQ	M_{CL}	Mo (dync-cm)	R (km)	f_o Hz	$\Delta\sigma$ (bar)	r (meter)	d (cm)	h (km)
20	0.7	1.2×10^{17}	6.8	35	2.50	28	.030	4.0
22	0.8	1.2×10^{17}	7.0	35	2.50	28	.030	4.0
27	0.3	2.4×10^{16}	8.0	30	0.30	32	.004	4.0
58	-0.3	4.8×10^{15}	9.6	40	1.50	24	.010	6.0
21	1.2	1.8×10^{17}	6.8	30	1.90	32	.020	4.0
		1.9×10^{17}	8.8	30	1.90	32	.020	
37	-0.1	1.9×10^{16}	7.0		.75	32	.020	
		9.6×10^{15}	10.8	40	.70	32	.020	2.0
		1.3×10^{16}	3.0		.75	24	.010	
50	-0.3	4.2×10^{15}	7.1		.30	40	.008	
		9.7×10^{14}	6.5	35	.29	28	.008	6.0
		2.0×10^{15}	8.3		.30	40	.009	
60	0.3	7.8×10^{16}	4.4		.90	40	.010	
		6.0×10^{16}	8.7	40	.88	40	.010	4.0
		3.4×10^{16}	5.6		9.50	24	.009	
65	-0.3	9.0×10^{15}	8.4		.30	28	.004	
		1.1×10^{16}	8.0	35	.30	32	.004	6.0
		1.7×10^{16}	7.3		.35	28	.004	
26	0.6	1.1×10^{17}	7.5		.46	52	.009	
		4.5×10^{16}	7.6	20	.50	48	.009	6.0
		9.0×10^{16}	7.6		.55	48	.009	
27		4.5×10^{16}	7.6	30		32	.005	6.0

$b = 0.57 \pm .03$ $\quad \log_{10} Mo = (16.15 \pm .05) + (1.09 \pm .08) M_{CL}$

$b = 1.9 \pm .14$ $\quad \log_{10} Mo = (14.78 \pm .15) + (2.6 \pm .2) M_{CB}$

their data indicate a zero magnitude event would correspond to a $Log_{10}(Mo)$ of about 16.4, with a slope of about 0.7. Depending upon which magnitude formula is used, the results from this study are, $Log_{10}(Mo) = (16.15 \pm 0.05) + (1.09 \pm 0.08) M_{CL}$ and $Log_{10}(Mo) = (14.78 \pm 0.05) + (2.6 \pm 0.2) M_{CB}$. Douglas and Ryall used a magnitude formula adjusted to the Wood-Anderson magnitude of their largest recorded event ($M_L = 2.0$). They also used S-waves rather than P-wave spectra. If one adopts the M_{CL} formula the Grass Valley events compare to the Fairview Peak events. Using the M_{CB} formula, the Grass Valley events are quite anomalous.

As suggested in The Geysers study, a low moment for a given magnitude may be an indication of attenuation effects. The corner frequencies for the Grass Valley events were generally in the 30-35 Hz range. Douglas and Ryall observed corner frequencies from 5 to 10 Hz. Differences are probably due to the observation distances. In Grass Valley the source-receiver distances were 5-10 km, compared to the 13-40 km range of the Fairview Peak events. Although Douglas and Ryall corrected for a Q of 250 and 400, these values may have been too high. For multiply recorded events, the corner frequency (f_o) for the Grass Valley events depended on azimuth and site geology. In general f_o was lower for the valley stations, which are underlain by low-Q alluvium, as compared to

bedrock stations. Therefore, the difference in the moment versus magnitude relation from one area to another might be accounted for by propagation path effects.

Because the commonly estimated stress drop, $\Delta\sigma$, is a function of f_o^3, the calculated stress drops of Grass Valley microearthquakes also differed from the stress drops of the Fairview Peak events. However, the lower moments tend to offset the higher corner frequency effect, i.e., $\Delta\sigma = 8.47\ M_o\ f_o^3/\alpha^3$, where α is the P-wave velocity. In general, the Grass Valley events have stress drop estimates an order of magnitude greater than the Fairview Peak events. Assuming the differences are real would imply that the two areas may be under the influence of different stress mechanisms. It may also be an indication that the Grass Valley events are the result of failure in unfractured material, whereas the Fairview Peak events are occurring on existing fractures. Douglas and Ryall (1972) also suggested that for different areas of occurrence near Fairview Peak, the difference in stress drop may be due to different source mechanisms. Although the Grass Valley events occurred over a much smaller region, there does not seem to be any correlation between stress drop and area of occurrence. This would suggest that all the events in Grass Valley are similar in relation to source mechanisms, as indicated by the fault plane solutions.

4.4 Explosion Data

4.4.1 P-Wave Velocities

In a study to determine if the presence of geothermal activity (hot springs) could be detected in the propagation characteristics of P-waves, a grid of stations was set out in Grass Valley. Studies by Iyer and Hitchcock (1975) have detected P-wave travel-time delays associated with areas of recent volcanic activity near Clear Lake, California. It is desired to know if shallow near-surface features could be detected by the use of such P-wave velocity studies.

Approximately 60 data points were taken at 500 meter intervals on lines E, D, H and at selected points between, (Figure 4-6). The data were reduced by assuming a zero delay time on bedrock at kilometer 0.0 on line D. To insure sharp arrivals and nearly vertical wave propagation, only large Nevada Test Site (NTS) nuclear explosions were used as sources for the P-waves in this initial study. The procedure was to use two bedrock reference stations on either side of the valley to obtain an apparent velocity end to end along the line. After the apparent velocity was determined the data were corrected, yielding relative delays for intermediate stations. This assumes that the bedrock on both sides of the valley is similar and represents a regional

Figure 4-6

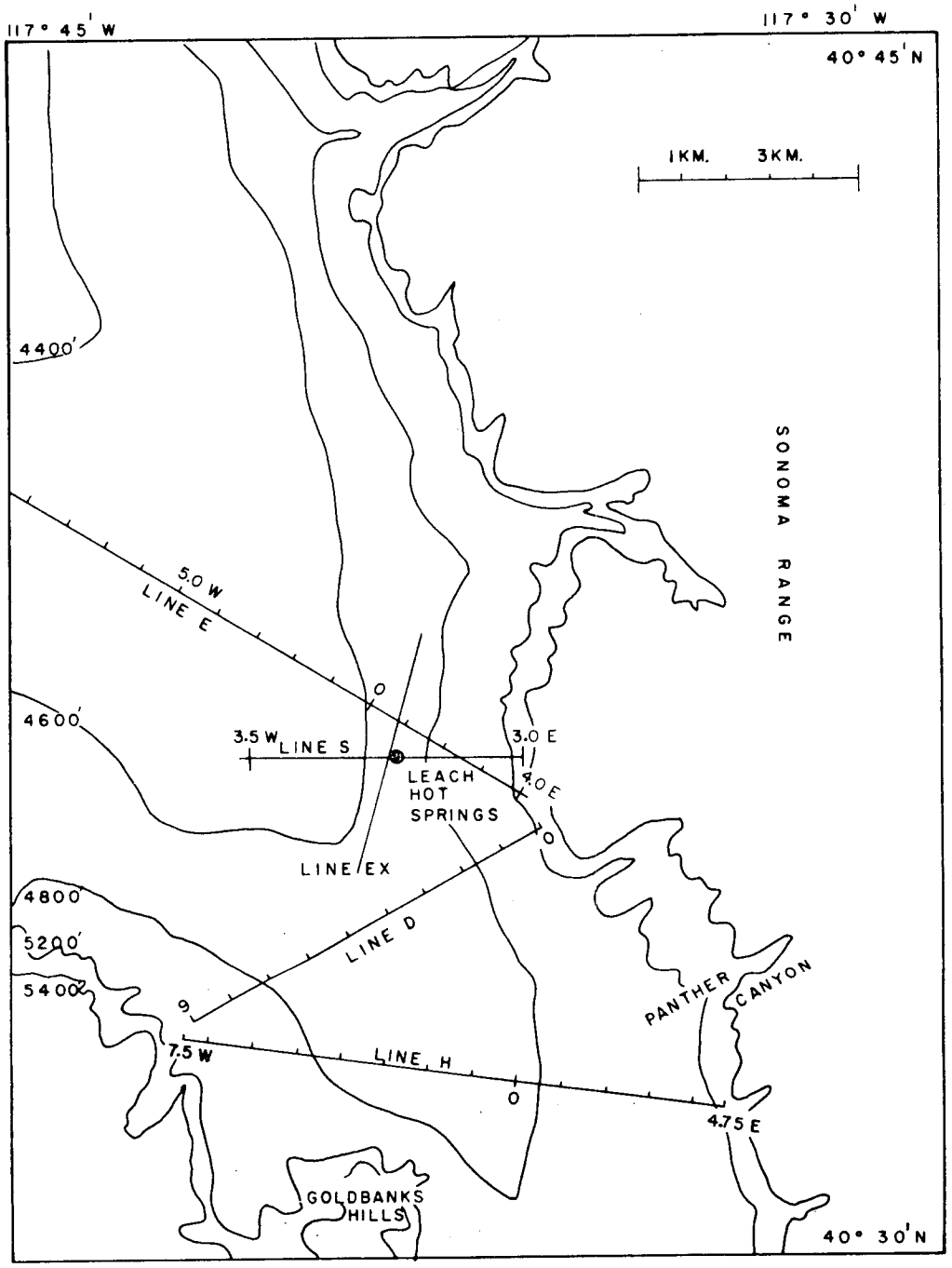

LEACH HOT SPRINGS
QUADRANGLE

Primary area of study with data line locations. For comparison to other figures note the relative positions of Panther Canyon and Leach Hot Springs.

phenomenon. Because the NTS explosions were relatively infrequent, a comparison with delays from daily mine explosions 40 kilometers to the east was made. The results were almost identical. Therefore, the majority of P-wave data points were from the nearby mine explosions. The contoured data are shown in Figure 4-7. A negative delay implies a faster velocity with respect to bedrock and a positive delay suggests a slower velocity compared to bedrock.

As expected, the slower P-wave velocity of the sediments produces delays, with the larger values occurring towards the center of valley where the sediments are thickest. Two significant anomalies were revealed. The most obvious is the negative P-wave delay, or advance, in the hot springs area. This advance is thought to be due to densification of sediments from the continual deposition of silica from hot springs activity. Additional evidence for densification is seen in the high gravity gradients surrounding the hot springs (Figure 4-8). Later gravity reduction (Goldstein and Paulsson, 1977) suggests an excess mass of 2.5×10^8 metric tons around the hot springs. If a density contrast of 0.5 gm/cc is taken between the normal sediments and the densified sediments, and a shape of $\frac{1}{2}$ of a right circular cone for the plug of silica, then the plug would extend to a depth of 1 km with a width at its base of 0.8 km.

Figure 4-7

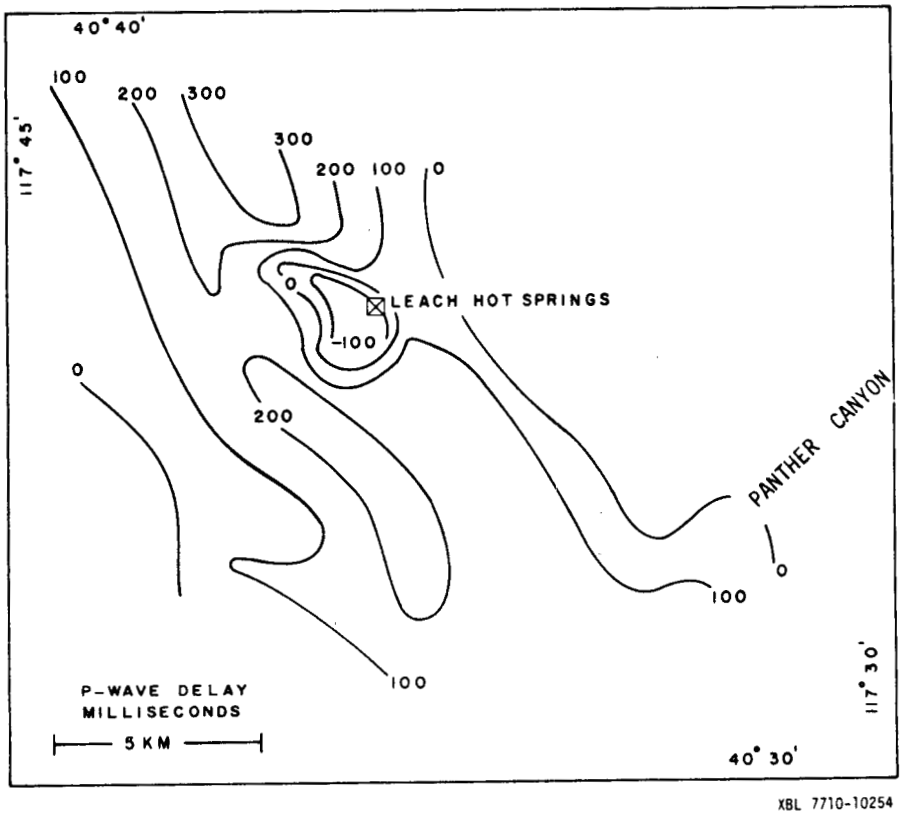

Contoured P-wave delay data, note negative delay or advance near the hot springs.

Figure 4-8

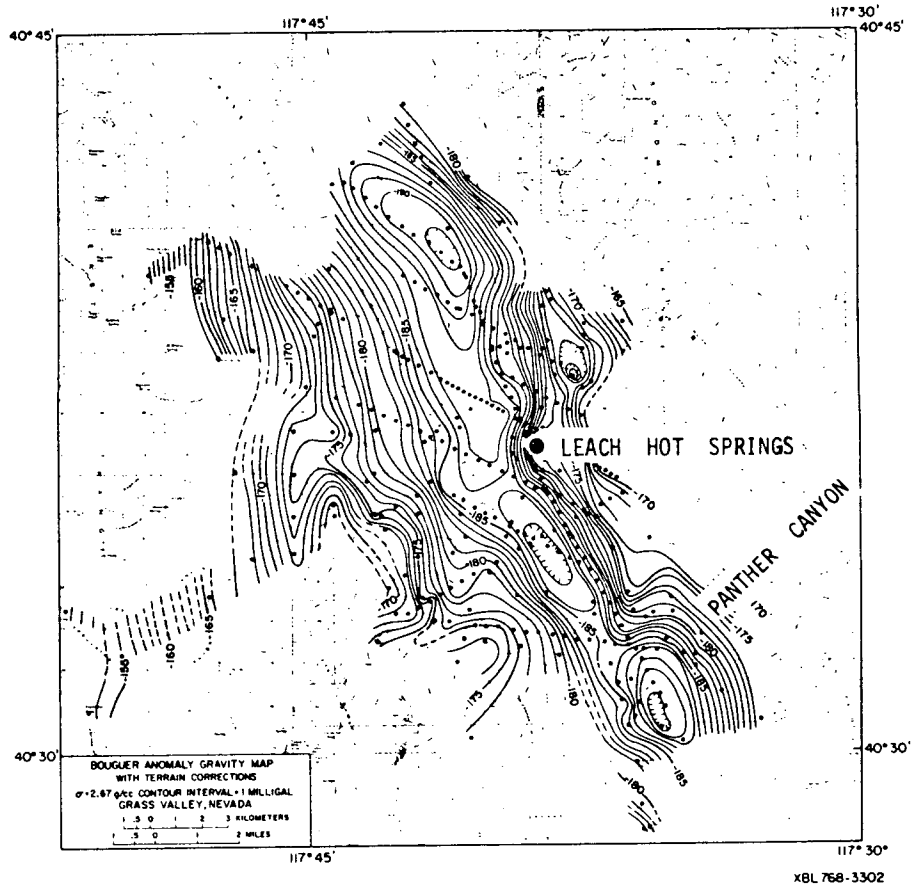

Bouguer gravity map with terrain corrections. Contours are in milligals (Beyer et al., 1976). Note the correlation with P-delay.

Assuming that this is the extent of the silica deposition, a velocity contrast of 1.5 km/sec (3.5 km/sec vs. 5.0 km/sec) would account for the 0.85 second average advance observed.

To confirm the presence of high velocity material in the hot springs area, a 12 element 550 meter N-S refraction line was set out across the hot springs. A total of four explosions were used, one at each end of the line and two offset 500 meters from the ends. The resulting data are shown in Figure 4-9. It is apparent from the shape of the travel-time curves that the structure associated with the hot springs is rather complex. However, it seems as if the velocity in the hot springs area is greater than the 2.0 km/sec found for near-surface valley fill. The highest apparent velocity is 5.5 km/sec just north of the hot springs. It should be noted that for accessability reasons the refraction line was placed approximately 30^{o} to the fault that is thought to be controlling the flow of the hot springs. The northern end of the line was on the downthrown side of the hot springs fault, where the majority of sedimentation and densification would be expected to occur. This may explain why the velocities on the northern end of the line are higher than the southern values. It is also possible that such effects as dip and horizontal refractions are playing an important role

Figure 4-9

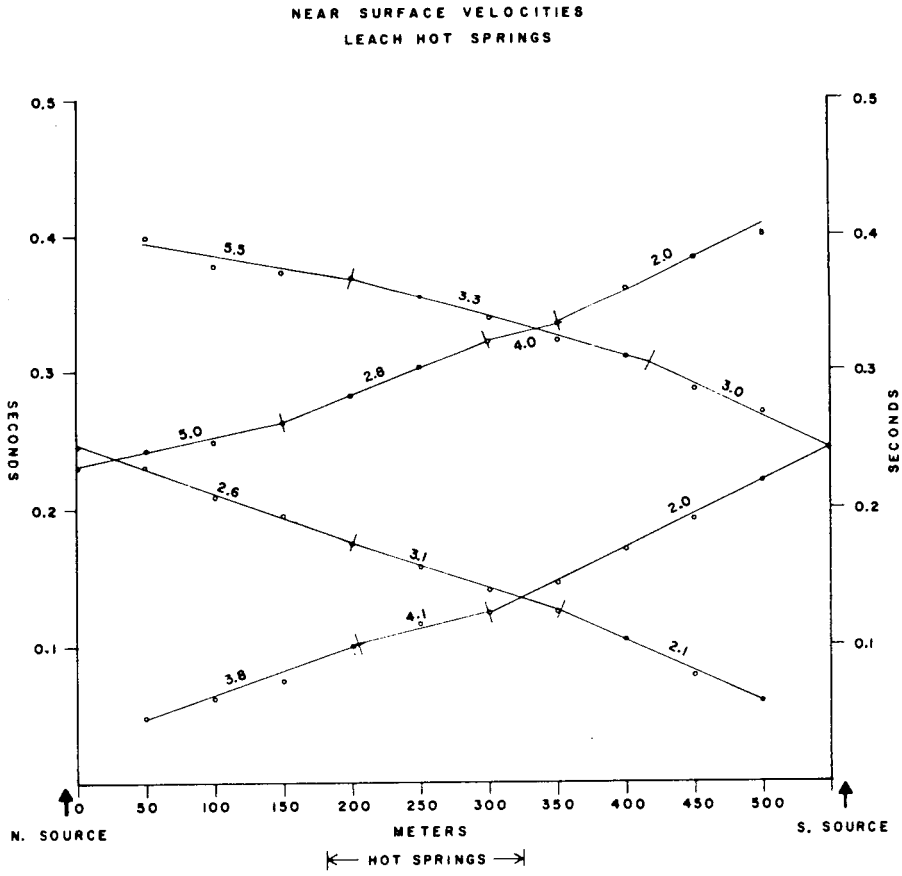

Data from shallow refraction study across the hot springs area. Numbers on curves indicate velocities in km/sec.

in determining the apparent velocity structure. The complexity of the structure around the hot springs will become obvious when the reflection profile data are presented in a later section.

A second P-wave velocity anomaly was found along line D, around kilometer 6, (Figure 4-6). It appears as a "nose" to the west in the 100 millisecond contour of the P-wave delay data (Figure 4-7). This "nose" is also apparent in the gravity data (Figure 4-8). If the P-wave velocity is controlled mainly by depth to bedrock this anomaly may be an upwarp in the basement structure. However, from the topographic map it is not apparent that this is the case. This P-wave anomaly also corresponds to a heat flow high, Figure 4-36. Further evidence relating this P-wave anomaly to the basement structure will be presented in the section on heat flow modeling.

4.4.2 Attenuation Data

During the P-wave velocity studies it was noticed that the frequency content of the waves traveling through the hot springs area differed significantly from other travel paths in the valley. For paths through the hot springs area, the high frequency content was preserved. This was especially obvious for high frequency sources such as local microearthquakes. Figures 4-10 and 4-11 are an explosion and a microearthquake, respectively, recorded at 3 different sites and displayed for

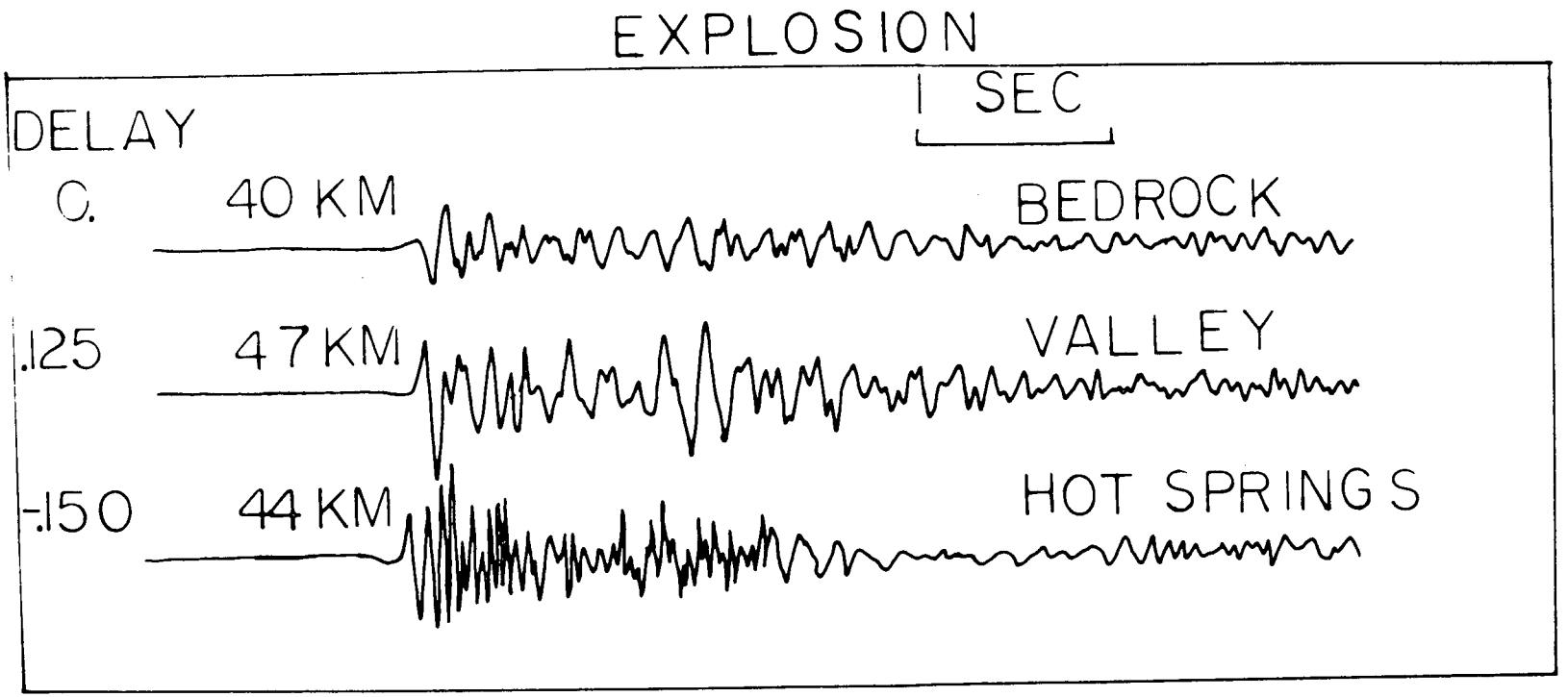

Figure 4-10

Explosion seismograms from three different sites. Note the high frequency content of the hot springs record.

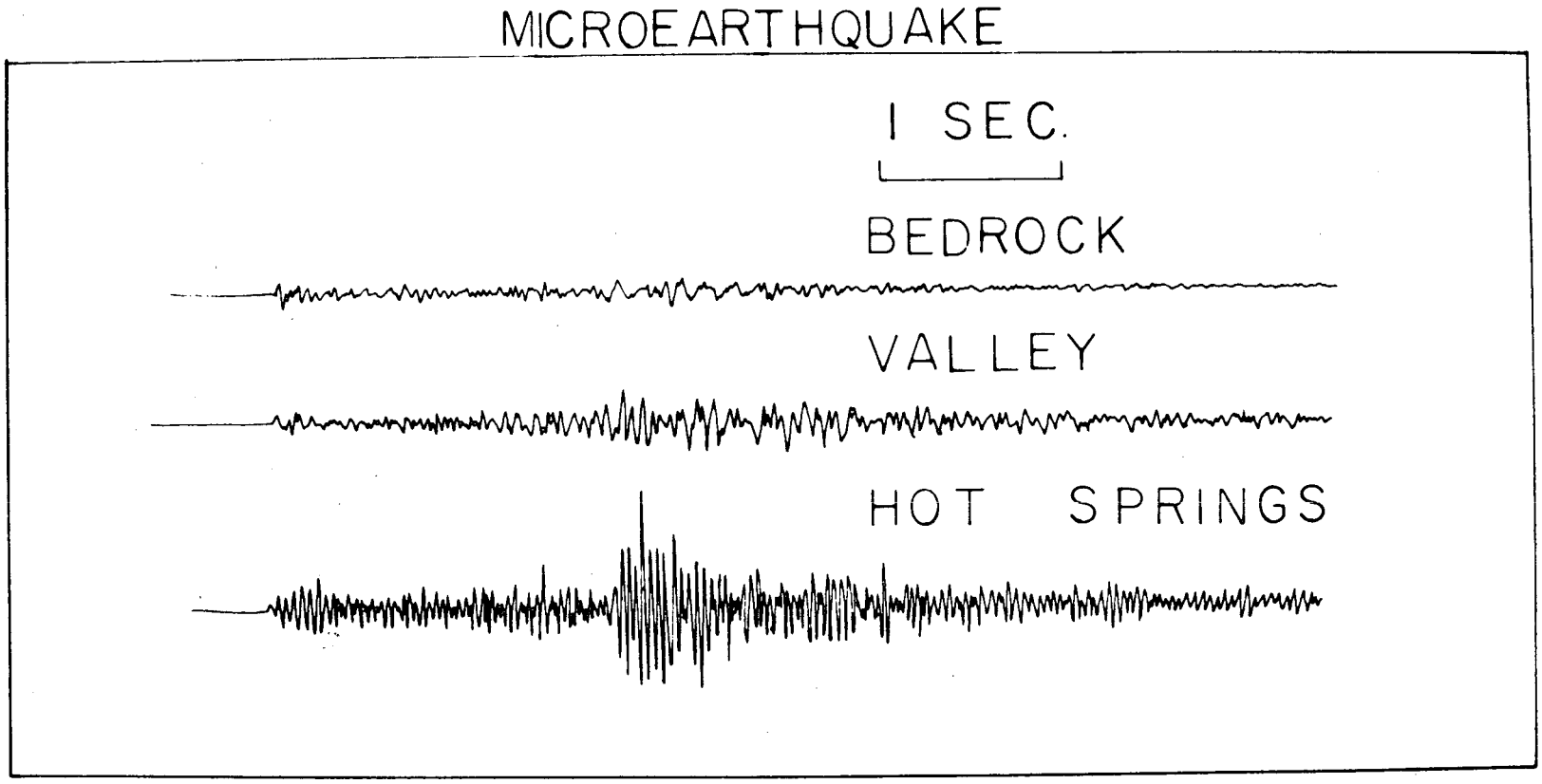

Figure 4-11

Microearthquake seismograms from the same sites as Figure 4-10. Again, note the high Q effect of the hot springs region.

comparison. In both cases, it is quite obvious that the structure is affecting the frequency content of the waves. All instruments were identical and the seismograms were corrected for different gains.

In an attempt to quantify this effect a line of stations was set out across the hot springs to record several mine explosions (Line S Figure 4-6). A line of nine stations with 500 meter spacing centered at the hot springs was used. Two additional stations, 1 and 11, were used as reference points on bedrock and alluvium respectively, i.e., stations 3.0 E and 3.5 W, Figure 4-6. All geophones and instruments were identical. The records from each site were digitized at 200 samples/sec, antialias filtered, and displayed to select the appropriate P-wave window. After the window length was selected (0.5 to 1 second) the signals were tapered with a 10% cosine taper, the mean removed and zeros added to total 256 points. The signals were transformed to the frequency domain by a fast Fourier transform and the instrument response was removed. Figure 4-12 shows the P-waves taken for analyses, the resulting displacement spectra, and the reduced spectral ratios. The reduced spectral ratios were obtained by using a reference spectrum that was the average of all eleven stations and then smoothed with a 10 point moving average. Each individual spectrum was then smoothed with a 10 point moving average and ratioed to the reference spectrum.

Figure 4-12

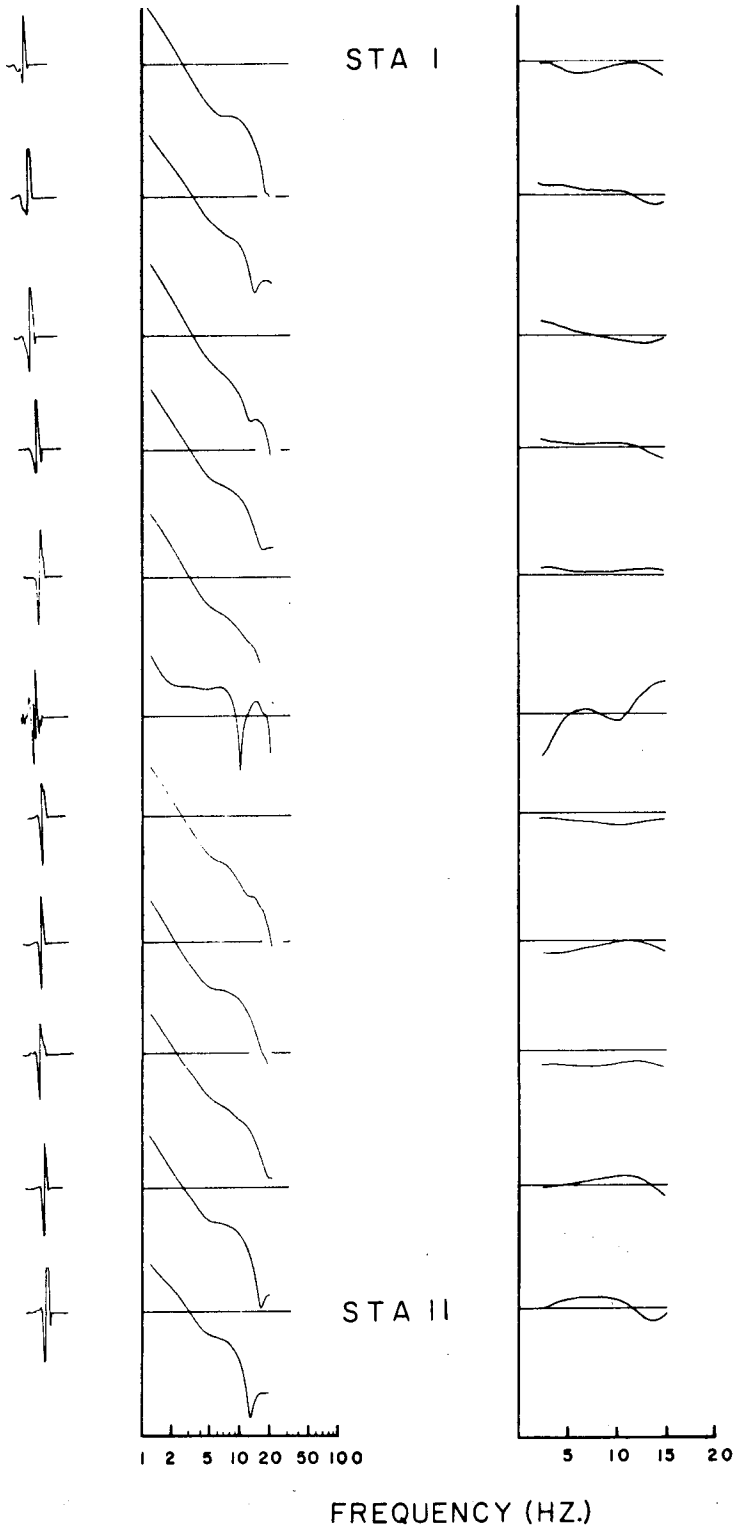

P-wave signals, spectra and reduced spectral ratios with respect to smoothed reference spectrum (see text). Note anomalous behavior at the hot springs, STA 6.

The resulting reduced spectral ratios are shown in the third column of Figure 4-12. Because extensive smoothing was performed to emphasize only significant effects, only a qualitative analysis of Q variations is within the quality of the data. As can be seen in Figure 4-12, the P-wave displacement spectrum and the reduced ratio for the hot springs station, station 6, are significantly different from the others. The positive slope of the reduced ratio suggests a higher Q through the hot springs area. As was concluded from the velocity data, the hot springs area is dominated by materials that are probably much denser than the surrounding rocks. However, the Q anomaly suggests that densification is confined to the immediate area of the hot springs. Because of the relatively large amount of work required for Q analysis, and close control on instrumentation, only one line of data was reduced to obtain Q structure. Therefore, it is difficult to compare P-wave velocity with P-wave Q data in detail. Both anomalies however, are quite localized, the attenuation more so than the velocity. It is of perhaps great interest that the severe signal attenuation off the hot springs area, both at bedrock and alluvial sites, indicate that the loss is accomplished in the shallowest kilometer or so of the crust. Implications are that greatly improved signal bandwidth may be obtained at moderate depth of source burial in tectonically active areas.

4.5 Refraction and Reflection Data

To gain additional information on fine structure of the valley and hot springs, two Vibroseis (registered trade name, Continental Oil Co.) reflection profiles and one refraction line were run. It was desired to know not only the structure of these areas but the applicability of this type of study in exploring for geothermal resources in a Basin and Range environment. If detailed surveys can provide structural evidence for the source of the hot springs, it may be possible to extrapolate this information to other Basin and Range structures where the surface manifestation of hot water is not observed. However, to carry this experiment to its logical conclusion would require confirmatory drilling based on the data, which has not yet been done.

Because of the high cost of commercial reflection profiling, the coverage of the valley could not be as extensive as for the other geophysical methods. Two lines were selected in areas of high potential and other geophysical data: line E and a cross line through the hot springs, line EX (Figure 4-6). (See Figure 4-13 for other data on line E.) The reflection profiles extended from approximately km 2.5 east to km 4.5 west on line E and along line EX through Leach Hot Springs. The refraction line extended from km 2.75 west to km 2.0 east on line E. The source points for the refraction line were at kms 7.5 west, 5.0 west, 2.75 west, 0.35 west,

Figure 4-13

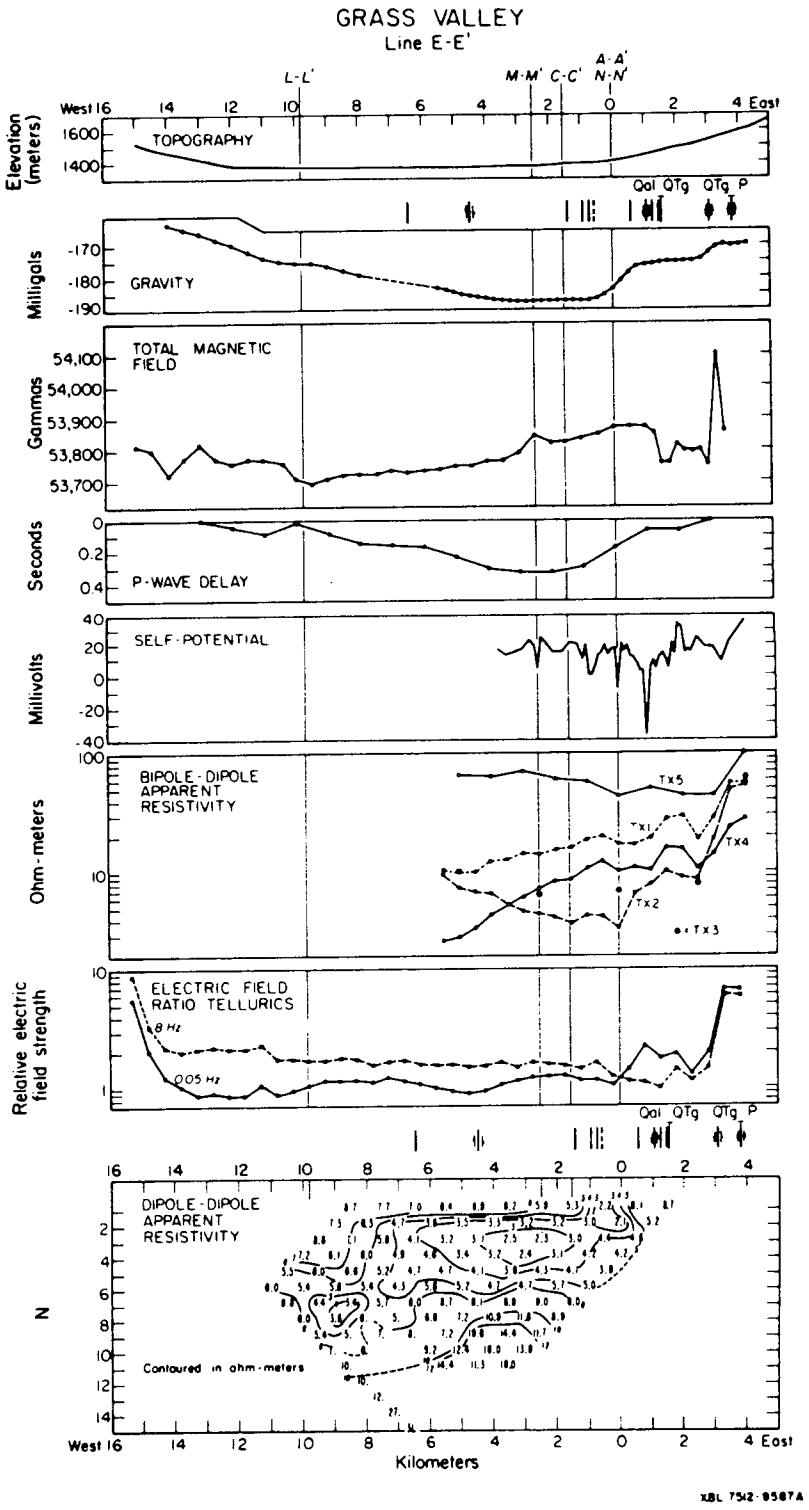

Composite of geophysical data along line E. (Beyer et al., 1976)

2.0 east, 3.65 east and one point 7.1 km off the east end of line E. Figures 4-14 through 4-19 are the reflection profiles displayed in migrated form (finite difference), conventional (polarity normal) and relative amplitude (polarity normal) for line E and line EX, respectively. The refraction data are displayed in Figures 4-20 through 4-25. The field work, May 23-26, 1976, and data reduction was done by Western Geophysical Company of Houston, Texas at a cost of $26,000. The parameters used in the study are listed in Table 4-2.

4.6 Regional Refraction Data

Although north central Nevada is known to be an area with high heat flow, there is no universally accepted model to explain it. Previous studies (Eaton 1963, Stewart et al., 1964 Hill and Pakiser 1966, Prodehl 1970) involving crustal refraction work in eastern and central Nevada have suggested crustal thinning may be responsible for the above average heat flow. However, north central Nevada had not been traversed previously by any such studies at the outset of this investigation. In an effort to improve the understanding of the regional crustal structure and upper mantle velocity, three (NTS) nuclear explosions were used as sources in a special study during 1976. The majority of the measurements were made with the explosions Fontina and Chesire

Table 4-2

Vibroseis Parameters

Instruments:	DDS-888
Format:	SEG-C (32 BIT, Floating Point)
Pilot:	58 - 12
Length:	16 Seconds
Sweeps:	16/V.P., reflection profiling, more for refraction
Vibrators:	4
Coverage:	1200%
V.P. Interval:	330'
Group Interval:	165'
Traces:	48
Spread:	4455' - 660' - 660' - 4455'

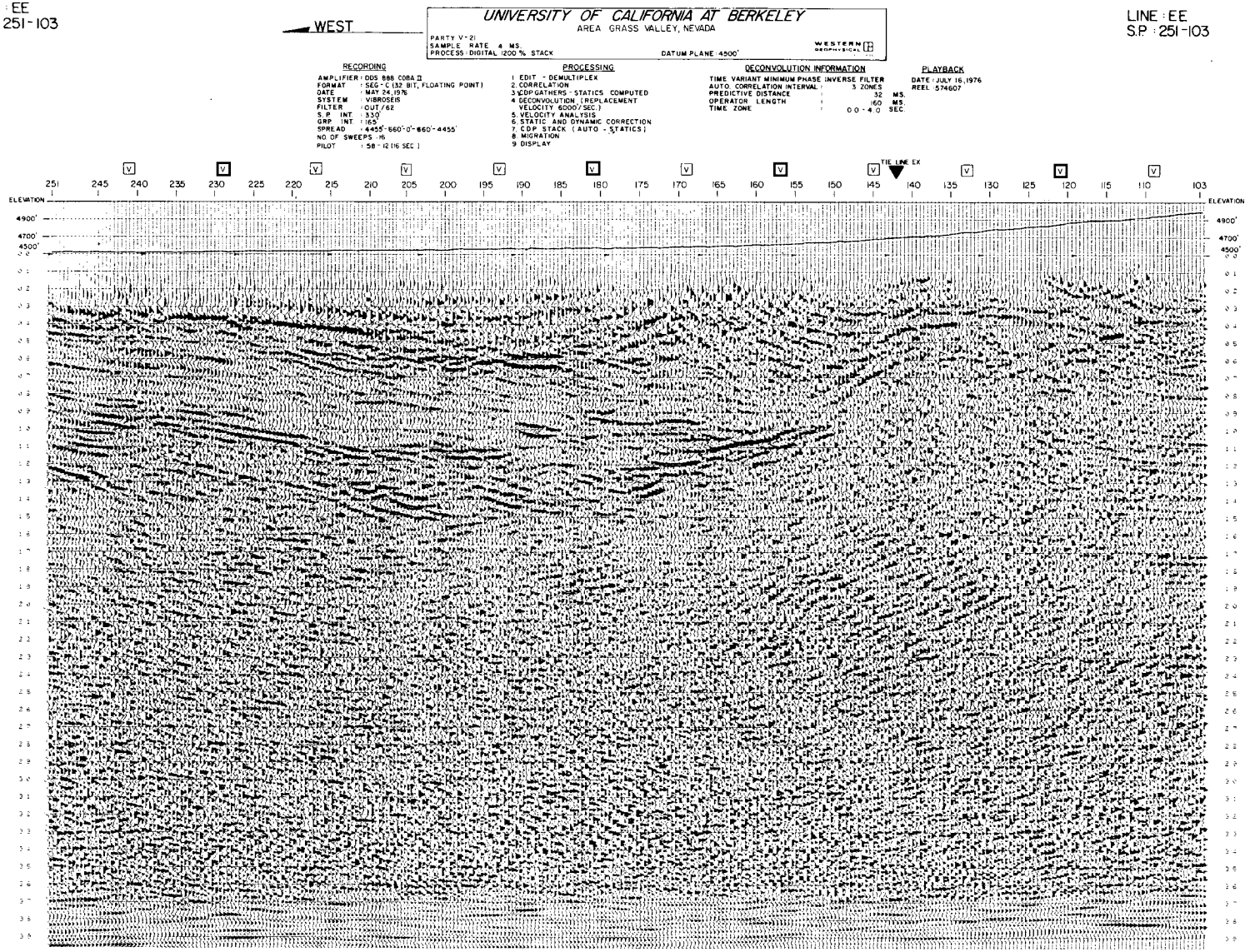

XBB 768-7630

Migrated reflection profile along line E, between points 4.75 west and 2.75 east.

Figure 4-14

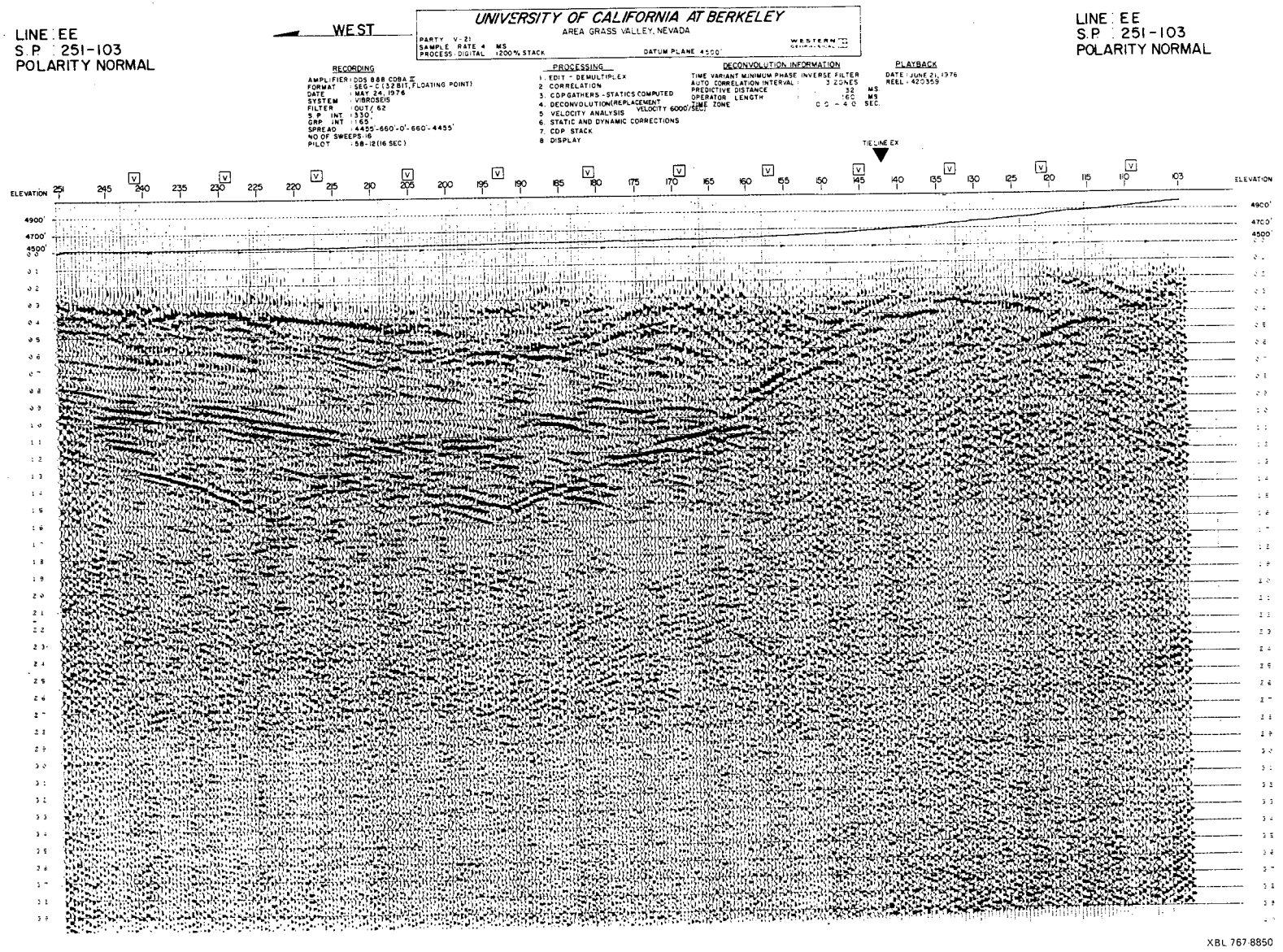

Conventional reflection profile along line E, between points 4.75 west and 2.75 east.

Figure 4-15

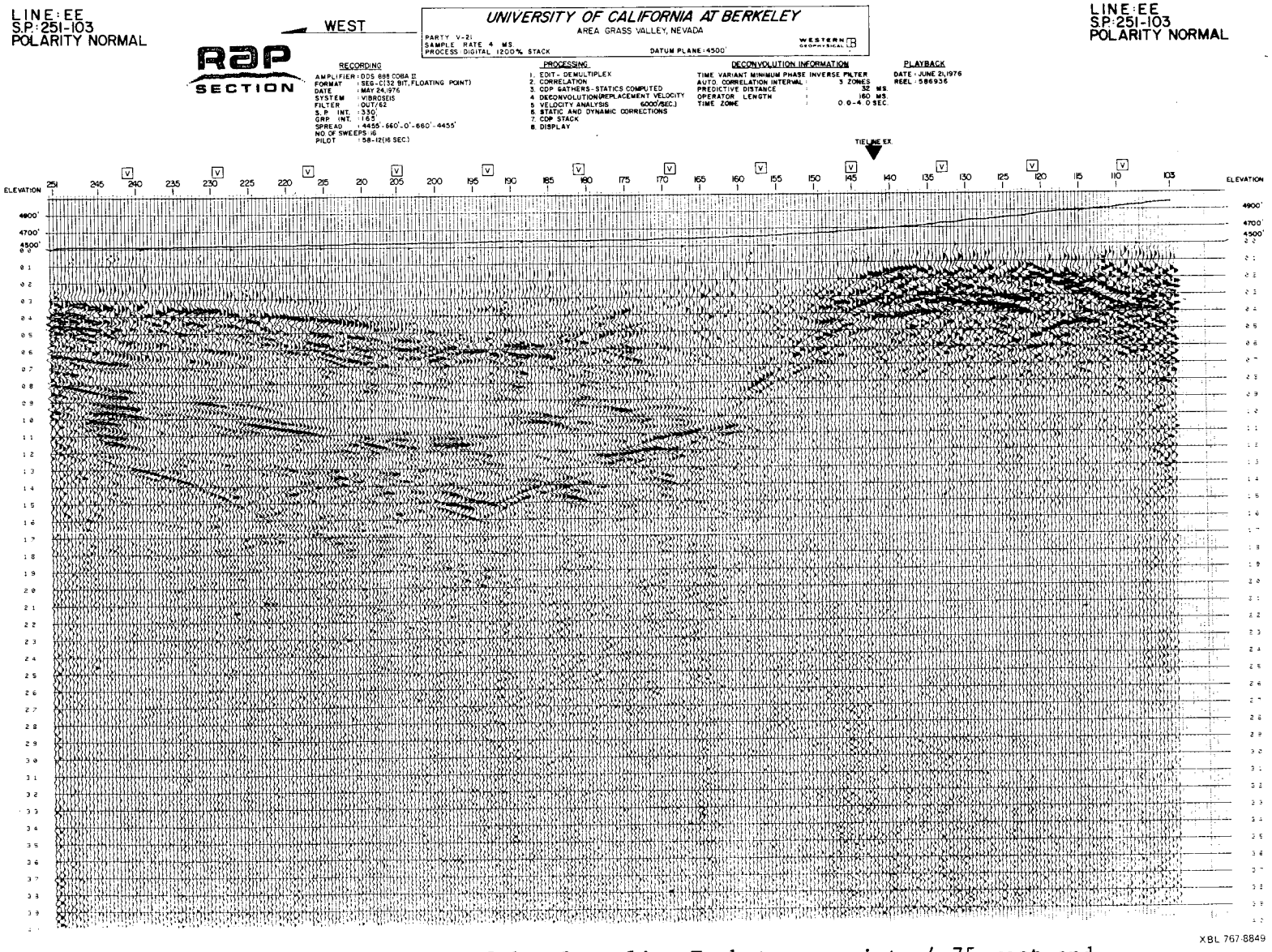

Relative amplitude reflection profile along line E, between points 4.75 west and 2.75 east.

Figure 4-16

Figure 4-17

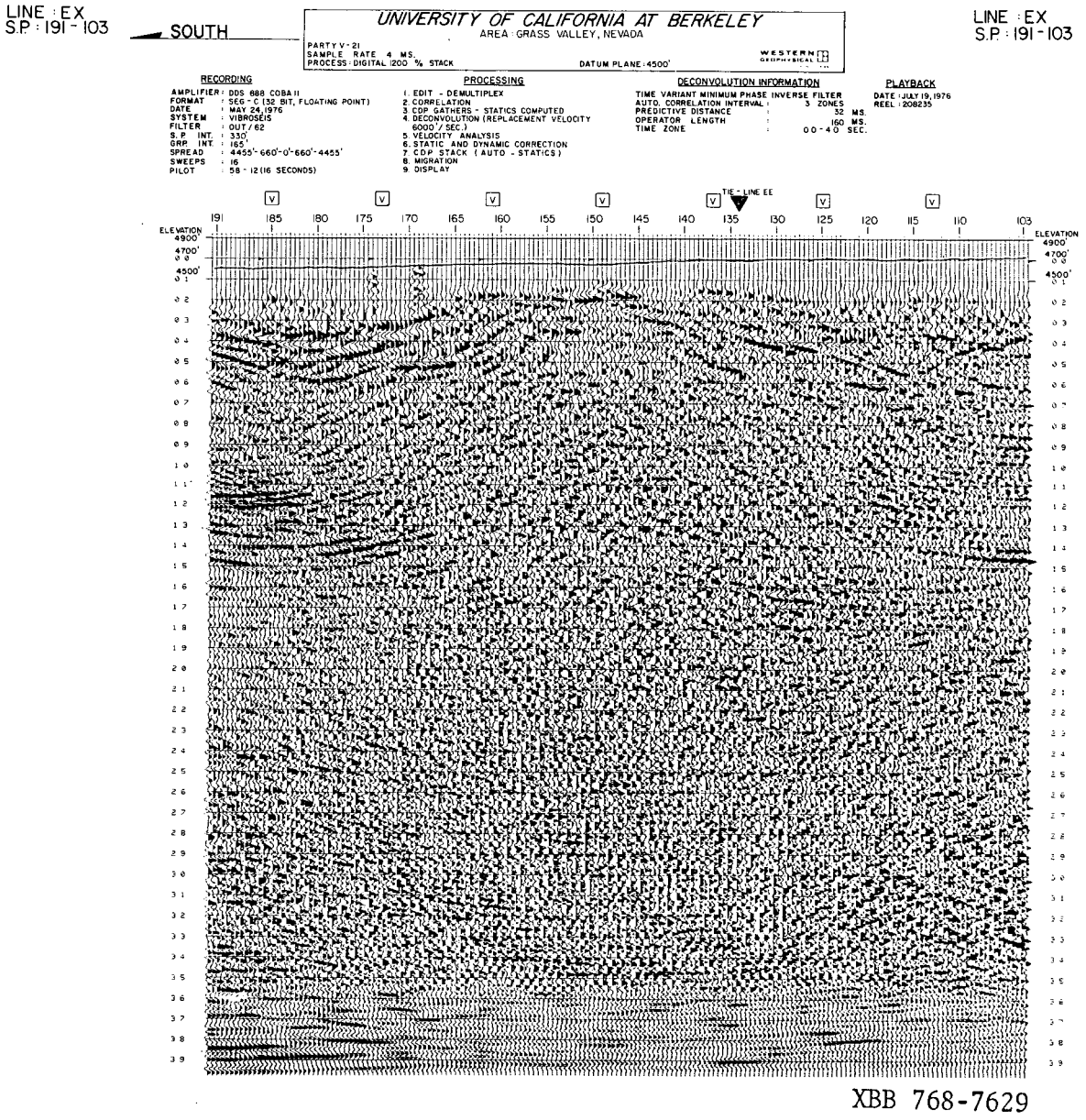

XBB 768-7629

Migrated reflection profile over hot springs area, line EX.

LINE: EX
S.P 191 -103
(POLARITY NORMAL)

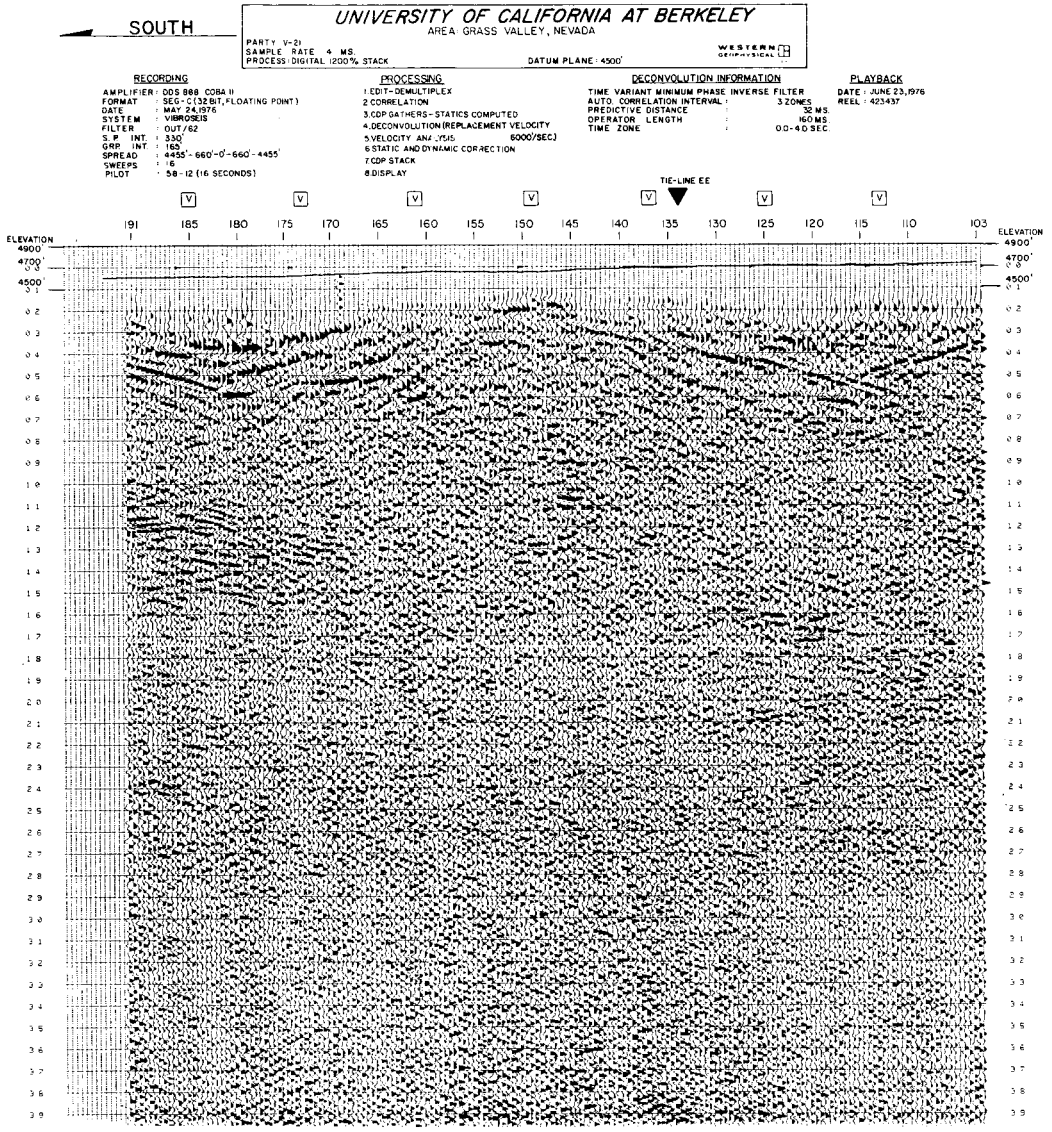

XBB 768-7628

Conventional reflection profile over hot springs area, line EX.

LINE: EX
S.P 191 -103
(POLARITY NORMAL)

Figure 4-18

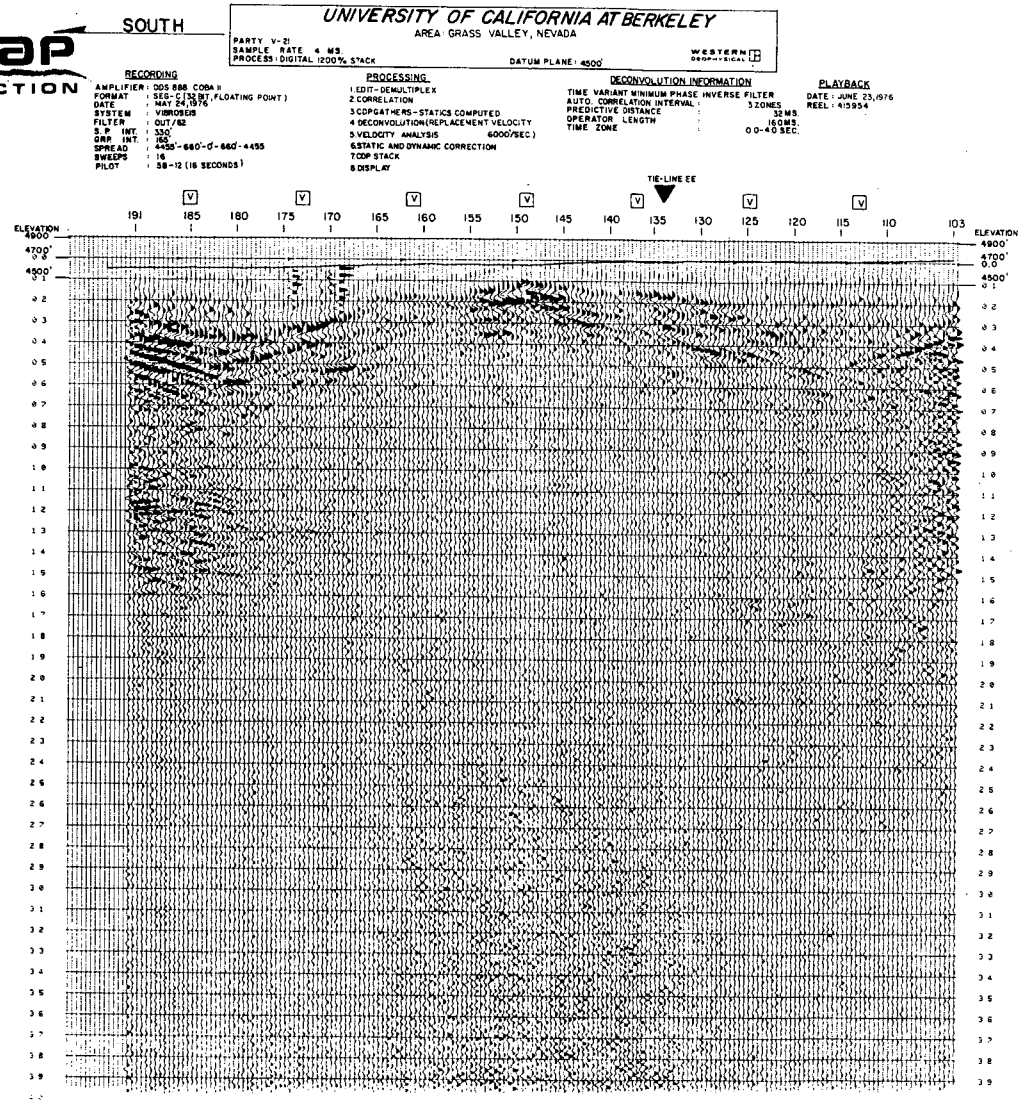

XBL 767-8848

Figure 4-19

Relative amplitude reflection profile over hot springs area, line EX.

Figure 4-20

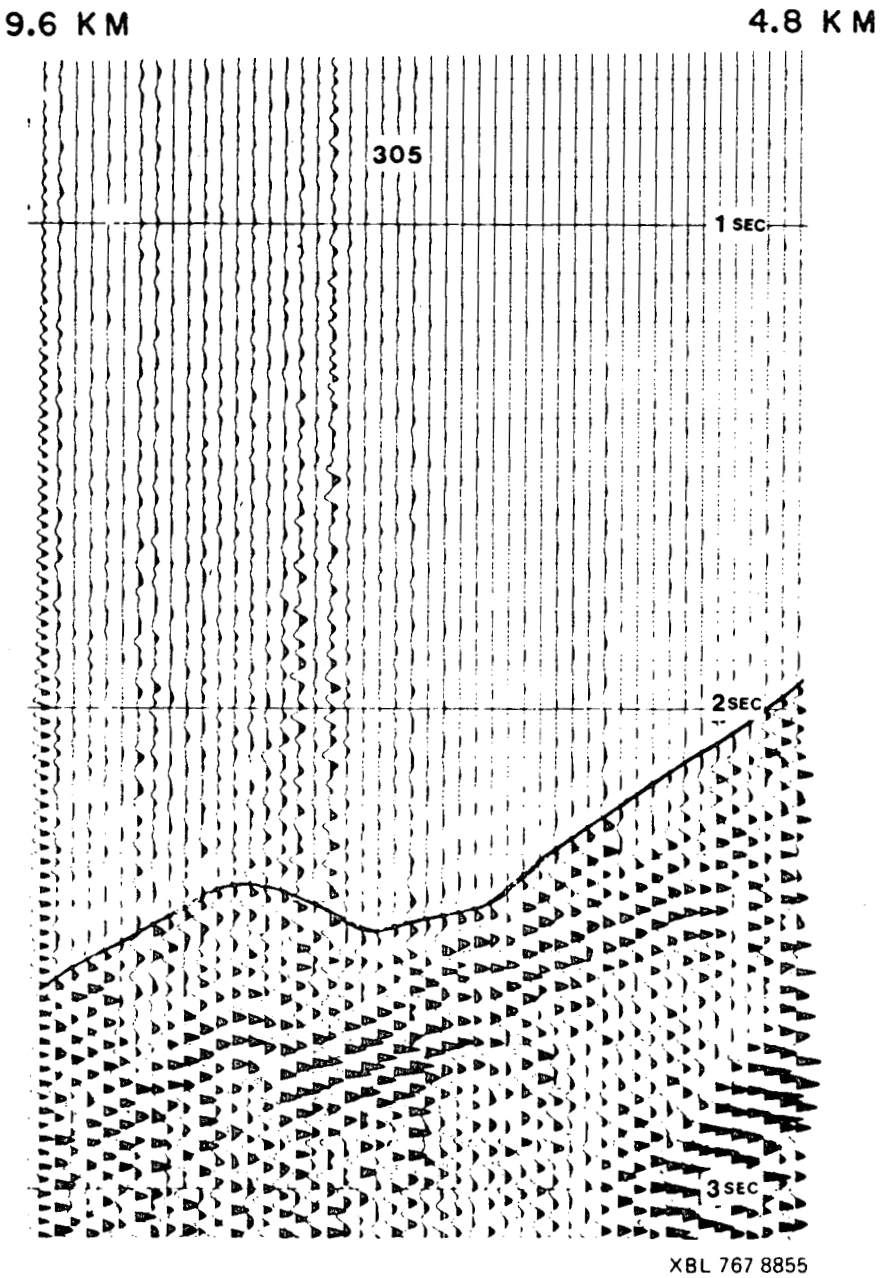

Refraction data between 2.0 east and 2.60 west, line E. Vibrator source is at point 305 or 7.5 west, line E. Note advance in data around km 0.0.

Figure 4-21

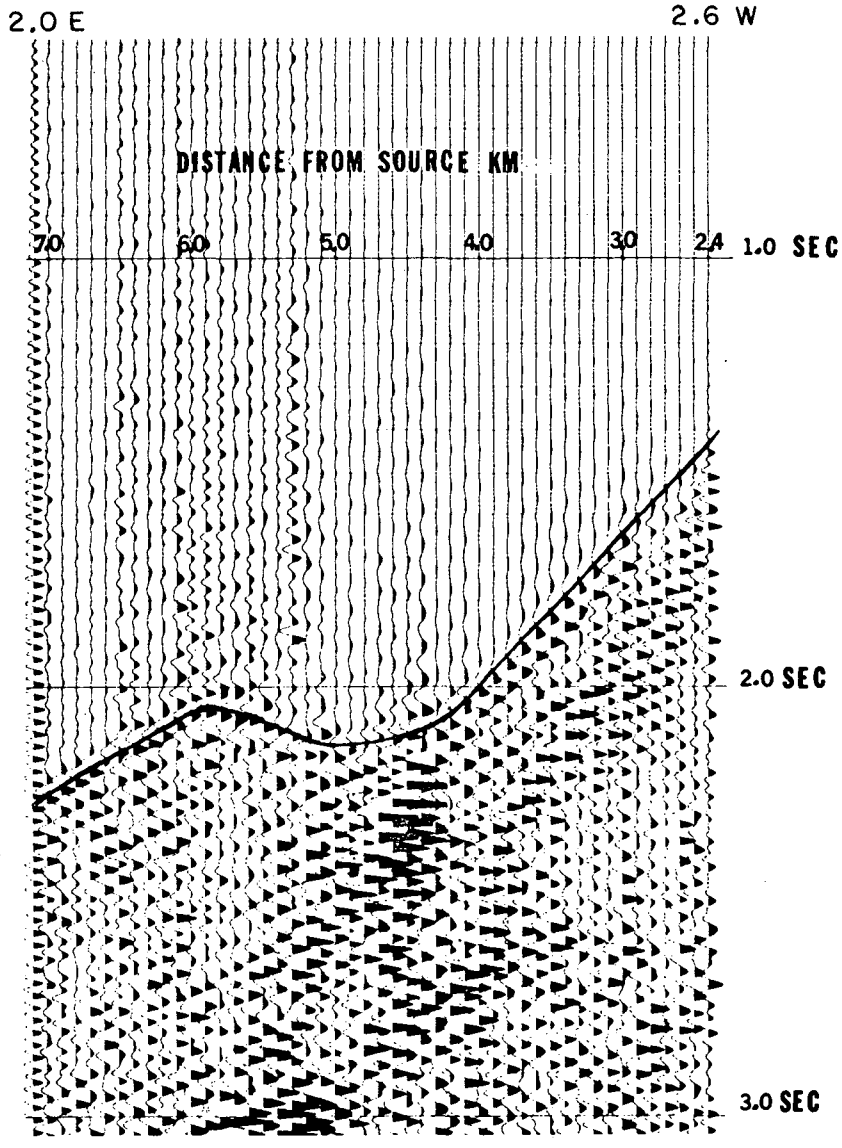

Refraction data along line E with vibrator source at 5.1 west line E. Note advance in data around km 0.0.

Figure 4-22

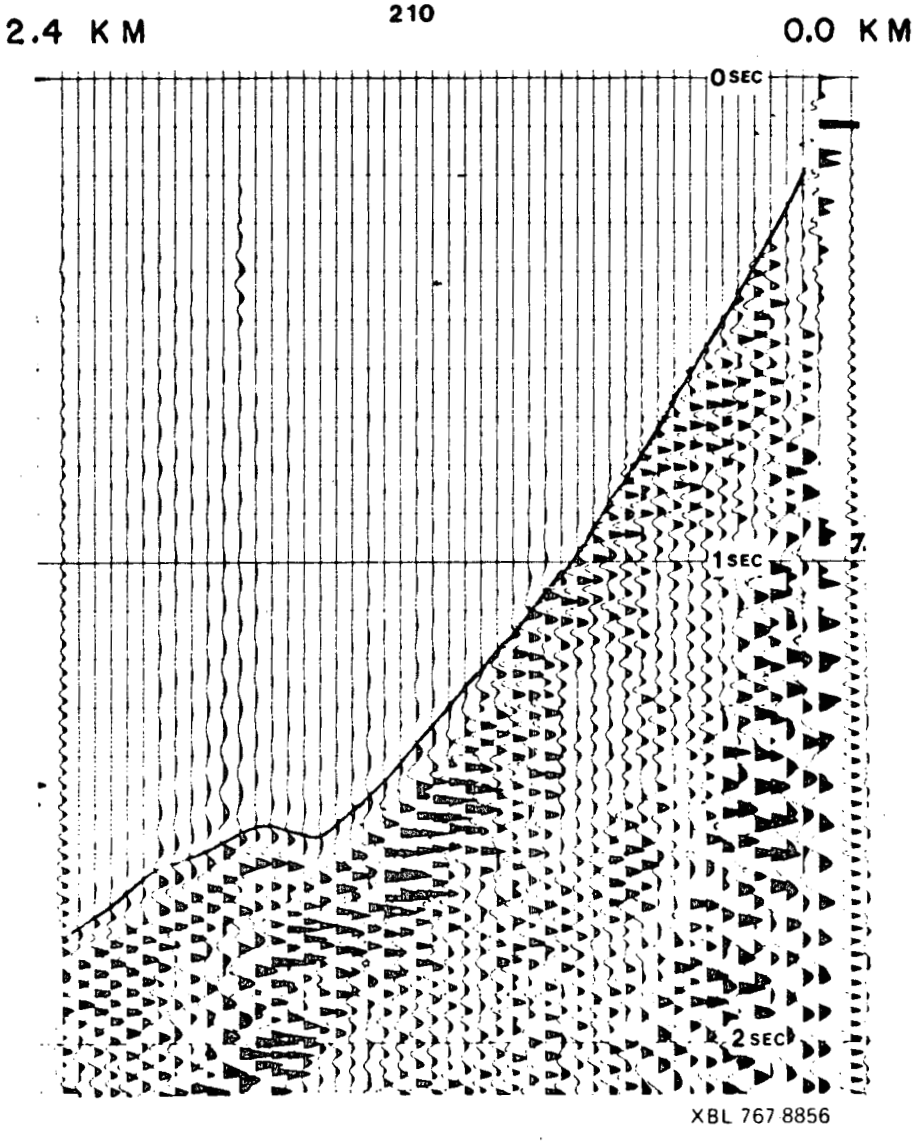

Refraction data along line E, vibrator source at 2.75 west, line E. Note the decrease in advance as source approaches 0.0 line E.

Figure 4-23

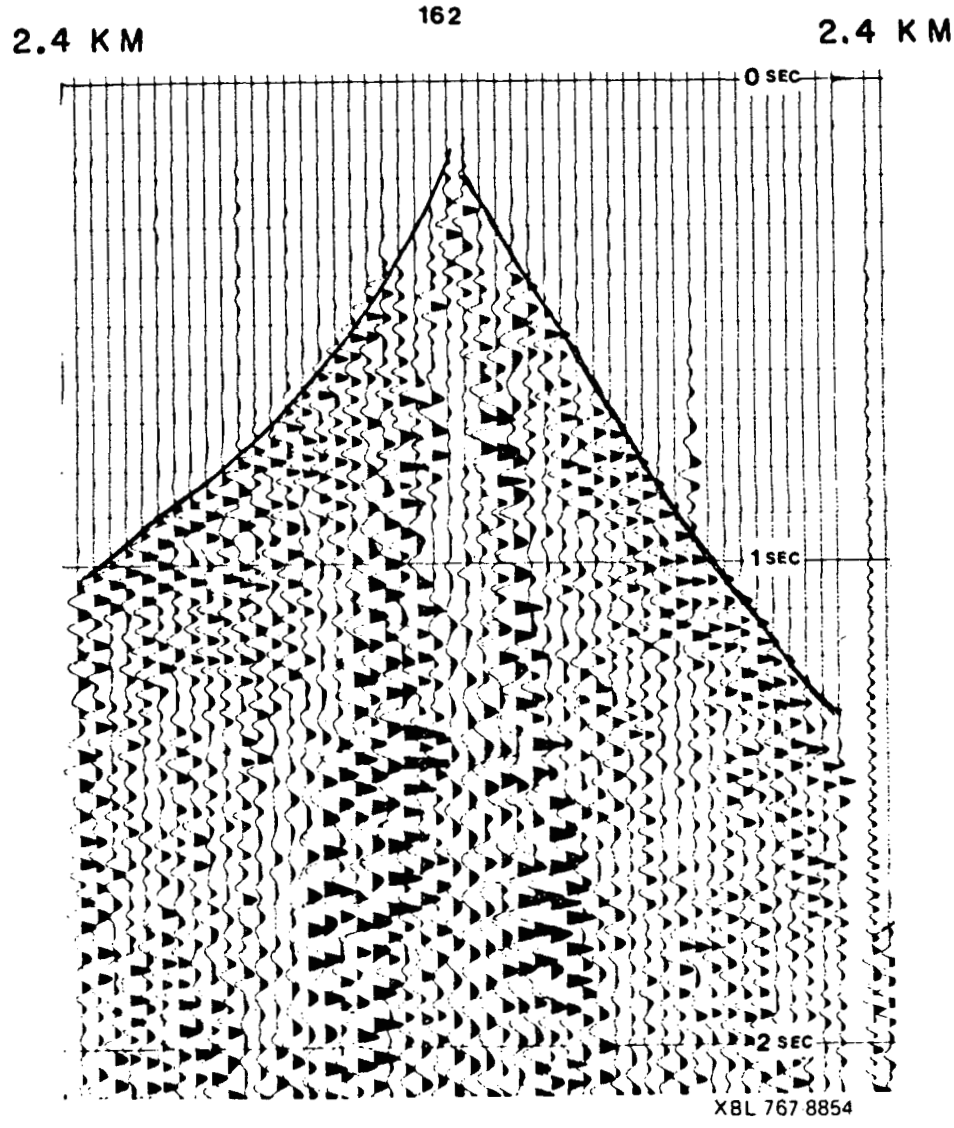

Refraction data along line E, vibrator source at 0.25 west line E. Note the lack of advance in data. Also note the higher velocities towards the east end of the line compared to the valley side or west end of the line.

Figure 4-24

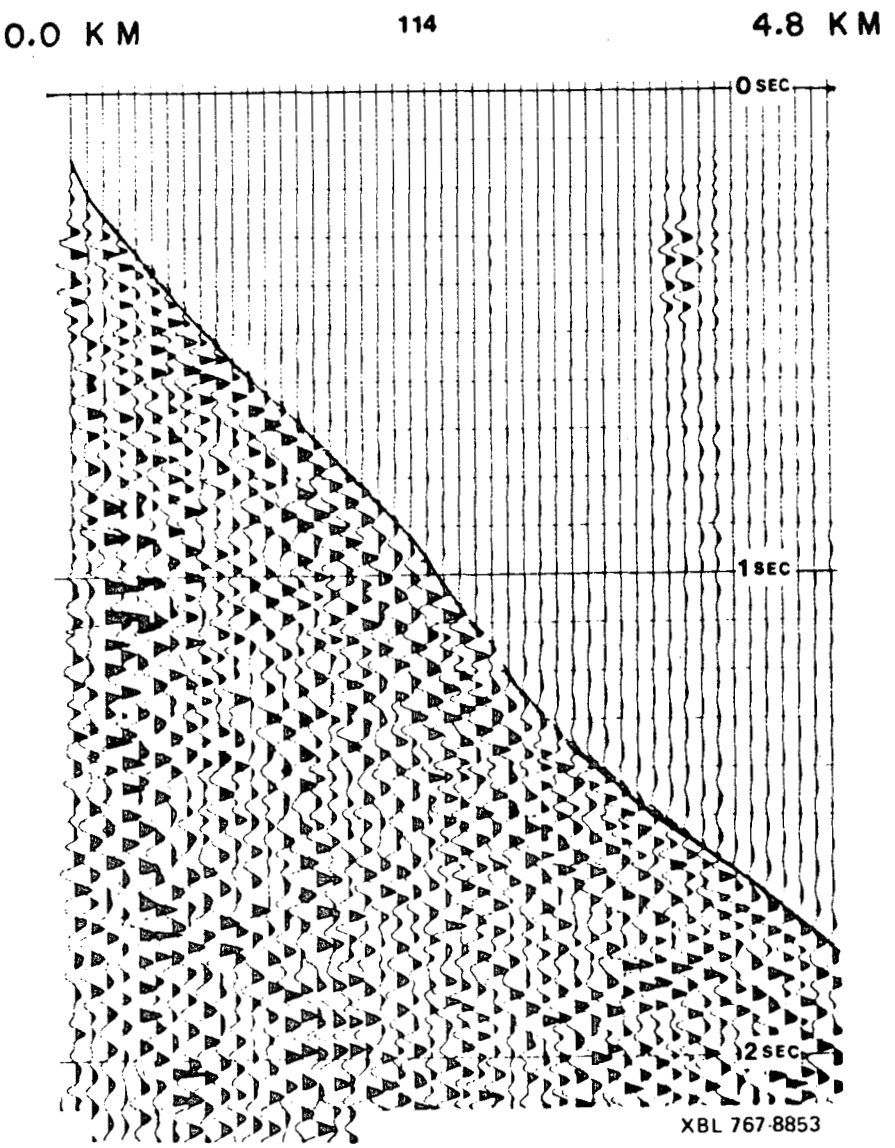

Refraction data along line E,
vibrator source at 2.0 east.

Figure 4-25

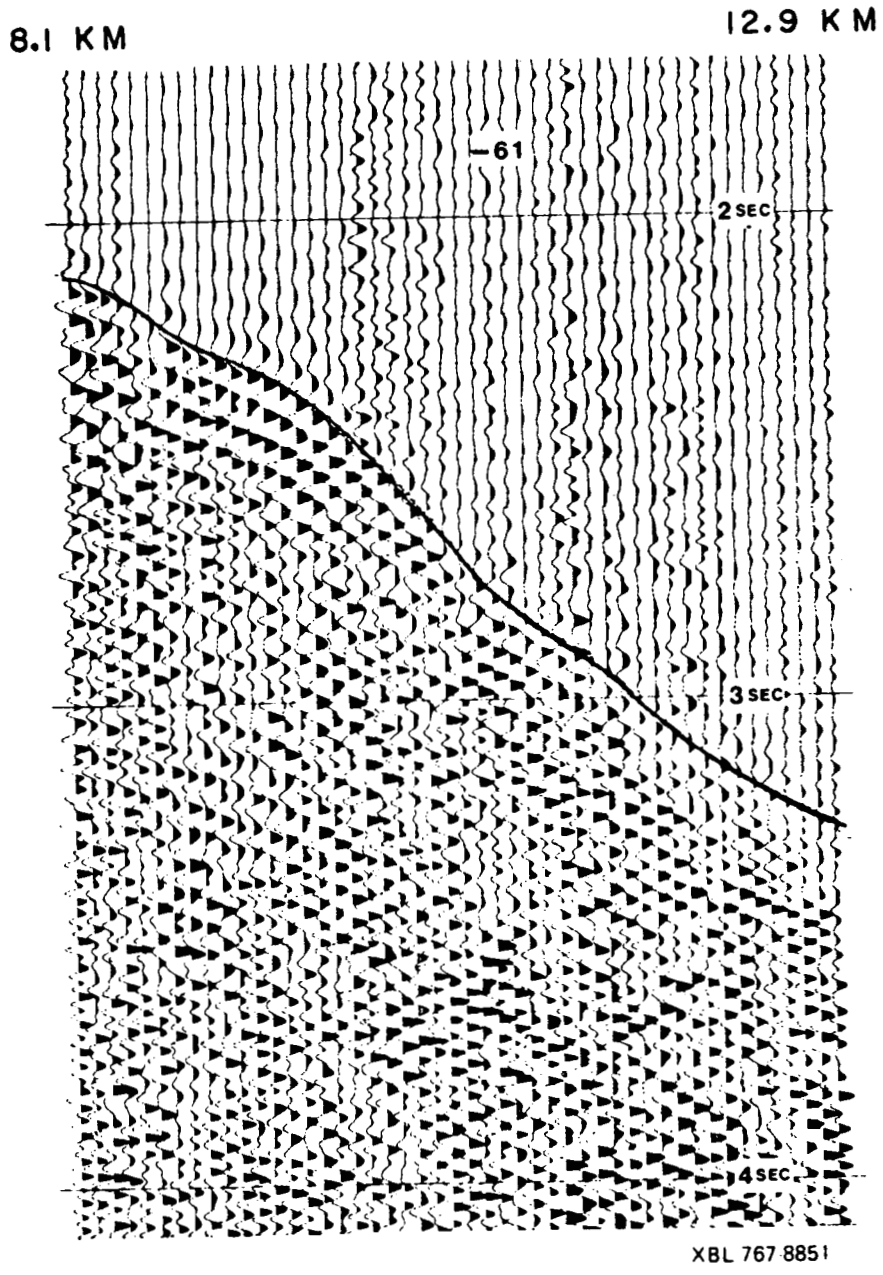

Refraction data along line E, vibrator source 7.1 km off east end of line E.

(February 1976). These stations are indicated by triangles in Figure 4-26. The stations indicated by circles recorded a smaller explosion (Banon) during August of 1976.

A wide east-west profile was selected, traversing the Battle Mountain heat flow high from east of Wells, Nevada to west of Lovelock, Nevada. Seismographs placed in pairs separated 50 to 70 km on radial lines from NTS included 14 temporary MEQ-800 smoked-paper instruments, one permanent station, BMN and the temporary array of radio-linked stations in Grass Valley. The stations were placed to determine local values of apparent P_n velocities and absolute travel times in a search for regional variations.

Because studies in Grass Valley revealed that P-wave delays of 0.2 to 0.4 seconds are common in sediment-filled valleys, care was taken to locate all stations on bedrock. Times on the MEQ-800 records could be read to ± 0.05 seconds or better. The times on the tape recorded stations in Grass Valley could be read to ±0.005 seconds. Because the large sources and the high gains used, there was little ambiguity in first arrival times. All stations were located by use of an altimeter and USGS topographic maps (15' and 7.5').

Pertinent station location information and travel times are given in Table 4-3. The raw times were corrected for clock drift and elevation differences using 4.0 km/sec.

Figure 4-26

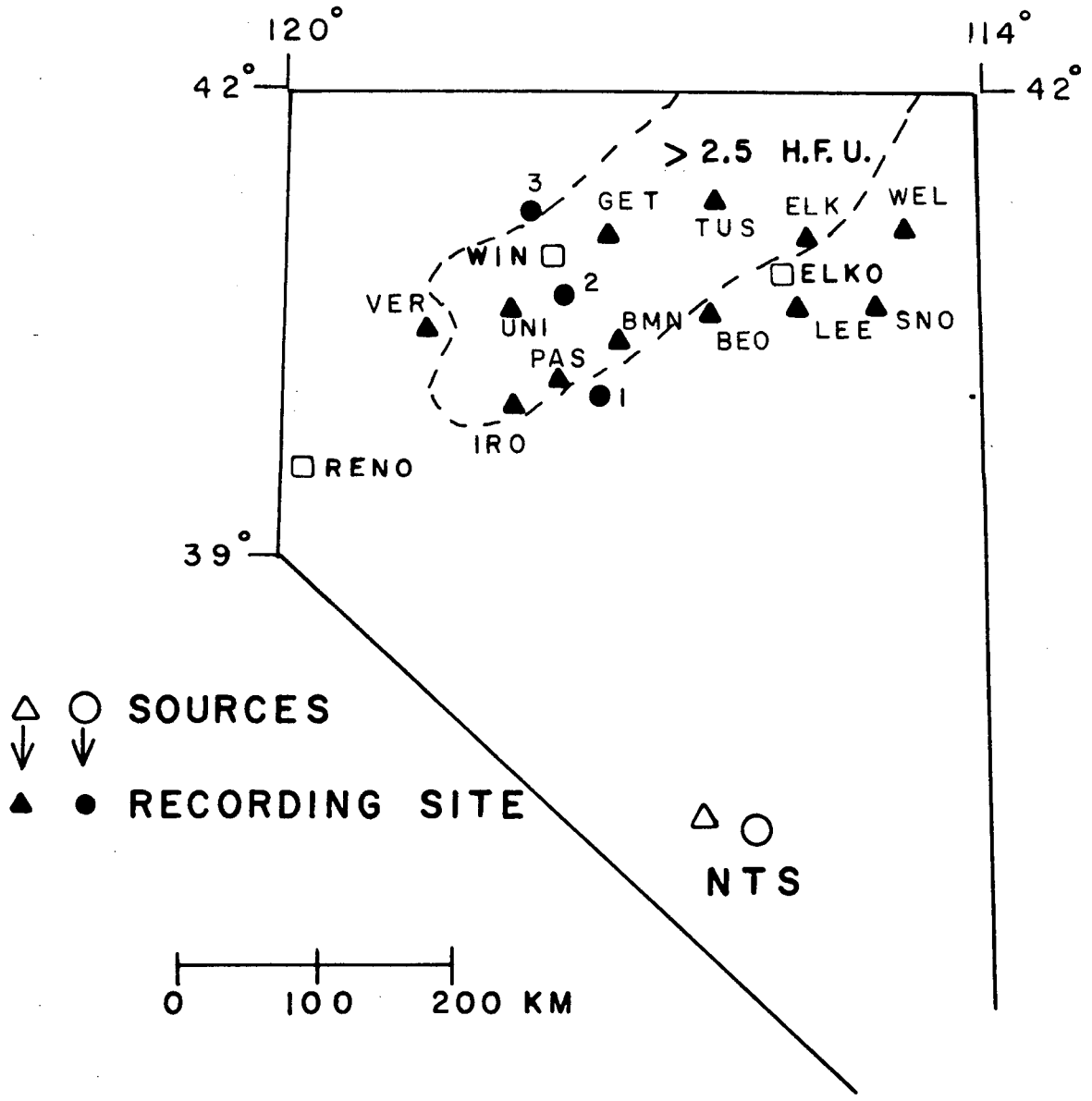

XBL 7710-10292

Station and source locations for regional refraction study in relation to high heat flow area.

Table 4-3

Station Locations & Arrival Times
For Regional Refraction Study

STATION	LOCATION		ELE (m)	Δ(km)	CORRECTED TIME (sec)
VER	40.415°N	118.799°W	1140	408.29	58.29
IRO	39.976	118.170	1288	339.56	49.55
UNI	40.549	118.120	1758	395.58	56.44
PAS	40.202	117.777	1525	349.08	50.69
GET	41.137	117.275	1667	438.65	61.68
BMN	40.431	117.222	1515	360.75	52.19
TUS	41.320	116.233	1909	450.15	63.47
BEO	40.640	116.442	1454	374.10	53.88
LEE	40.616	115.601	1798	379.28	54.76
ELK	40.963	115.660	1606	416.16	59.16
SNO	40.691	115.059	1818	399.41	56.88
WEL	41.155	114.726	1818	457.33	63.97
1	40.043	117.291	1503	340.66	49.88
2	40.589	117.603	1505	407.58	58.01
3	41.189	117.928	1424	476.62	67.16

	SOURCE INFORMATION		(UTC)	LOCATION		M_L
1-12-76	'Fontina'	1445	00.160	37.242°	116.420°	5.9
1-14-76	'Chesire'	1130	00.160	37.271°	116.488°	6.3
8-26-76	'Banon'	1430	00.168	37.125°	116.082°	5.1

A least squares fit to all arrival times at all stations gave a P_n velocity of 8.10 ± 0.07 km/sec, with an intercept of 7.69 ± 0.04 sec. For each station pair a P_n velocity was obtained using the differential travel time and the differential radial distance from NTS between the two stations. The resulting data are shown in Table 4-4.

Previous studies (Herrin 1972 Thompson and Burke 1974) suggest a regional P_n velocity of 7.8 km/sec in this region. In this study, except for one station pair (2-3), all apparent P_n velocities were higher than 7.8, with the average being 8.10. Because the lines were not reversed the ambiguity between P_n velocity and dip cannot be resolved, and a component of south dip is possible with lower velocity. Further discussion and possible models will be given in a following section on heat flow models.

4.7 Interpretation

4.7.1 Microearthquake Occurrence

Compared to other areas of microearthquakes in Nevada, the rate at Grass Valley of 1-2 events/day is not anomalous. Westphal and Lange (1967) and Stauder and Ryall (1967) reported rates of up to 31 events/day in the Fairview Peak area of west-central Nevada. Oliver et al. (1966) observed up to 208 events/day with S-P

Table 4-4

Reduced Values of P_n Velocity for Station Pairs in Regional Refraction Study

STA Pair	dT (sec)	dΔ(km)	Velocity (km/sec)
IRO-VER	8.74	69.37	7.93
PAS-UNI	5.74	46.72	8.14
BMN-GET	9.49	78.02	8.22
BEO-TUS	9.59	76.31	7.96
LEE-ELK	4.46	37.06	8.31
SNO-WEL	7.09	58.02	8.18
1-2	8.13	66.95	8.23
2-3	9.15	69.06	7.55

times less than 5 seconds in the same area. In a micro-earthquake study in the Black Rock Desert of northwestern Nevada (Butler, 1974) over 400 events were recorded in 30 days, with 300 of these events occurring in one swarm. These studies indicate seismicity equal or greater than that of Grass Valley.

In June, 1965 Oliver et al. (1966) occupied a site within a few kilometers of the southernmost station of the North Pleasant Valley array (Figure 4-1). Although the site was occupied for only 10 hours, a rate of 14 events/day was observed. (Oliver et al. (1966) concluded from their study of microearthquakes in Nevada that high-gain short-term recording can provide representative estimates of seismicity in a region.) Because the study used only one station and included events with S-P times of up to five seconds, the microearthquakes recorded could have been in the southern part of Grass Valley. Due to the short recording time and uncertainty in microearthquake locations, it is impossible to conclude that the seismicity in Grass Valley has changed from 1965 to the 1976 level. If the seismicity in Grass Valley represents aftershocks of the 1915 Pleasant Valley event (magnitude 7.5), one would expect only a 5/6 reduction in the 1965 rate by 1976, with typical decay laws (Utsu 1969). The reduction from the uncertain estimate of 14 events per day may well imply aftershock activity,

though resolution of this question would require a 5-10 year sample. Ryall (1977) concluded that aftershock activity in the rupture zone of $M \geq 7$ event in Nevada occurs for about a century. In addition, he also concluded that for this region the recurrence rate of $M \geq 7$ events is on the order of a thousand years, implying that if the activity in Grass Valley is related to a major event it is aftershock activity from 1915 rather than foreshock activity to another large event.

The Grass Valley events are off the northern end of the 1915 event fault trace. It has long been hypothesized that aftershocks are not always associated with the focus of the main shock, (Utsu, 1969). Stauder and Ryall (1967) observed that seismicity in the Fairview Peak area, which they associated with the 1954 magnitude 7.1 event, was concentrated towards the ends of the surface breakage. In a description of the 1915 event and its characteristics, Jones (1915) hypothesizes that the Pleasant Valley fault may extend further north of the observed surface breakage, up Panther Canyon separating the Sonoma and Tobin Ranges (Dashed Line, Figure 4-3), where much of the microearthquake activity is located.

A relation of the observed microearthquake activity to the hot springs is questionable. Although Russell (1896) described the fault associated with Leach Hot

Springs as post Quaternary, Jones (1915) found no evidence of movement during the 1915 event.

The northeast-southwest trend in the microearthquakes may be another indication that the activity is related to regional tectonic stresses rather than geothermal activity. Goldstein and Paulsson (1977), from a detailed interpretation of the gravity data in this area, hypothesized the existence of northeast-southwest trending normal faults extending between Panther Canyon and the Goldbanks Hills. Although it is not apparent in the topography, two northeast-southwest trending swells separate the -190 milligal contour, Figure 4-13, south of Leach Hot Springs and northeast of the Goldbanks Hills, indicating basement highs beneath the valley sediments trending southwest-northeast. These basement structures may reflect a physical barrier between the locale of microearthquake activity and the heat source responsible for the hot springs activity.

Figures 4-27 and 4-28 illustrate the seismicity of Nevada and recent fault breakage, respectively, from large events. It is apparent that Grass Valley is on the northern end of a seismically active zone. Suppe et al. (1975) hypothesized a rigid plate approximation to present day tectonics of the Western United States. In this model, Grass Valley lies in a zone of northwest-southeast extension (Figure 4-28b), consistent with the

Figure 4-27

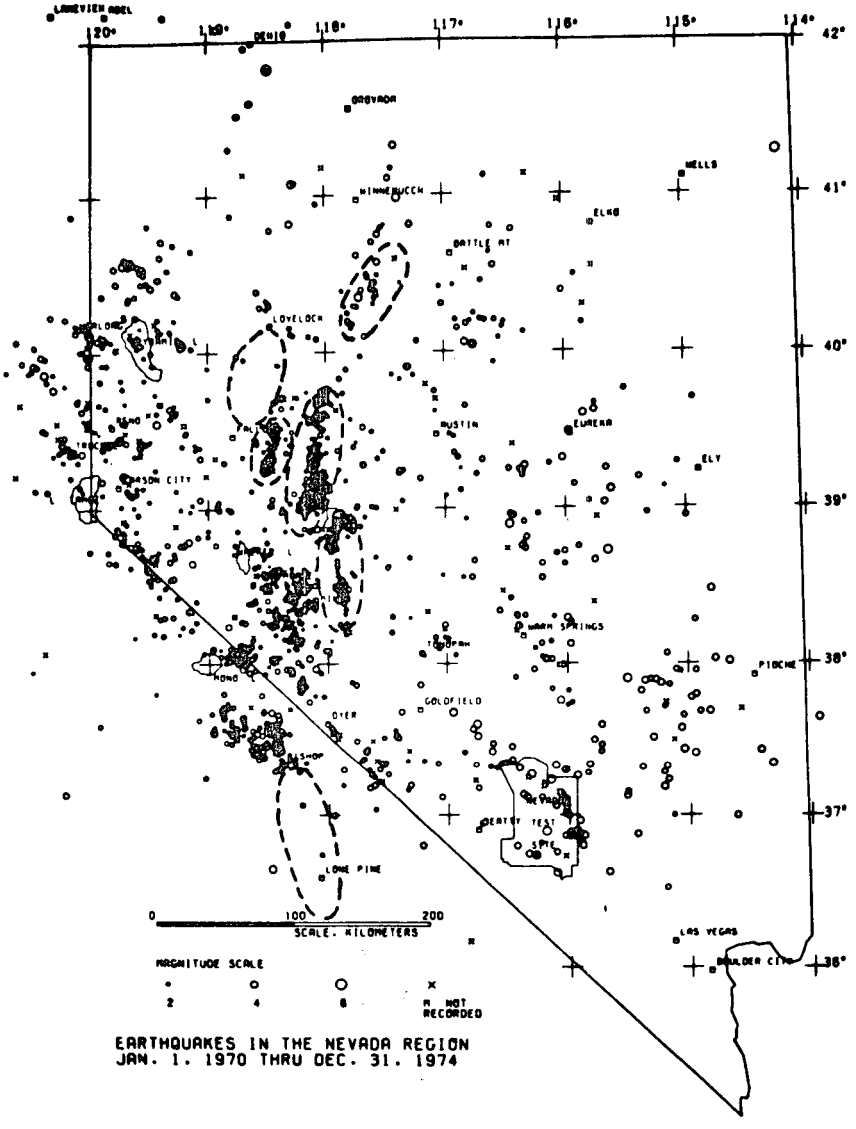

Nevada seismicity 1970-1974, M≥ 1, note the regions outlined by dashed lines. Grass Valley lies within the northern-most area. (Ryall, 1977)

Figure 4-28

(b)

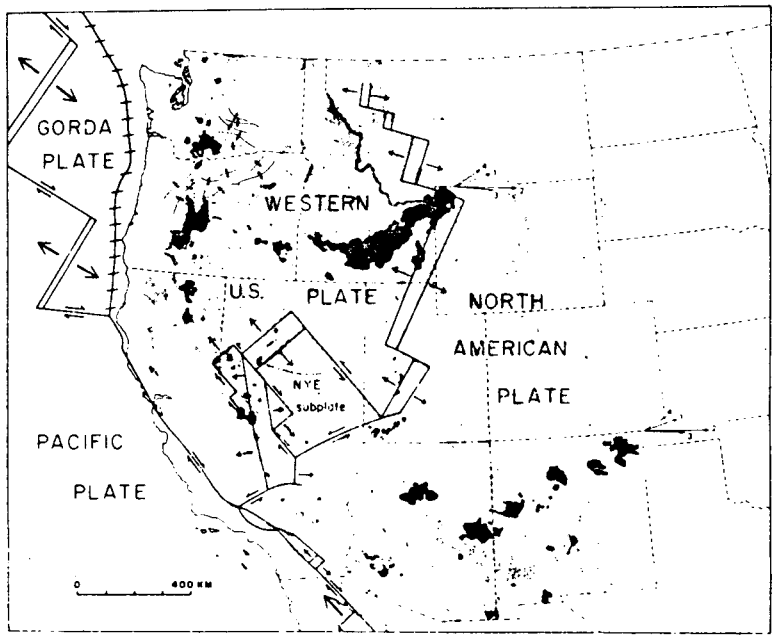

(a)

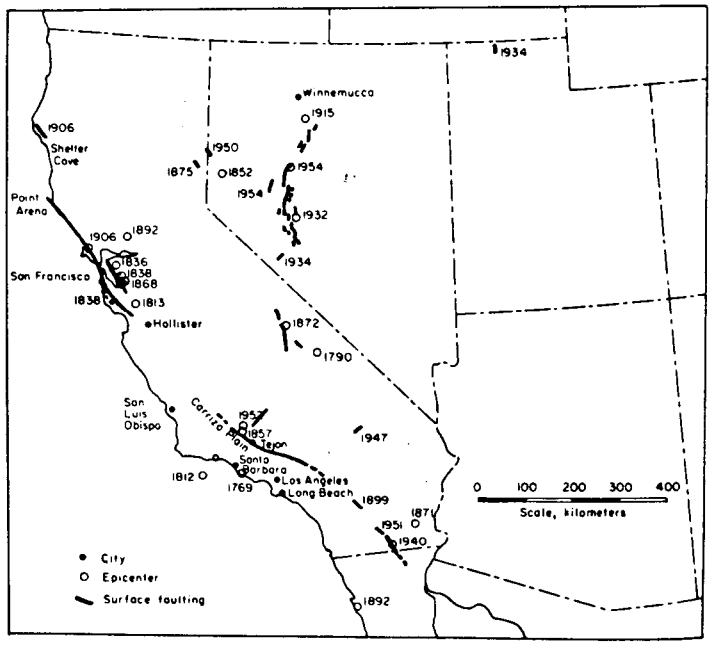

(a) Recent fault breakage in Nevada-California regions. (Ryall et al., 1966) 1915 marks the southern end of Grass Valley.

(b) Tectonic model of Western U.S. (Suppe et al., 1975)

fault plane solutions observed and the faulting mechanisms implied by the gravity interpretation of Goldstein and Paulsson (1977).

Considering regional tectonics and seismicity of Nevada, the observed microearthquakes thus are not unusual. The northeast-southwest trend of microearthquakes in Grass Valley can be explained as a termination fault to the 1915 Pleasant Valley fault. Stauder and Ryall (1967) suggest that microearthquakes at the southern end of the 1954 Fairview Peak fault breakage indicate a termination fault cross cutting the main fault. The presence of the microearthquakes at end of a major fault zone is further evidence that their origin is tectonic rather than geothermal. There is some evidence, however, that the microearthquakes may be an indication of higher than normal temperature gradients. All events located were at depths less than 8 kilometers. Although there are few other studies of microearthquakes in Nevada, most events are located at depths of 10 to 15 kilometers with very few events above 5 kilometers (Stauder and Ryall 1967, Westphal and Lange 1967, and Ryall and Priestly 1975). The shallow events in Grass Valley may indicate higher temperatures in this part of Nevada compared to areas where microearthquakes are occurring deeper. Although the data are not available at the present time, it would be interesting to compare the depth of microearthquakes across the Battle Mountain

heat flow high. Dietrick (1974) concluded that the process of stick-slip is an important mechanism for earthquakes on shallow faults. Because increasing temperatures inhibit stick-slip and promote stable gliding, the maximum depth of microearthquakes in a region may define a threshold temperature. This assumes that other mechanisms which influence stick-slip (stress, embrittlement of material and slip surface roughness (Stesky, 1977)) are constant from one region to another, which may not be the case.

In general, high b-values have been associated with aftershock sequences (Mogi, 1966), low stress (Scholz, 1968) and shallow earthquakes (Wyss, 1973). The b-values obtained using the two different coda formulae are 0.57 and 1.90. The b-value obtained using maximum amplitudes is 1.1. The correct value for comparative analysis is not known. The value of 1.1 is consistent with other Nevada studies. Given the difficulty in estimating the b-value it is impossible to make a definitive statement on its normalcy. A more quantitative measure of earthquake occurrence is required before any such evaluation can be made. The same problems with coda length magnitudes encountered at The Geysers occur in this study. Because of potential attenuation effects and variations of site geology, none of the b-values determined are reliable enough to support the conclusion that the Grass Valley microearthquakes indicate an

anomalous situation with respect to other Nevada microearthquakes. This situation may well pertain to all such attempts documented in the literature.

4.7.2 Microearthquake Source Parameters

The difficulty in obtaining magnitudes of the Grass Valley events also renders the moment versus magnitude relations a poor data set on which to base conclusions. As observed in The Geysers study, propagation path effects could not be separated from source effects, even at distances of 5 km or less. Of the source parameters determined, none showed a systematic variation with azimuth or depth except for corner frequency, which may be due to a combination of radiation pattern and Q effects. Additionally, in locating the events, the depths of most events were constrained at 2, 4, 6, 8 or 10 km. Conclusions about the variation of source parameters with depth or azimuth are thus tenuous at best.

The Q's necessary to raise the lower corner frequencies observed, when a single event was observed at different stations, to the highest observed value, were consistently close to 100. Previous microearthquake studies in Nevada used values between 250 and 400 to correct for Q. If the value of 100 had been used in the other studies, corner frequencies for the corrected spectra would be higher, possibly as high as the 20-40 Hz

range observed for most events in this study.

Whether any of the source characteristics are due to an anomalous situation related to geothermal activity cannot be determined from data. These events do not exhibit any significant properties that would suggest such a relation. Only when this area, or another area in Nevada, is shown to be a region of geothermal activity coinciding with microearthquake activity of obvious distinguishing characteristics, will studies of microearthquakes be significant in exploring for geothermal activity in Basin and Range environments.

4.7.3 Velocity and Attenuation

It is impossible to conclude from the velocity data alone that steam is present at depth beneath the hot springs area. The P-wave advance suggests that no steam is present. In a steam dominated environment, the lack of pore fluids alone would produce reduced P-wave velocities. That this effect may not dominate is evident in The Geysers data. The possibility cannot be ruled out that the structure or densification of material in the hot springs area, compensates for a velocity decrease from the presence of any steam. The near surface refraction studies indicate a maximum velocity between 5.0-5.5 km/sec. The magnitude of the P-wave advance indicates that a near-surface velocity increase alone cannot be responsible. The relatively broad gravity high supports

the notion of densification and associated high velocity distributed over a significant depth.

P-wave velocity data may be useful in determining broad structural contrasts. Assuming an average velocity of 3.0 km/sec for the sediments and 4.5 km/sec for bedrock, the maximum delay of 0.3 seconds would predict an alluvial thickness of 0.9 km at mid-valley. Thompson (1959) calculated that the valley fill in a Basin and Range valley (near Austin, Nevada) to be 1.65 km thick. He assumed a density contrast of 0.5 g/cc with a gravity anomaly of about 28 milligals. Assuming the same density contrast, the gravity anomaly of 15 milligals for Grass Valley yields a depth to basement of 0.88 km, which agrees well with the P-wave result.

P-wave delay studies can thus be useful in determining general structure of an area, especially if additional velocity data are available from refraction studies. The method is relatively efficient. In this study with two people, one source per day from the nearby mine, 6 mobile stations, and two reference stations, approximately 2 weeks were required to gather the data. Compared to other studies such as gravity or electrical methods this is quite fast. Also, the data reduction is not as involved compared to other methods. Depending upon background noise and size of source, the maximum distance from source to receiver

could be 100 km. If announced nuclear explosions were available as in this study, the major prospects in the Western United States could be covered. Because 4.5 Hz geophones were used, teleseismic data were not available. If longer period geophones had been used, the source of the P-wave would not be the limiting factor, but rather the size of the target structure. That is, at longer wavelengths it is difficult to delineate fine structure.

As stated previously, the detail in the attenuation measurements did not approach that of the P-wave delay studies. However, the effects seen in the vicinity of the hot springs, appear so anomalous that few if any other areas in Grass Valley are likely to exhibit such behavior. The attenuation analysis was prompted by the peculiar visual records at stations very near to the hot springs. As seen in Figure 4-12, the effect is limited to a very small region around the hot springs ($\sim$1km). On the other hand, in The Geysers region the preservation of high frequency waves was demonstrated over a region several kilometers wide. It is not known if high Q is associated generally with geothermal activity. The anomalous structure in Grass Valley is of limited size. At other measurement sites in Grass Valley no unusual attenuation effects were noted. We conclude therefore, that P-wave velocity and attenuation analyses if useful in delineating the geothermal reservoir in

Basin and Range structures, indicate an anomalous zone in Grass Valley of very small size for commercial prospects. Rather, it may be that such effects indicate only shallow conduits in the hydrothermal system.

4.7.4 Reflection Profiles

Figure 4-29 presents an interpretation of valley structure from the reflection data along line E. As expected, a series of normal faults is indicated, downthrown toward the valley. The general structure agrees very well with the structure implied by the P-wave delay and gravity data. The reflection data delineate fine structure that is averaged out in the gravity and P-wave data. The areas of interest in relation to geothermal activity are probably the major faults which may extend sufficiently deep to permit circulating water to reach the heat source. From these data it seems the most likely location for a geothermal reservoir would be near the edges of a valley. In this case, it would be near 0.0 on line E in Figure 4-29, where the major boundary fault could be intersected at 5000 to 7000 foot depth. There is an interesting zone of reflectivity at 1.7-2.0 sec in the 0.0-1.0 E region, possibly multiple energy, but an attractive alternative is deep structure associated with a possible reservoir.

Also evident in Figure 4-29 are the different layers in the valley sediments. To determine thickness and

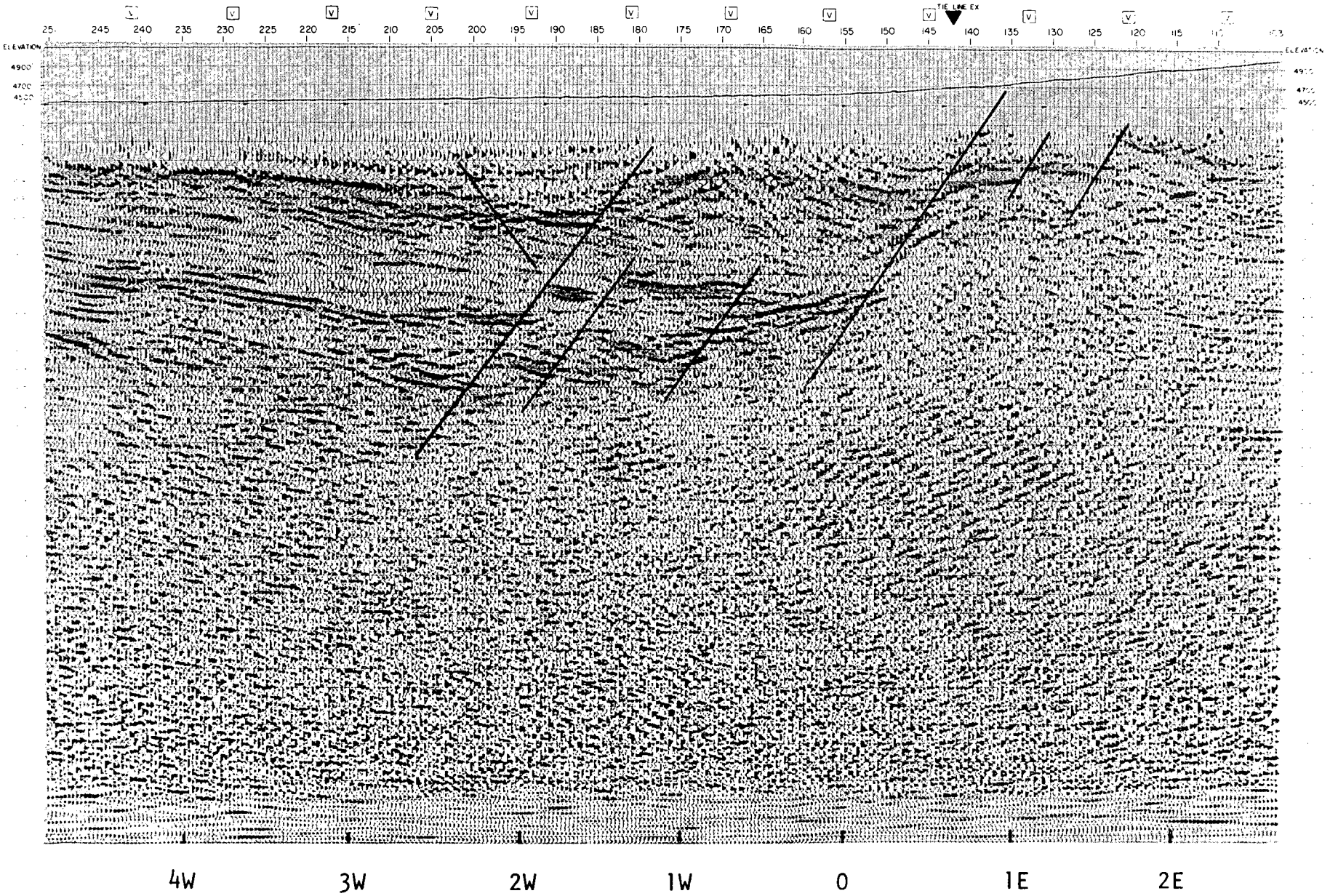

Figure 4-29

Interpretation of a migrated reflection profile along line E. The symbol ▽ at the top of the section indicate locations of velocity analysis.

XBB 760-10053

velocity for these beds, data from the refraction line was complemented by velocity analyses from the reflection data (the points of velocity analysis are marked by V at the top of the reflection profile). Several examples of the reflection velocity analyses along line E are shown in Figures 4-30, 4-31 and 4-32. The right half of Figure 4-31 is an example of a velocity analysis in an area of complex structure such as point 157 on line E (Figure 4-29), where lack of coherent reflected energy precludes definition of clear rms velocity peaks (black dots on plots). This is particularly true in the hot springs area (Figure 4-33).

From the refraction data and velocity analysis of reflection data and velocity analysis of reflection data, a finite element model of line E was constructed (Figure 4-34). The computer program used for calculating synthetic seismograms was developed by Smith (1975). The resulting synthetic seismogram section (Figure 4-35) should be compared to Figure 4-21. The significant features of Figure 4-21 are the negative apparent velocity between 5.0 - 6.0 km and the large amplitude increase around 4.5 km. These features are apparently due to the high-velocity path up the fault zone providing first arrivals propagating in the reverse direction for about 1 kilometer back from the fault trace. Amplification results from the constructive interference of this

Figure 4-30

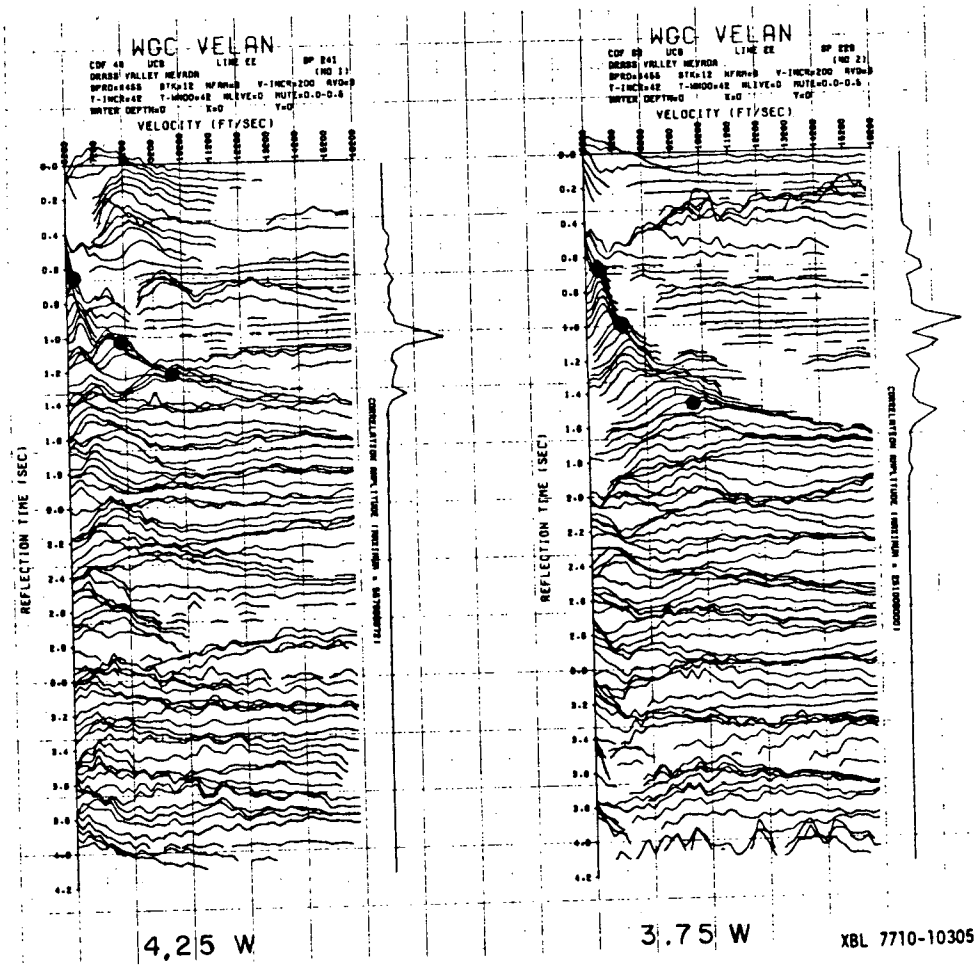

Velocity analysis at 4.25 west and 3.75 west line E. Black dots are points of maximum reflection, indicating velocity transistions or layering within the section.

Figure 4-31

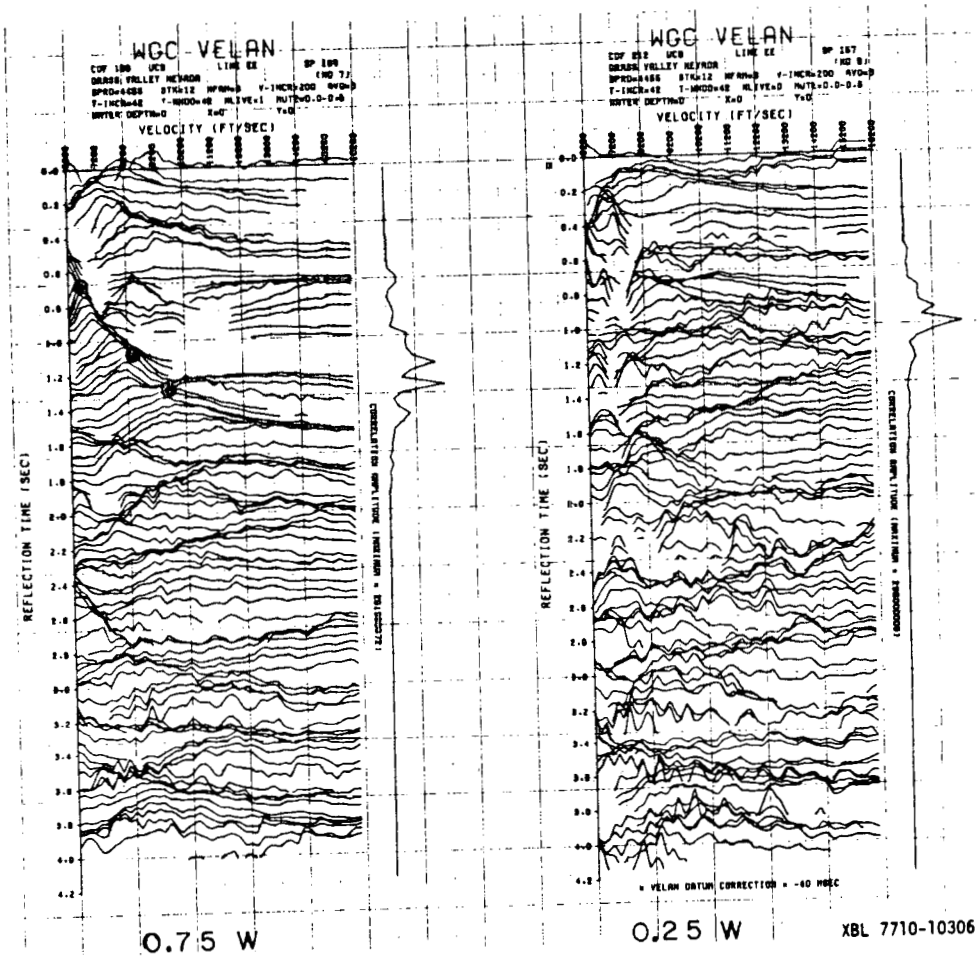

Velocity analysis at 0.75 west and 0.25 west line E. Note the lack of reflections over the fault zone at 0.25 west.

Figure 4-32

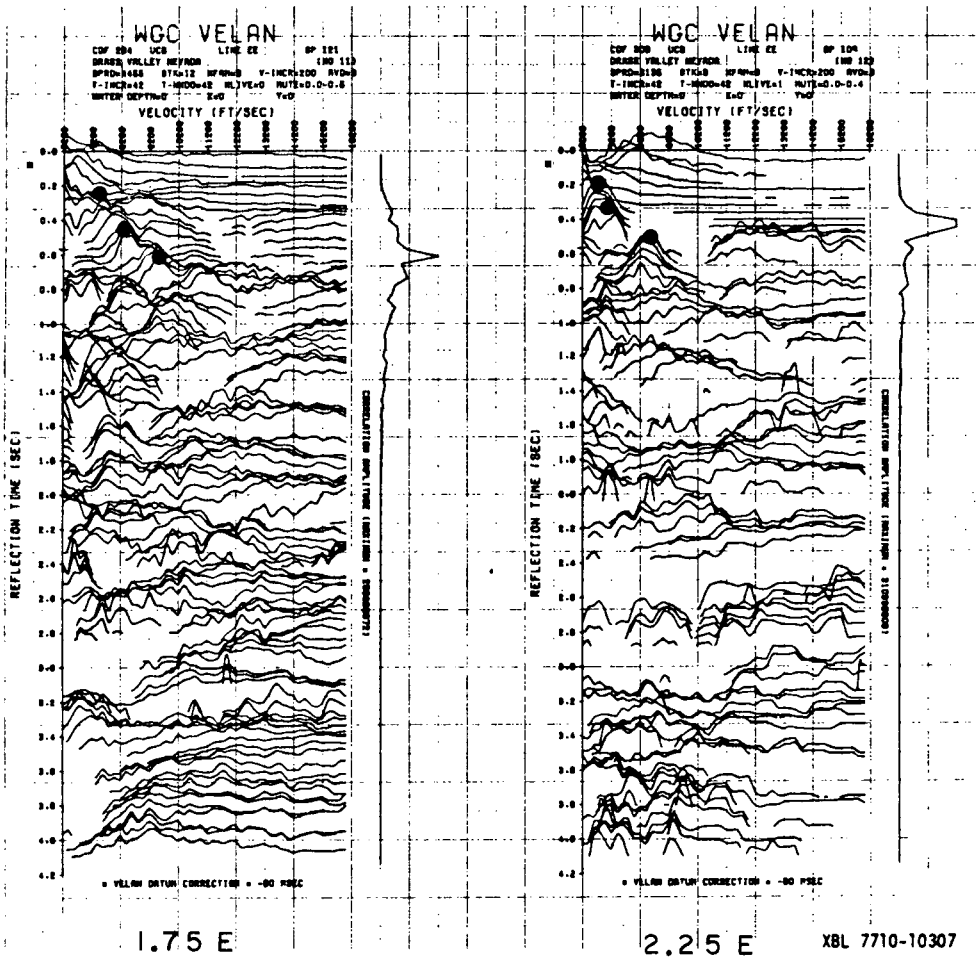

Velocity analysis at 1.75 east and 2.25 east, line E. Note that the reflections are closer to the surface, indicating thinning sediments.

Figure 4-33

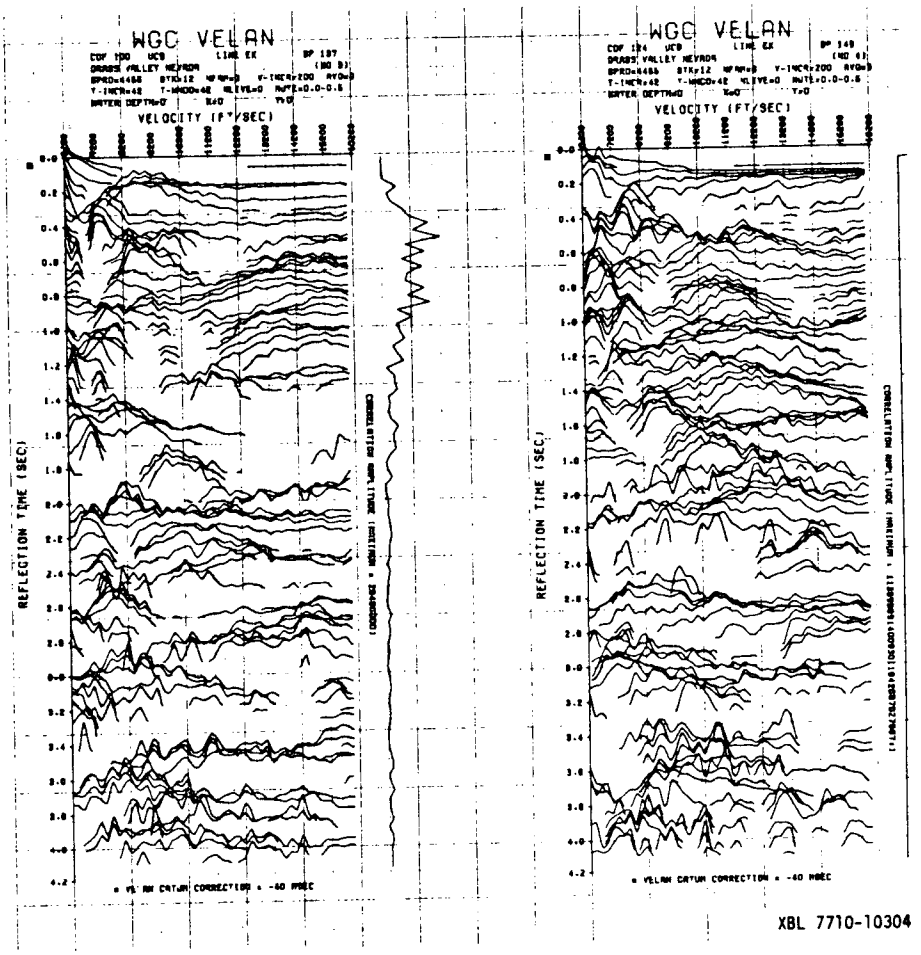

Velocity analysis at points over the hot springs. Note the lack of good reflections.

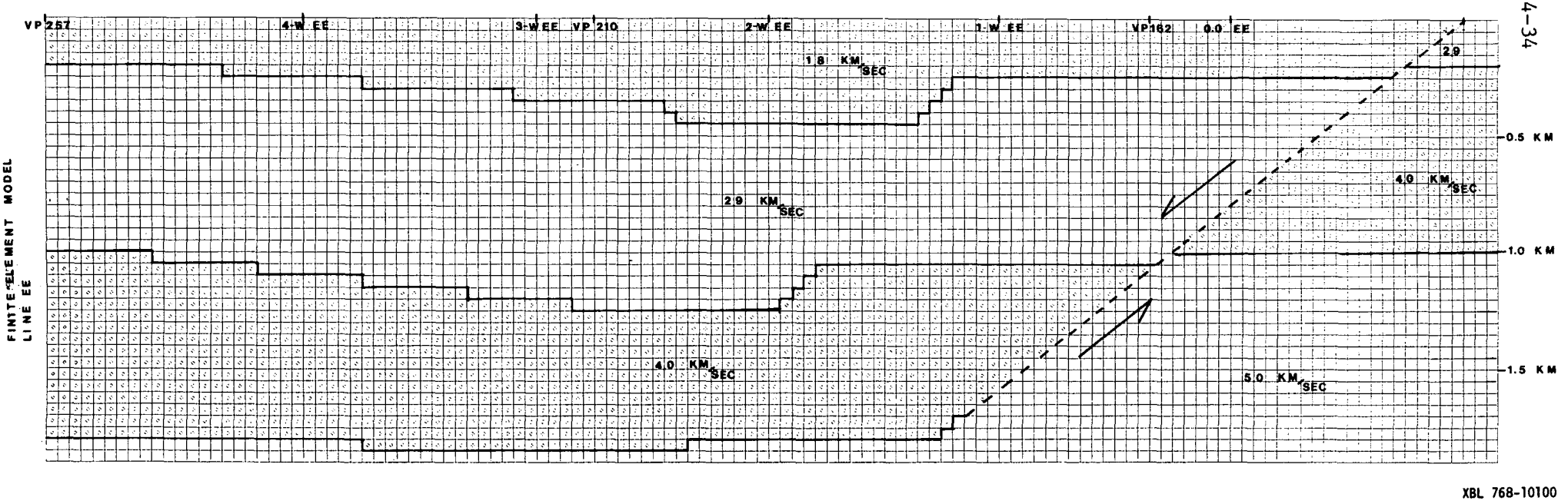

Figure 4-34

Finite element model of Grass Valley between 5.1 west and 1.25 east, line E.

Figure 4-35

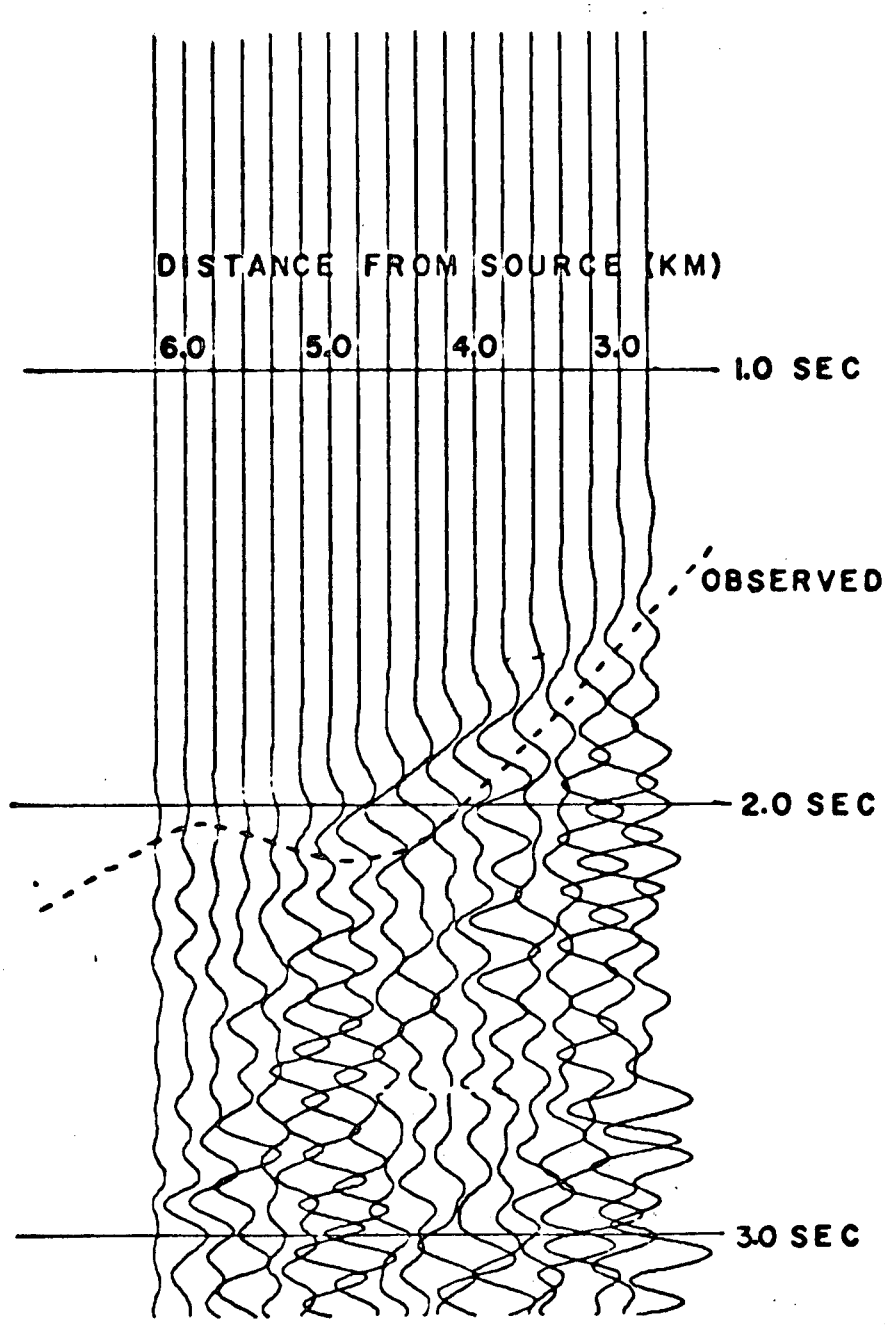

Synthetic seismograms from finite element model. Compare this figure to Figure 4-21.

arrival with the "normal" first arrivals. As can be seen in Figure 4-35, the calculated result is in fair agreement with the observed, illustrating the validity of the model in explaining the observation. The negative apparent velocity is not as pronounced as the observed. The amplification effect is illustrated although it is at 5.0 km rather than 4.5. The discrepancy between the calculated and the observed could be reduced by refinement of the model. The indicated adjustment would be a combination of higher velocity on the upthrown fault block and a shift of the high velocity to the west, perhaps representing silicification in the down-thrown block.

Closer comparison of Figures 4-35 and 4-21 show that the observed frequencies are much higher than the calculated. This is due to the minimum element size allowed in modeling the desired region. The maximum allowable number of nodes in the program was 5000. The area 2 km by 6.25 km modeled gives a minimum element size of 50 meters. To reduce ringing, attenuation and dispersion, it is recommended by Smith that eight elements per wavelength be used. Fewer elements per wavelength reduces the amplitudes. Even for 5.0 km/sec, appreciable attenuation begins at 12 Hz. From the observed data in Figure 4-21, the frequency of the waves are 20-30 Hz, the source being a Vibroseis with a 12-60 Hz sweep. The simplest model source is a step function

or boxcar of arbitrary length. However, to reduce ringing it is recommended that a pulse length of 3.7 times the propagation time across one element be used, again limiting the choice of parameters. Finally, because of the time (computer as well as human) involved in fine-tuning the model further computation is not warranted at this stage of the exploration. A single run to obtain the information to plot Figure 4-35 cost $175.00. It is possible that finite element modeling of refraction data, if computationally economical, may provide constraints on reservoir structure in areas of moderately complex geology.

4.7.5 Regional Refraction Study

As noted earlier, the apparent regional P_n velocities from this study are higher than generally thought true for the upper mantle in this region. Because all the data are from unreversed lines, and because the interval over which data were obtained is only 135 km, there are several possible explanations for the discrepancy.

The first and most probable cause would be a sloping crust-mantle interface. If one assumes a true velocity for the mantle material of 7.8 km/sec, an average crustal velocity of 6.25 km/sec, and an apparent velocity of 8.1 km/sec, the resulting dip would be 2.75°.

A value of 2.75^{o} is not unreasonable. This would imply a crustal thinning to the north of approximately 6.5 km over 135 kilometers. Although these values are plausible, an argument against such an explanation is that the high apparent P_n velocities are observed over a very wide region, much wider than the high heat flow region which also may be due to crustal thinning. Assuming the thinning has occurred long enough ago to allow heat transfer through some 30 km of crust, i.e., $t \sim L^2/h$ where t = time, L = linear dimension, h = diffusivity, and with L = 30×10^5 cm, h = 0.01 cm^2/sec, then t = 9×10^{14} sec or 28 million years. This also assumes that the additional heat flow is due to an increased gradient below the crust, rather from sources within the crust. If the thinning is a relatively recent phenomenon (10-15 million years) then only the seismic manifestation would exist, with the elevated heat flow occurring later.

A second explanation for the high P_n velocity would be a systematic velocity increase in the crust as one proceeds northward. Assuming a 60 km distance over which the change would have to occur, a 30 km crust, and an average velocity at the southern station of 6.25 km/sec, the average crustal velocity increase necessary to account for an apparent velocity increase to 8.10 km/sec (from the true value of 7.8) would be to 6.5 km/sec over the 60 km distance. Although this 4%

crustal velocity increase is not drastic, a systematic velocity increase over the entire sampled area does seem unlikely. It should be noted that Hill and Pakiser (1966) observed a northerly increase in crustal velocity along a line from Eureka, Nevada to Boise, Idaho, although the increase did not occur until a region 50 km north of the area studied in this experiment. On the other hand, Hill and Pakiser did note a near-surface, northerly velocity increase (2.0 km/sec to 4.5 km/sec) in an area common to this study. A thin 4-5 km thick layer suggested by the Hill and Pakiser model could account quite easily for the apparent velocity increase.

A final explanation for the high P_n velocity is that it is real. Because the lines were not reversed this possibility cannot be totally discounted. However, gravity data (Woollard and Joesting 1964) indicate crustal thinning may be occurring over part of the region. Again, though, the Bouguer gravity high observed (approximately 20-30 m/gal) does not correspond to the total area over which the high P_n velocity is observed. Also, crustal velocity increase would probably imply an associated density increase.

It seems, therefore, as if a combination of factors may be involved in an explanation of the observed P_n velocity of 8.1 km/sec. Additional refraction work with reversed lines, and possibly deep reflection work through the high heat flow area can provide data

necessary to resolve the present ambiguities. An additional explanation consistent with normal P_n velocities will be presented in the next section on heat flow modeling.

4.7.6 Heat Flow Modeling

To gain additional insight on the significance of seismological data in geothermal resource exploration, the data were considered combined with regional and local heat flow studies. The resulting analysis is not intended to be an exhaustive or comprehensive study of all probable models for the heat flow anomalies observed in a Basin and Range environment. Other studies, such as those of Sorey (1975), Cathles (1977) and Lachenbruch and Sass (1978), are better directed toward such purpose. This study is intended to explore the compatability of conclusions from seismological and heat flow data.

Figure 4-36 shows the available heat flow data in Grass Valley contoured in heat flow units (hfu), 10^{-6} cal/cm^{2}sec. The data are from heat flow studies in 82 shallow to intermediate depth holes, (18 to 400 meters, Sass et al., 1977). The depths of the holes were selected on the basis of a careful study to determine at which depths reliable data could be obtained in Basin and Range valleys. A first set of deep wells (200 meters) was drilled to determine at which depth surface effects and water flow would no longer influence

Figure 4-36

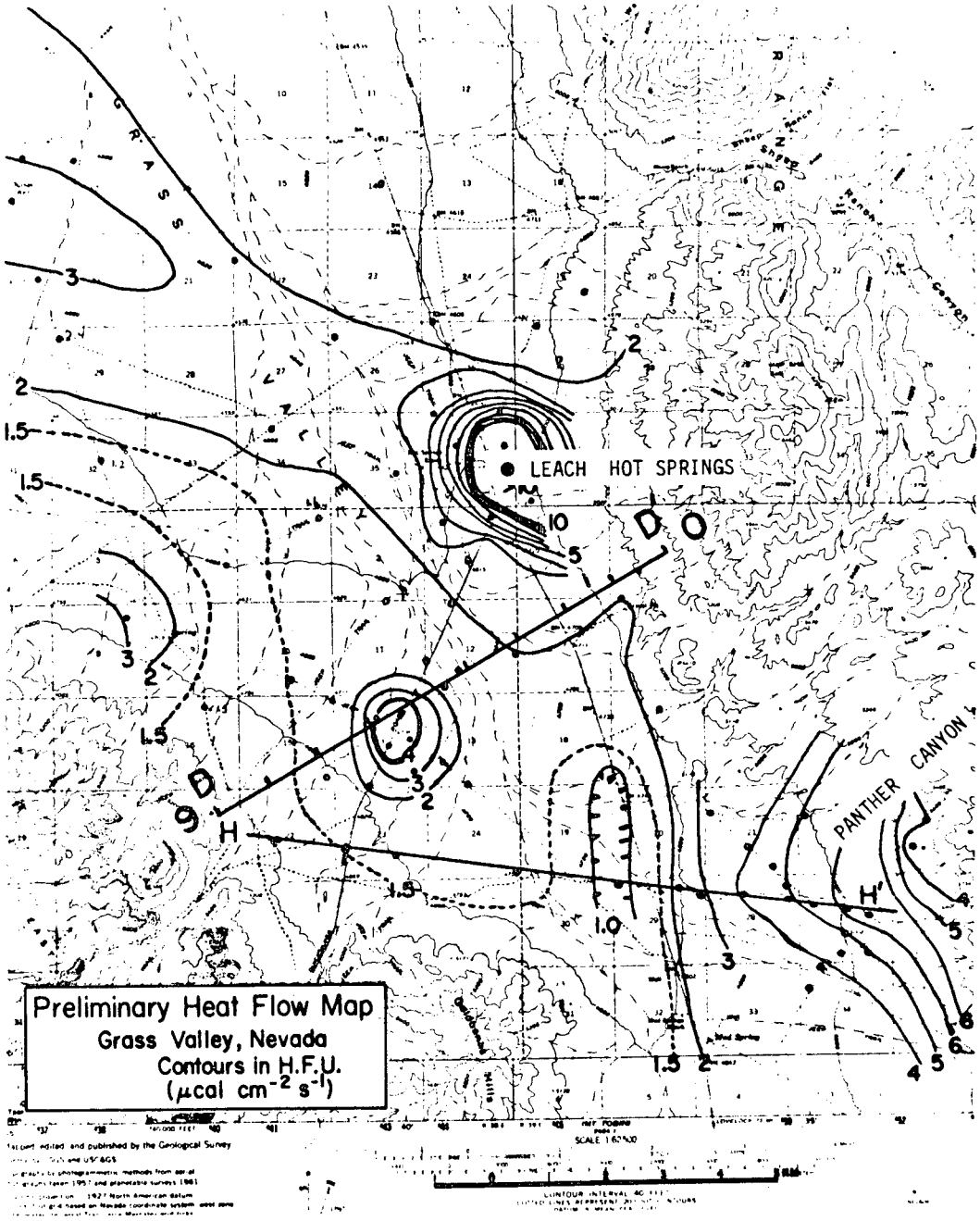

Contoured heat flow values in Grass Valley (hfu) (Lachenbruch et al., 1977).

the data. On the basis of these holes, intermediate depth wells were drilled (50-150 meters). Both the deep and intermediate holes were carefully backfilled and sampled every 5 meters for thermal conductivity. Based on these holes and the observations of shallow temperature versus temperature gradients and heat flow at depth, a series of shallow holes (15-18 meters) were drilled to obtain detail around known anomalies or isolated deeper holes. A single sample of cuttings from the lowermost 5 meters of the shallow holes was retained for conductivity measurements.

Two different methods were used to determine thermal conductivity. After obtaining cores (deep and intermediate holes only) a needle probe was used at spacings between 5 and 15 centimeters along the core. Sass et al. (1977) state a reproducibility of $\pm 3\%$ for these measurements. When cores were not available, the thermal conductivity of the solid component of porous sedimentary rock was determined from measurements on cuttings. These measurements were made every 5 to 10 meters for all holes. The reproducibility is estimated to be $\pm 10\%$ for this method.

Temperature logs were run in all holes within a few days of completion and at least once a month after completion. It was found that the temperature gradients in the upper 10-20 meters are systematically higher than

at greater depths, most likely due to the lack of water above 20 meters, causing lower conductivity.

The measured conductivities varied between 2 and 6 x 10^{-3} cal/cm sec deg for the sediments. Because of poor sorting the conductivities varied from hole to hole, but generally increased with depth. Although values as high as 15 x 10^{-3} cal/cm sec deg were found for bedrock in an adjacent valley, 10 x 10^{-3} cal/cm sec deg was taken as the thermal conductivity of bedrock for modeling purposes. For a detailed description of the heat flow study in Grass Valley, the reader is referred to Sass et al. (1977).

As can be seen in Figure 4-36, there are three anomalies of interest. The first and most obvious is the high heat flow associated with the hot springs area. Two additional anomalies are also apparent, the 4 hfu near the center of the valley along line D, and the 6 hfu anomaly near the east end of line H. It was fortunate lines D and H, along which the P-wave and gravity data were taken, traversed the 4 and 6 hfu anomalies, respectively.

The high heat flow at the hot springs is probably due to the flowing water; however, the other two anomalies have no surface expression of water flow, such as sinter deposits or springs. For this reason, purely conductive models were used to model the observed heat flow at the

4 and 6 hfu anomalies. Several conductive models were tested for fit to the hot springs heat flow. Also, several mass flow models were used to explain the heat flow in the vicinity of the hot springs.

These three areas were modeled with an integral finite difference program (Lippmann et al., 1977) using the seismic and gravity data for information on alluvial thickness overlying bedrock in the valley. The conductivity used in the models are not the exact values found at each site, but are meant to be average values for the different sediment and bedrock materials. Except for special cases, the conductivities were within the limits of measured values. In the models requiring mass flow, the density of water was 0.9 g/cc, having a heat capacity of .878 cal/deg mole. No porosity or permeability is required by the program. The flow is handled by keeping the mass flow between nodes constant. The user is required to pick the element size and flow rates such that the velocity of flow is physically reasonable. In this case the total flow was known and the element size was adjusted to give reasonable velocities of flow. The background heat flow for most conduction models was 3.5 hfu. This value was chosen because it was the average value of heat flow measured between the valleys in the mountains, presumably bedrock. Steady state conditions were considered to be present when the maximum

temperature change was less than 0.005^{0}C for two successive time steps ($\Delta t \approx 10^{4}$ to 10^{5} years).

Figure 4-37 compares the P-wave delay, gravity and heat flow data for line D. As can be seen, there are highs in all the data sets around kilometer 6 on line D. The P-wave delay and gravity highs can be explained by an upwarp in the basement structure beneath the sediments. But, could an upwarp in a higher conductivity material (i.e., basement) with a constant heat flow from beneath, also explain the high heat flow?

To answer this question, 5 kilometers of the western end of line D was modeled by several purely conductive models shown in Figure 4-38. The thickness of the sediments was determined by P-wave and gravity data. The thermal conductivity of the sediments, K, was varied between 2 and 6 x 10^{-3} cal/cm sec deg. Also shown in Figure 4-38 are the results of the modeling, with the observed and calculated heat flows and isotherms in ^{o}C.

Figure 4-38 demonstrates that it is quite easy to account for the observed heat flow without the presence of any convection effects beneath the surface. The observed heat flow matches the calculated heat flow very well, except where the bedrock (K=10) thins towards the valley edge. These low observed values may be due to water descending along the faults bounding the valley, thus suppressing the heat flow.

Figure 4-37

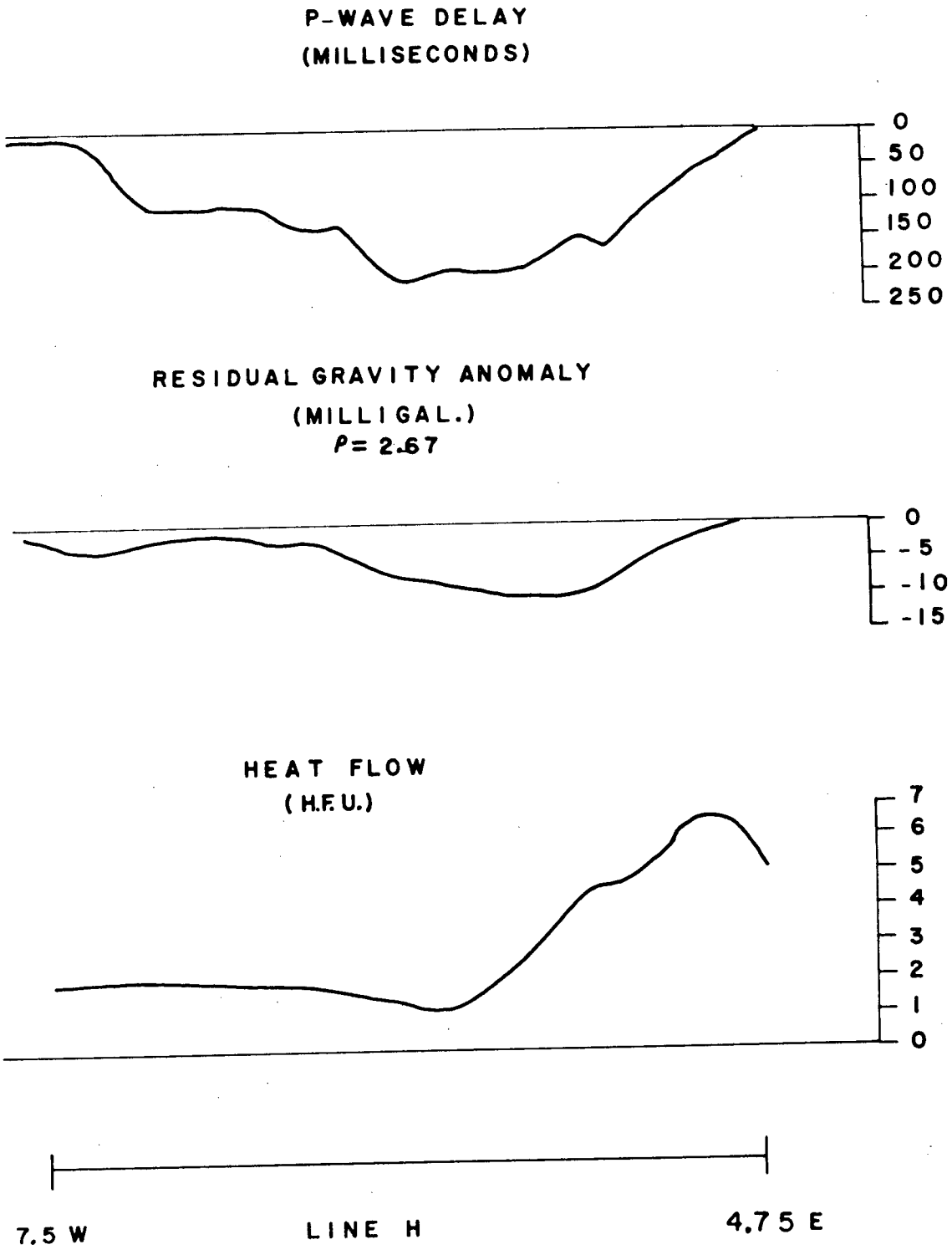

P-wave, gravity, and heat flow data along line D in Grass Valley.

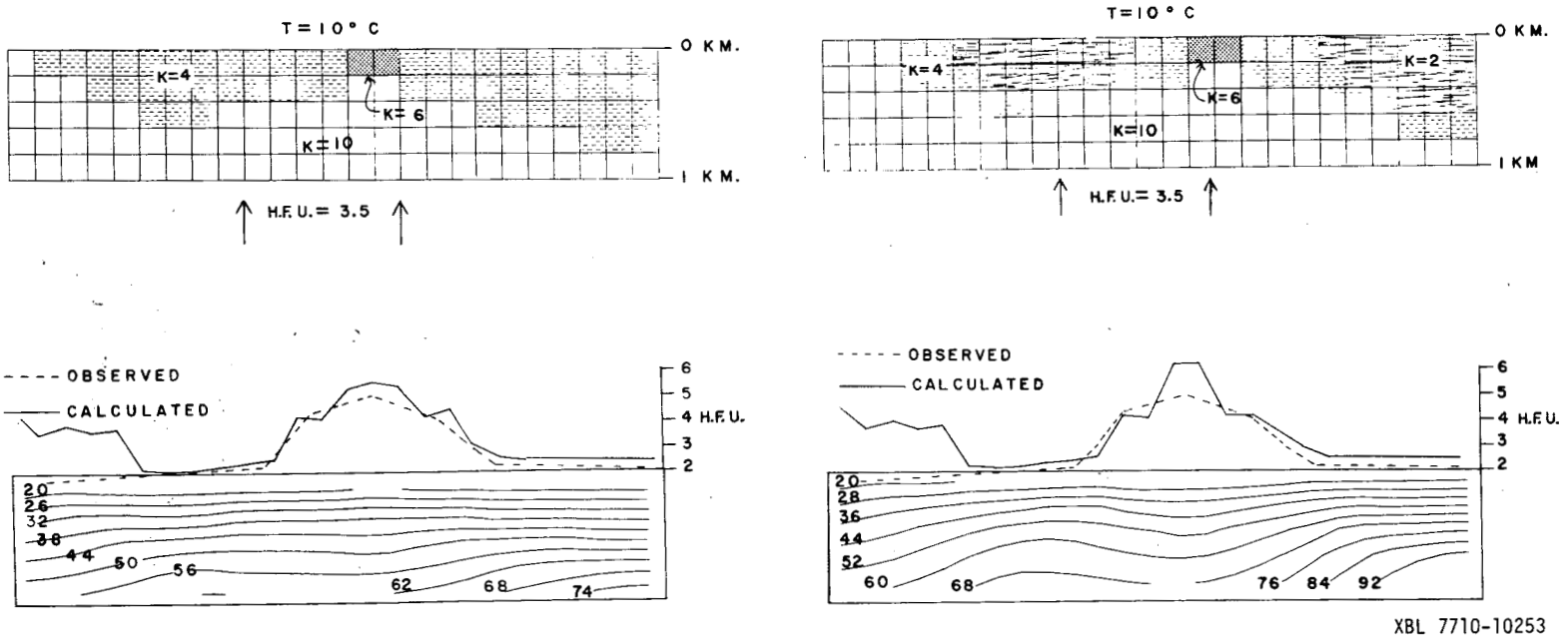

Figure 4-38

Several conductive models, boundary conditions and results for line D. Isotherms in ^{o}C.

Subsequent to this modeling, a deeper hole was drilled (400 meters) through the center of the 4 hfu anomaly. Bedrock was encountered at 350 meters, with a normal conductive gradient to this point. However, further drilling encountered temperatures no higher than 56°C. Therefore, it seems that water is descending along faults bounding the valley, is heated to 56°C, then circulates along basement faults to the sediment-basement interface. Small heat flow anomalies of this type may be due to shallow hydrologic effects coupled with anomalous conductivities from bedrock highs not evident in the surface topography or geology.

Figure 4-39 shows the P-wave delay, gravity and heat flow data along line H. In this case there is poor correlation between heat flow and basement topography. Also, the size of the heat flow anomaly is much larger than the anomaly observed on line D.

Figure 4-40 shows several models used to explain the observed heat flow by conduction. Assuming reasonable conductivities the calculated heat flow could not be made to equal the observed heat flow along line H. Also of note are the isotherms in the models. If conduction is responsible for the heat flow anomaly, the temperature beneath the low conductivity layer in the center of the valley at 1 km depth would be over 100°C. These models reflect one of the limitations of modeling a geological

Figure 4-39

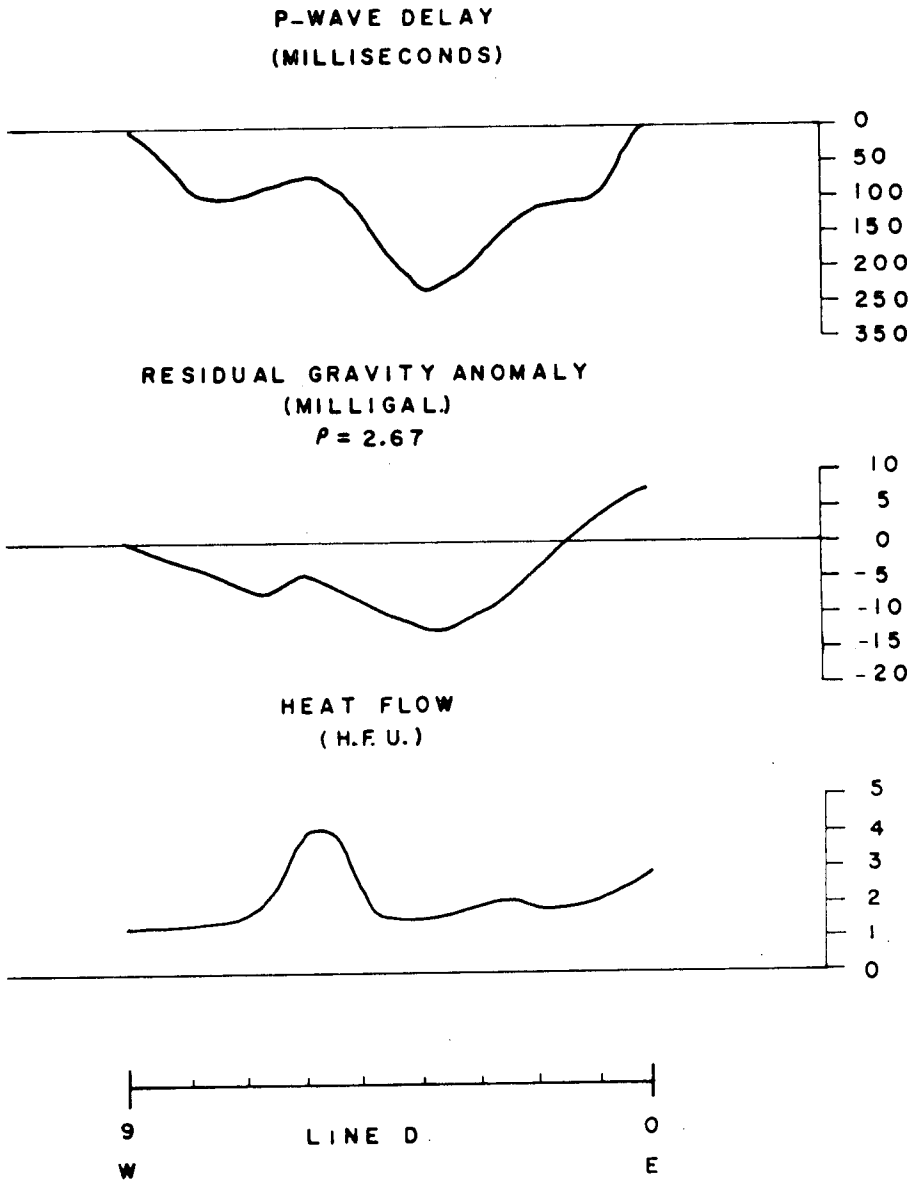

P-wave, gravity and heat flow data along line H in Grass Valley.

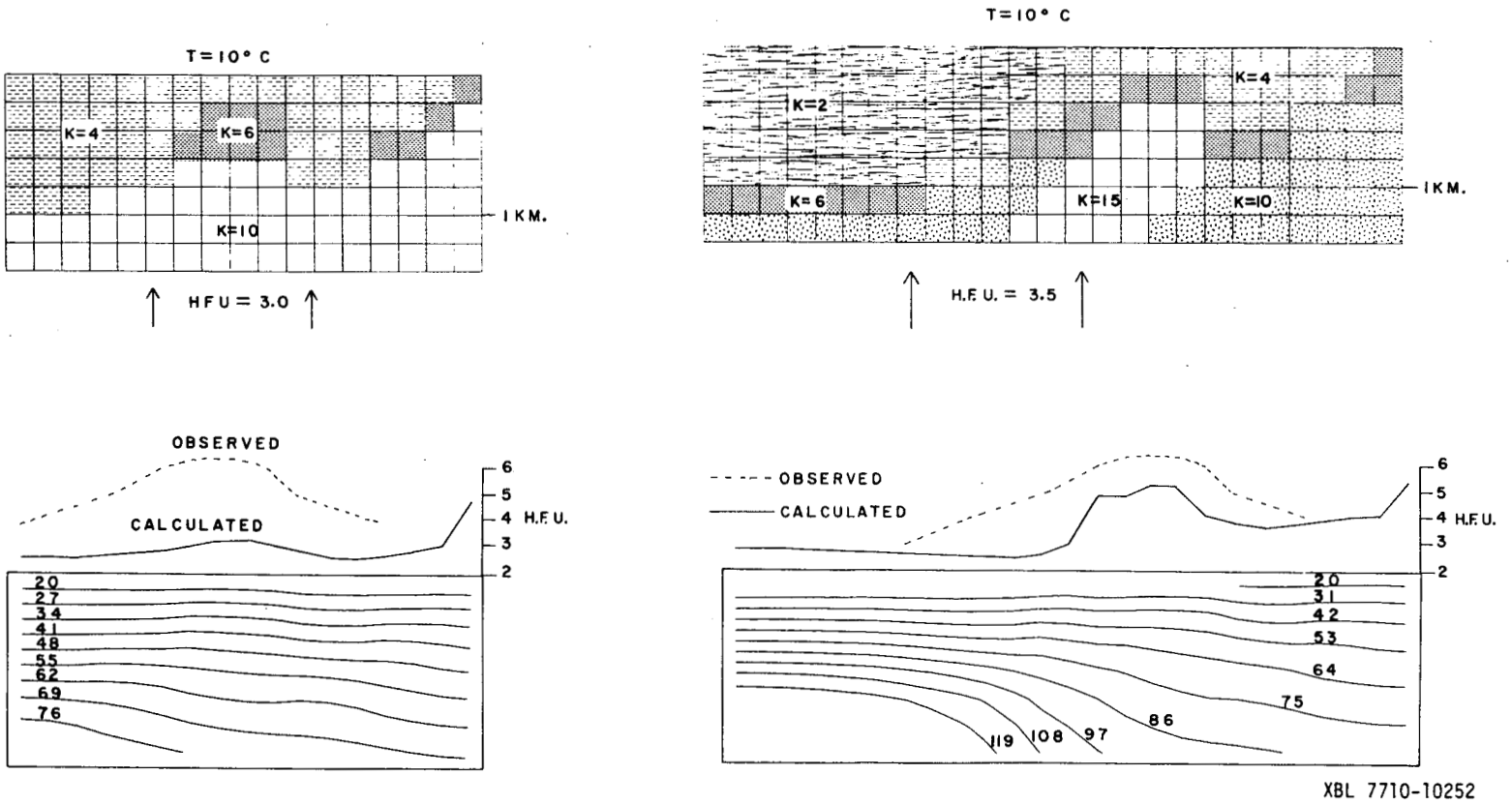

Figure 4-40

Several conductive models, boundary conditions, and results for line H.

phenomenon, the size of the model is limited by computer requirements. That is, given a certain flow of heat into the bottom of a model, steady state requirements dictate the temperature gradient; i.e., heat flow, $q = -K \text{ grad } T$, where K = thermal conductivity and T is the temperature. Therefore, to balance the heat budget for a limited model area requires a larger temperature gradient where the conductivity is low.

It seems as if conduction alone cannot easily account for the heat flow along line H. The hydrologic effect thought to be partially responsible for the heat flow anomaly on line D may also be occurring in this region. However, the low heat flow which would be expected where the water is on a downgoing path is not observed on the edges of the valley as in the previous case along line D. However, the downgoing water may be in a region that is greatly removed from the high heat flow. This would imply that the water may be circulating on a path that is much deeper than the route apparently taken along line D.

To explore the heat flow due to an intermediate depth reservoir which is kept at a constant temperature from hot water fed to it by deeply circulating water, the model in Figure 4-41 was used. This model is meant to simulate a valley with sediments having conductivity of 4 and 6×10^{-3} cal/cm sec deg, underlain by bedrock

Figure 4-41

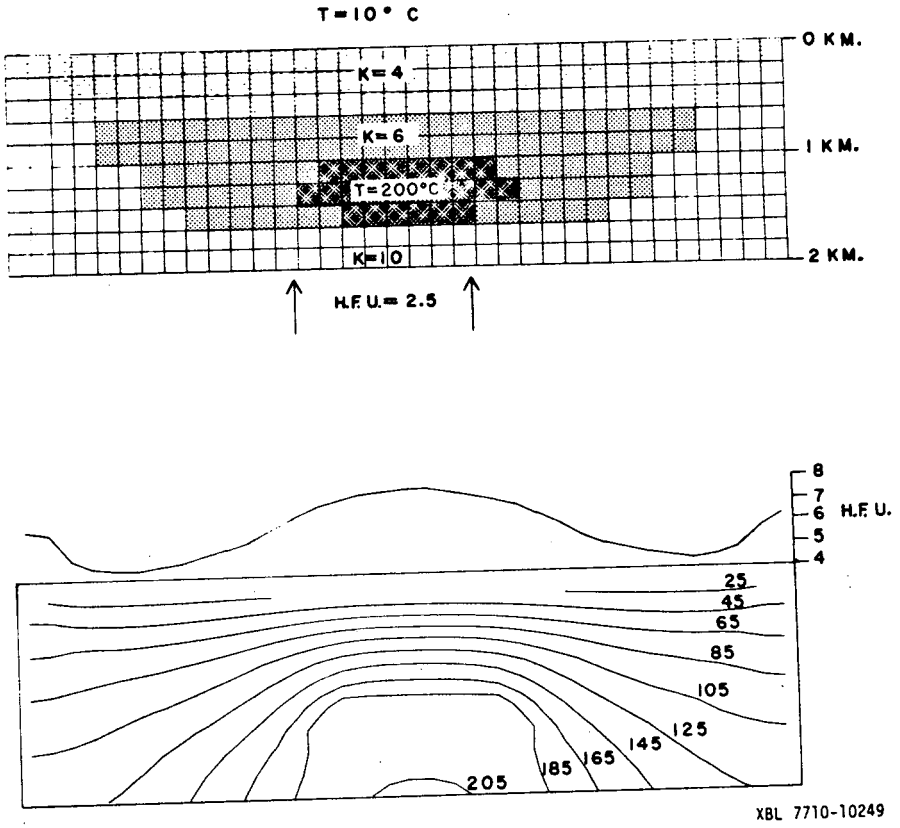

Model of a 200°C reservoir at the base of the sediments for a Basin and Range valley. Heat flow is conductive.

with conductivity approximately twice that of sediments. Again, the only mode of heat transfer is conduction, with similar boundary conditions as previous models. The dark region in Figure 4-41 is held at 200°C (to simulate a constant temperature reservoir) until steady state conditions were reached. As can be seen in Figure 4-41 the heat flow observed at the surface is not much greater than the observed heat flow value in the southern part of Grass Valley. Comparing Figures 4-40 and 4-41, it can be seen that the shape of the anomalies are also similar, implying similar depths and temperatures may be realistic. However, there is a disappointing aspect to this explanation. The deep water flow is probably controlled primarily by the faults. Because of the times involved for the heat from a reservoir buried one to two kilometers to reach the surface (500,000 to 1 million years), the conduits supplying the reservoir may have been cut long before in a seismically active region. On the other hand, the faults serving as conduits may be of such a scale that even major earthquakes would not disturb the water flow. Therefore, although unlikely, the southern heat flow high may be indicative of elevated temperatures within a few kilometers of the surface.

Turning to the hot springs region, it was apparent from the discharge of hot water, (95°C), the heat flow is not dominated by conduction. However, it is not

known if the shape of anomaly could be accounted for by a thin conduit of flowing water without the presence of a deeper reservoir.

Therefore, a model was adopted that assumed equilibrium had been reached between a silica plug surrounding a hot water conduit and its surroundings, such that a temperature gradient existed between the bottom and top of the conduit-plug system, with the temperature at the top being the observed 95°C. Several gradients of the silica plug were adopted; $T = 95^{\circ} + 11\ (Z)^{\circ}C$, and $T = 95^{\circ} + 30\ (Z)^{\circ}C$, where Z is the depth in kilometers. The first gradient simulates water that has penetrated to a depth of some 4 km and there heated to the temperature of its surroundings. Then either by a convective or artesian process the water rises along a conduit, at a rate such that it cools to 95°C by the time it reaches the surface. The second gradient simulates water that has penetrated to greater depths and has been heated to a higher temperature. These models assume that the cooling experienced by the water on its upward journey is done by conduction with its surroundings. The temperature of the conduit-plug was held at its original temperature gradient. Such factors as mixing with cooler water will be treated later. The size of the plug was determined by P-wave delay and gravity data.

As can be seen from Figure 4-42, the difference

Figure 4-42

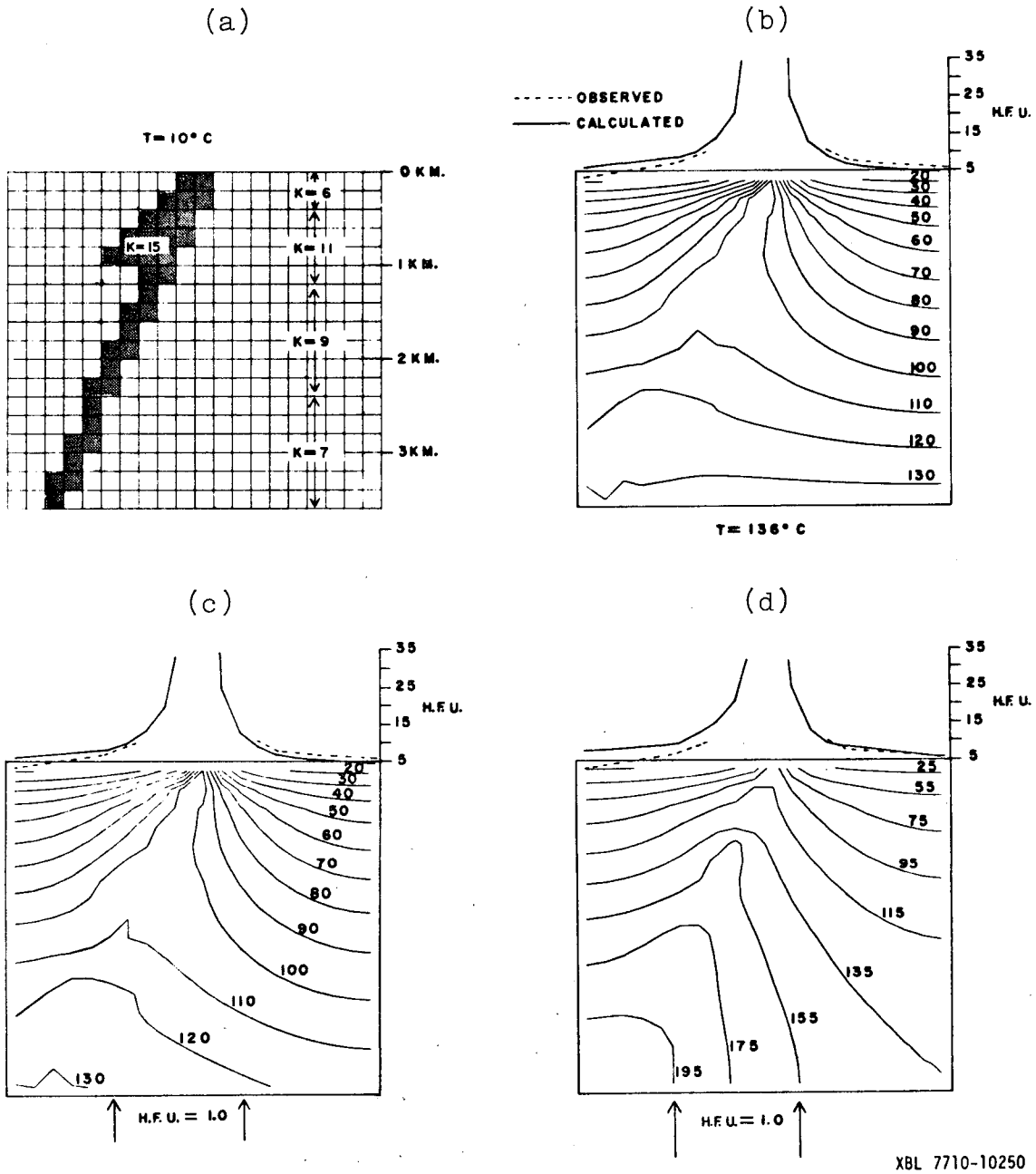

Conductive model of a silica plug. Results b and c represent the same gradient with different boundary conditions. Result d is with a higher temperature gradient for the silica plug.

between the three models is slight. However, the model assuming the higher gradient seems to give too high a value for the heat flow at the surface. These models also demonstrate that water heated to values not greatly exceeding temperatures predicted by normal gradients is sufficient to account for the observed heat flow.

Do the flow rates which would heat and cool the water to the values assumed in the previous models correspond to the observed flow rates? The models in Figure 4-43 were designed to answer this question. The observed flow from the hot springs is approximately 6 g/sec. If the conduit in which this water flows is 500 meters wide and extends to a depth of 10 km, how hot would the water get, and to what temperature would it cool if it took the path in Figure 4-43? The given rate of flow and dimensions of the elements correspond to a velocity of 42 cm/year. From Figure 4-43 it is apparent that the water would heat to only a temperature of 55°C and would cool to 45° by the time it reached the surface. If the area of contact was greater, such that the velocity of flow was less, i.e., 0.42 cm/yr, the water would heat to nearly 300°C, but because of the slow rate of travel it would also cool to 20°C by the time it discharged at the surface.

Therefore, either the surface water observed at 95°C is coming in contact with much higher temperatures than anticipated, or the water spends more time at depth.

Figure 4-43

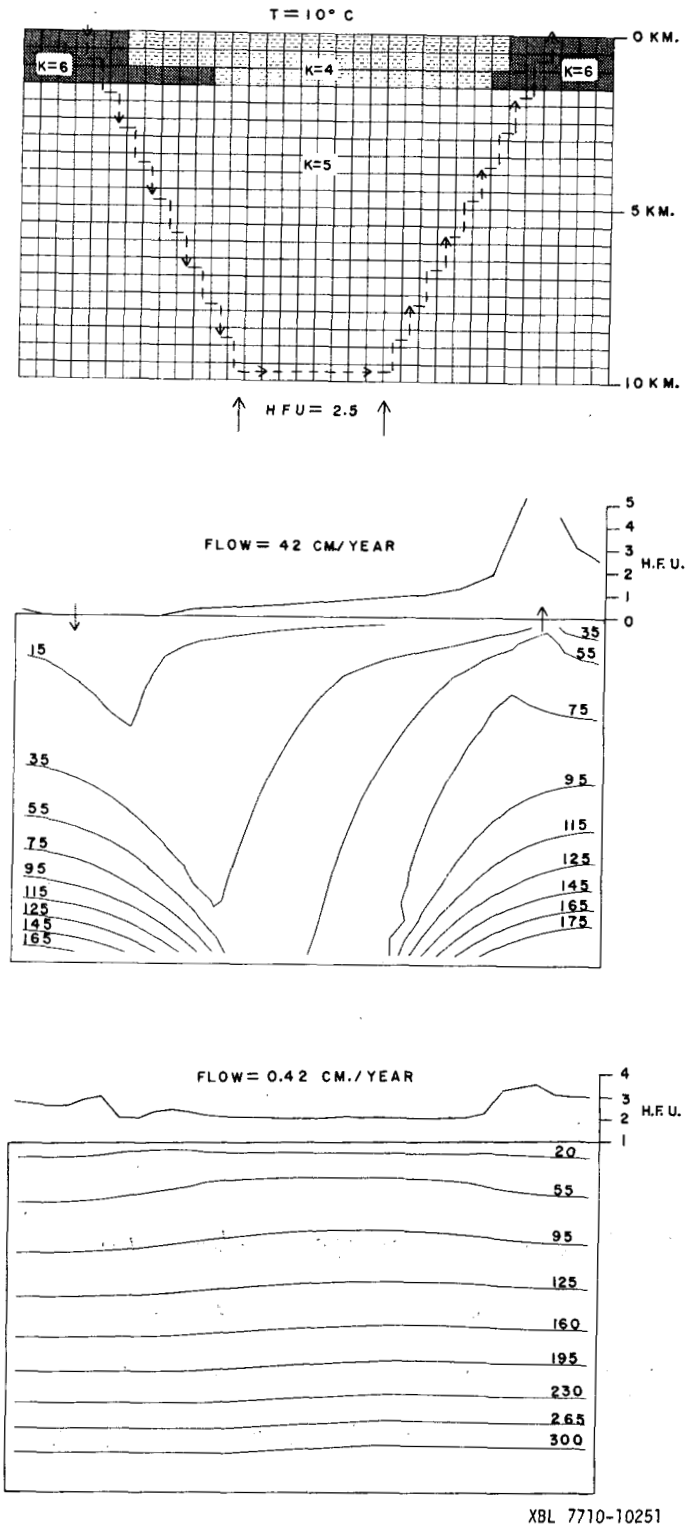

Conductive model of water flowing along hypothesized faults at different rates.

To model the heat flow from the hot springs and the immediate vicinity, with the additional constraints of the observed temperature, flow and possible mixing, the model in Figure 4-44 was adopted. This model assumes that the water exists long enough at depth or in contact with a hot pluton to be heated. Then by either convection or an artesian process the water rises along a conduit, such as a fault bounding the valley. However, before the water reaches the surface it is mixed with cooler water from the near surface, 10°C in this case.

The magnitude and shape of the calculated values are in good agreement with the observed. Therefore, this may be a plausible model for Basin and Range hot spring activity. This also implies that a reservoir need not exist to explain the observed heat flow. It should also be noted that the location of the mixing point could influence the shape of the heat flow anomaly, the more symmetrical the shape, the deeper the point of mixing. However, near-surface thermal conductivities would also influence the shape of the heat flow anomaly.

Although Figure 4-44 is a simple model with a simple path for the water, it demonstrates that the structure of the valleys in Northern Nevada may be controlling hot water generation and flow. Undoubtably, the real situation is much more complicated, with many intersecting water paths and heat sources. To model all the cases

Figure 4-44

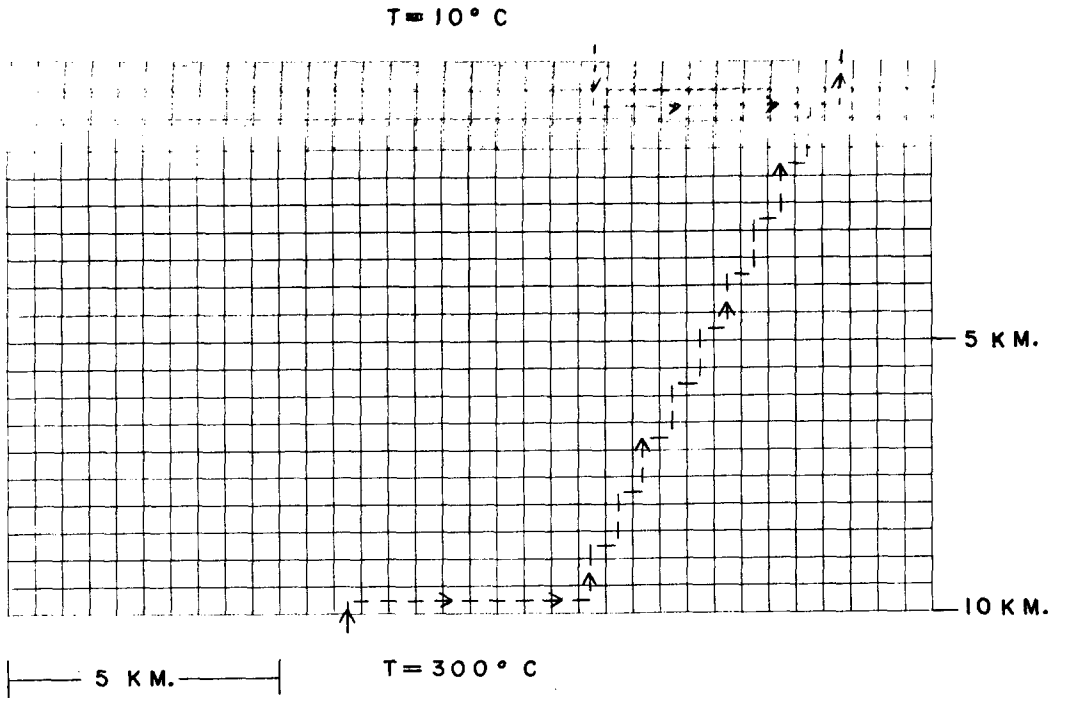

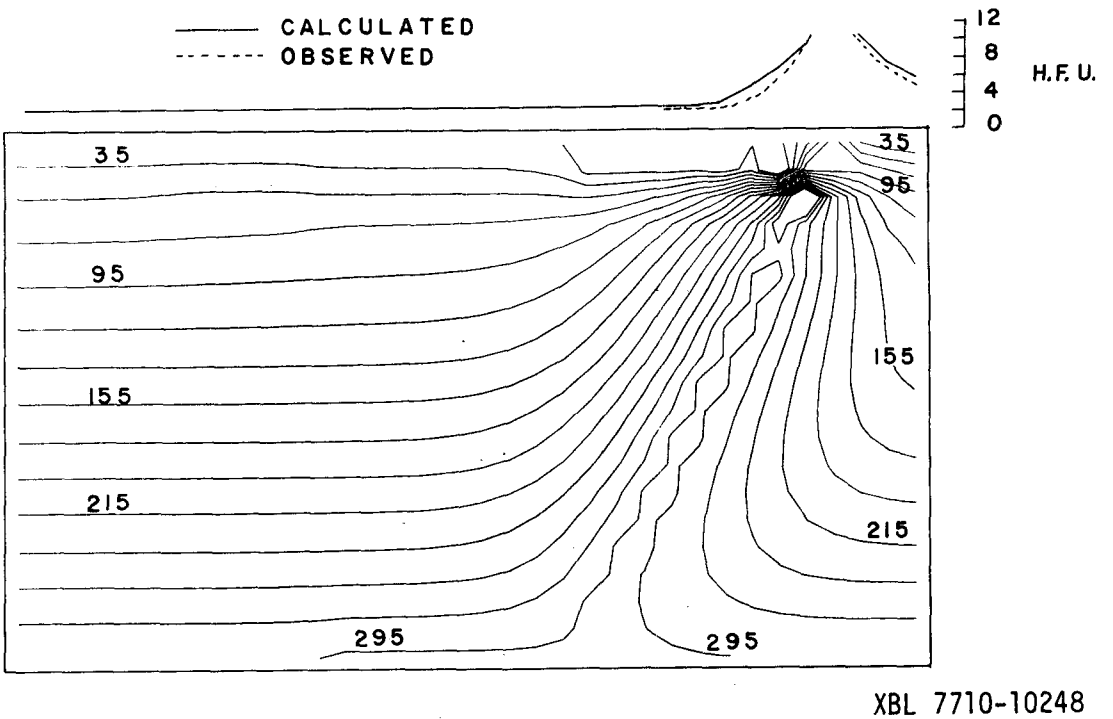

XBL 7710-10248

Conductive model of water flowing from a 300°C zone. Before reaching the surface the water is mixed with 10°C water. The total volume and temperature of the water at the surface are constrained to the observed values.

is clearly unrealistic. However, by using other information such as P-wave velocity, gravity, and possibly seismic reflection data as additional constraints, a more realistic model may be obtained.

Finally, for completeness, several regional models will be presented. The origin of the high regional heat flow in northern Nevada has long been a topic of debate. Presented in Figures 4-45 and 4-46 are two models that are physically reasonable. Figure 4-45 presents a hypothesis that the above-normal heat flow is due to a crustal intrusion. Several researchers (Landisman and Chaipayungpun, 1977, Stanley et al., 1977) have reported intercrustal low resistivity zones on the order of 1-10 ohm-meters. Preliminary magneotelluric work in Grass Valley (Mosley and Morrison, personal communication) indicates similar widespread phenomenon at depths of 10-15 km. Stanley et al. (1977) claim that the low resistivity zone seen beneath the Snake River Plain-Yellowstone area corresponds to the 700°C isotherm. However, most studies indicate higher temperatures are required to produce resistivities of 1-10 ohm-meter in basaltic and granitic rocks (Parkhomenko, 1964). If the low resistivity is due to increased water content and only moderate (500-700°C) temperature, one would not expect to see a P-wave delay. However, Eaton et al. (1977) also reported P-wave delays beneath the Yellowstone region. Therefore, because such effects as crack

Figure 4-45

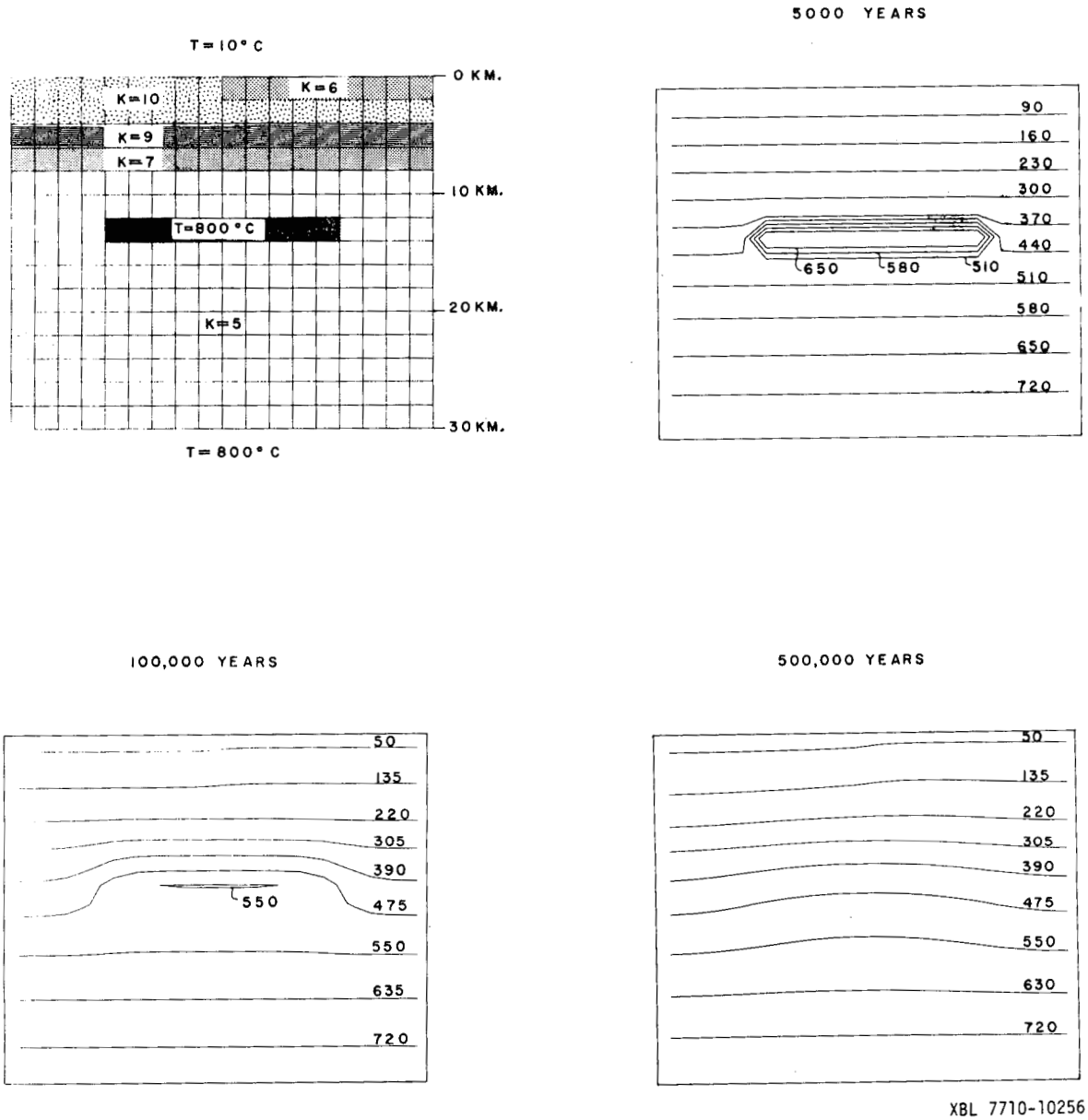

Crustal heat flow model with 800°C intrusion.

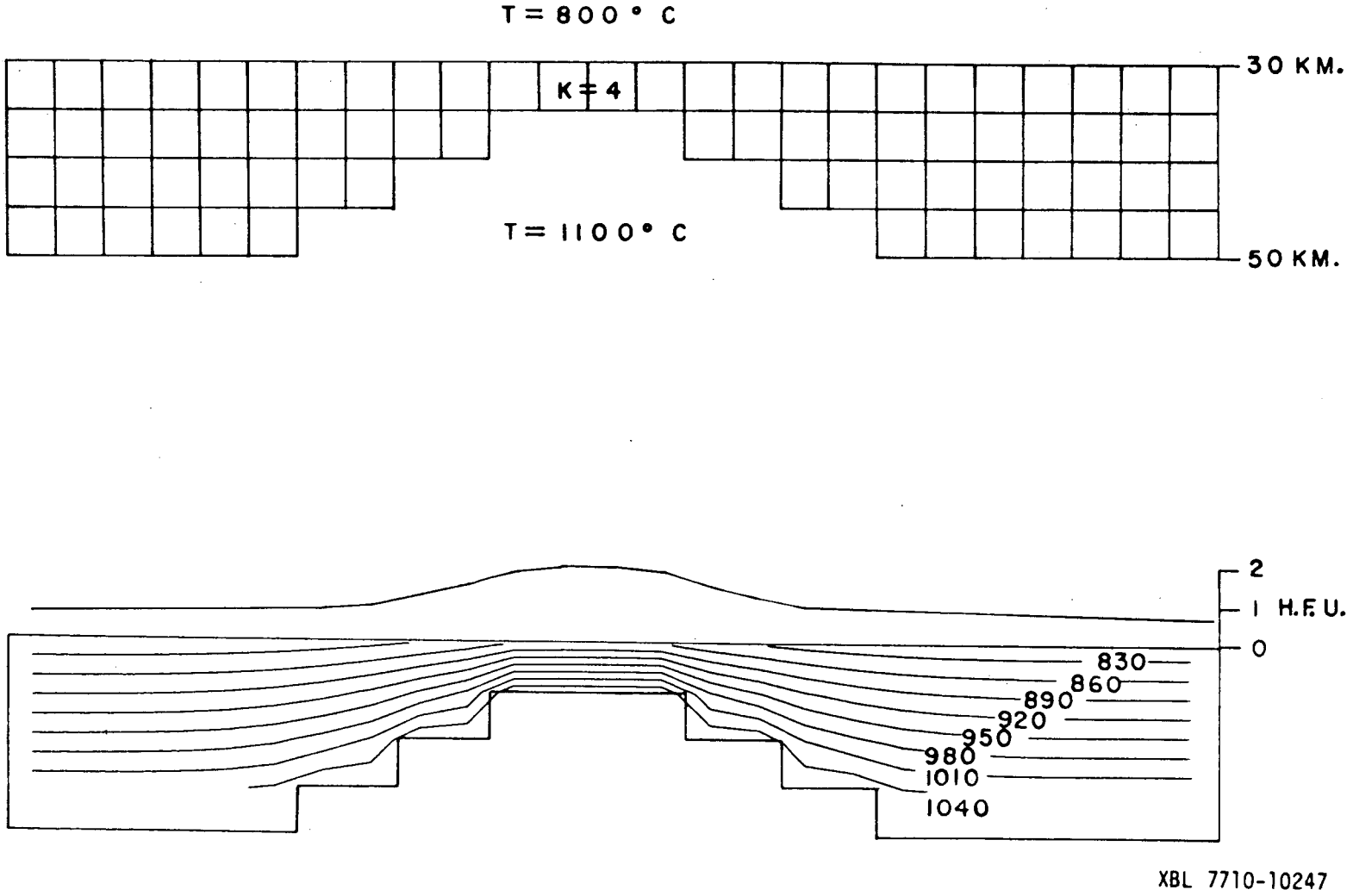

Figure 4-46

Conductive model for top of the mantle, with a hot spot or plume being present.

orientation, water content, permeability, and porosity make it difficult to estimate the true temperature, 800°C was adopted as the value that would produce a resistivity of 1-10 ohm-meter. In addition, the model was given a heat generation of 1×10^{-13} cal/g sec and a temperature gradient of 26°C/km. Without any intrusion, this model would produce a heat flow at the surface of 1.3 hfu. It was desired to know the effect of an intrusion 2 km thick, 20 km long, and 12 km deep on the surface heat flow. There is almost no effect at all. What little effect is seen is after the temperature of the intrusion has dropped to nearly ambient conditions. Therefore, the simultaneous observation of high heat flow and low resistivity at depth would imply that the area of low resistivity is still hot due to periodic reheating from successive intrusions.

Figure 4-46 is another model that may explain the high heat flow. The heat flow observed at the surface is a combination of the heat flow from the crust (from such factors as intrusions, radioactivity and convection of water) and the heat flow into the bottom of the crust. If for some reason the 1100°C isotherm is upwarped at the top of the mantle, i.e., a plume or hot spot is beneath this region, then the heat flow would double, as demonstrated in Figure 4-46. Therefore, the additional heat flow would be 1.0 hfu for a total of 1.8 hfu into

the bottom of the crust and an overall total at the surface of 3.1 hfu (i.e., 1.8 + 1.3).

This model, besides giving near correct regional surface heat flow, is attractive from another point of view. If the hot spot is no longer beneath the region of high heat flow, the temperatures at the base of the mantle may not be as high as when the hot spot was present. Even when the hot spot was present, the temperature at the base of the crust was only 900°C. Therefore, the temperature at the base of the crust would not have to increase greatly to explain the observed high heat flow. This may also indicate that the true P_n velocity beneath the Basin and Range (as opposed to the apparent P_n velocity which is measured) may not be as low as previously thought. In other words, because it takes so long (20-30 million years) for the heat to travel through the crust, the temperatures at the base of the crust may be normal now, explaining the higher P_n velocities observed in this study, yet it would still be possible to have high heat flow at the surface. This would also explain why the gravity, P_n and heat flow anomalies do not exactly spatialy coincide.

Further heat flow measurements and seismological studies may make it possible to resolve the difficulties with the present models of the Basin and Range tectonics.

Presently it seems as if the combination of anomalous subcrustal heat sources, crustal thinning, and deeply circulating water are combining to give the observed P_n velocity and heat flow anomaly.

4.8 Conclusions

In relation to Basin and Range properties, Grass Valley does not seem to be anomalous with respect to structure or microearthquake occurrence. There is no correlation between heat flow and the microearthquakes. The distribution of seismic activity indicates tectonic, rather than geothermal activity as the cause. Mechanisms are consistent with E-W tensional stress. Depths of events (1-8 km) suggest the possibility of a broad, shallow high temperature. Seismic wave velocities and attenuation porperties are anomalous only in the hot springs area, with indications that sediment densification as the cause. Due to the lack of comparative data and reliable magnitude estimates, no conclusions regarding peculiarities of source parameters can be made. Regional refraction studies indicate a thinning or higher velocity crust; however, there is little spatial correlation between high heat flow, high gravity (Woollard and Joesting, 1964) and the high P_n values, which are also thought to be a result of a thinning crust.

Heat flow modeling suggests minor anomalies can be conductive rather than convective in origin. Hot springs need not be supplied by a large volume reservoir, assuming the path of the water is long and deep enough to be heated. On the other hand, relatively shallow (2-3 km) and hot (200°C) regions do not produce large heat flow values at the surface ($\leq$ 10 hfu). Regional heat flow models indicate crustal intrusions are not sufficient to account for the high regional heat flow values. Either an anomalously thin crust or hot mantle are required to account for the Battle Mountain heat flow high.

It is unfortunate that no confirmatory drilling has been done in Grass Valley. Seismological methods can reliably determine structure, bedrock-alluvium contacts and fault locations. Because geothermal resources in a Basin and Range setting are probably hot water, many of the anomalies associated with a steam resource will not be present. Therefore, direct detection by seismological techniques is difficult. Associated properties such as high seismicity due to anomalous fluid flow, velocity and attenuation differences from silica deposition, unusual stress release, spatial and temporal occurrence characteristics, and source mechanisms of microearthquakes may be indicative of a geothermal resource. Until further case histories

of Basin and Range settings are provided, complete with confirmatory drilling, the utility of seismological methods, particularly microearthquake analysis, for geothermal exploration in the Basin and Range will remain in question.

CHAPTER 5

SUMMARY, CONCLUSIONS, AND RECOMMENDATIONS

5.1 Summary of Objectives and Methods

To asses the value of seismological methods for exploring and/or delineating geothermal resources, a known geothermal area, The Geysers, California, and a potential geothermal region, northern Nevada, were subjected to detailed studies of microearthquakes, P- and S-wave velocities, and P-wave attenuation. Additional studies to determine the relation between geothermal activity and structure in northern Nevada included commercial reflection and refraction, P_n refraction, and heat flow modeling.

Experimental and theoretical studies indicate that porosity, permeability, and pore fluid state are evident in the velocity and attenuation of P- and S-waves. In a search for anomalous propagation characteristics related to geothermal environments, seismograms from explosions and microearthquakes were examined for changes in frequency content and relative arrival times of P- and S-waves across the two regions. To uniquely define a "geothermal earthquake" the microearthquakes were compared to regional seismicity for anomalous spatial and temporal occurrence characteristics as well as for variation in source parameters inferred from the spectral characteristics of P- and S-waves. It was hoped

dynamical properties such as fluid movement, anomalous temperature and pressure gradients, and phase changes could be associated with the rate and manner of stress release of the microearthquakes in geothermal regions.

5.2 Conclusions

Seismological methods can produce data useful for both the exploration and the reservoir delineation phases of geothermal resource identification. Known geothermal areas seem unique, and any significance in anomalous characteristics in microearthquake occurrence or in wave propagation must be determined individually, or on a prospect-by-prospect basis. Anomalous characteristics that can be identified and related to geothermal activity provide potential for a methodology of estimating resource size and reservoir configuration.

Microearthquakes reflect the dynamics of a local stress system within the crust. Characteristics of microearthquakes must be examined in relation to regional seismicity and tectonics. The mere occurrence of microearthquakes in a region of high heat flow is insufficient basis for inference on the presence of a geothermal resource. Although earthquakes are abundant in some known geothermal areas, no phenomenon identifiable as a "geothermal earthquake" has been found. Microearthquake occurrence anomalies noted in

The Geysers cannot be separated from exploitation effects, though many of the microearthquake characteristics have little obvious relation to production of the field. Properties such as high corner frequencies, very shallow depths, anomalous occurrence rates and unusual moment - magnitude relationships in high heat flow regions or areas of suspected geothermal activity may well be indicators of a geothermal resource. As in the case of The Geysers, the spatial distribution of source parameters based on high frequency radiation of P- and S-waves, such as fault dimensions and propagation characteristics, source rise time, and stress drop may delineate high temperature and pressure gradients associated with steam boundaries in known geothermal regions. However, as was seen in both the Nevada and The Geysers study, even at several kilometers observation distances, attenuation can mask important spectral details at frequencies above 20-30 Hz. The occurrence of events on the edges of the steam zone in The Geysers indicates that microearthquakes could be useful in monitoring any reservoir expansion or contraction related to fluid withdrawal. Variations in temporal occurrence of microearthquakes in zones of high heat flow may indicate anomalous stress or materials, possibly due to geothermal activity. However, b-values must be obtained from reliable magnitude

estimates. Coda lengths were found to be an inadequate measure of magnitude in The Geyser and northern Nevada.

Anomalies associated with The Geysers microearthquakes were not evident in the Nevada events studied. Although this may be due to the nature of the geothermal resource, i.e., hot water versus steam, it is more likely because the Nevada midroearthquakes are tectonic rather than geothermal in origin. Thus, with virtually no case histories of successful discoveries, microearthquake analysis remains an unknown exploratory tool, particularly if utilized without other complimentary geophysical methods. It seems as if microearthquakes may be more valuable in monitoring and delineating known geothermal reservoirs as opposed to exploration use only.

A promising exploratory method involves mapping spatial variations in the propagation properties of P- and S-waves. Anomalies in velocity and attenuation of both types of waves make possible the estimation of pore fluid content and crack volume as well as the properties of the rock. Associated characteristics of geothermal activity, such as hydrothermal alteration and silicification, were evident in the anomalously high P-wave velocity and Q structure surrounding Leach Hot Springs in Grass Valley, Nevada. Similar high velocity - high Q anomalies were also found in the upper kilometer of The Geysers steam field. Deeper penetrating

waves in The Geysers indicated a lower velocity-lower Q region in the steam field compared to regional values. By utilizing S-waves from microearthquakes, Poisson's Ratio was found to be lower in the steam zone compared to the surrounding areas. Direct temperature effects are small at values characteristic of geothermal reservoirs. Only in the presence of a magma chamber or partial melt would the attenuation or velocity of P- and S-waves be affected directly. Because wave propagation anomalies due to the presence of steam are not evident in a hot water resource, direct detection of a geothermal resource in Basin and Range structure could prove difficult. P-wave delays are effected by alluvial thickness, but allow fairly detailed mapping of sug-surface zones of anomalous velocity and broad structural trends. Regional P_n studies in northern Nevada were useful for determining deeper crustal structure and possibly detecting evidence for a broad heat source. Although expensive, commercial reflection and refraction work can provide detailed structural information which may be relevant to fluid flow. In northern Nevada such surveys provided only confirmatory information to the knowledge gained from other geophysical investigations. If fault control of the reservoir is suspected, reflection studies can add valuable data in siting an exploratory well.

Simple heat flow models have demonstrated that localized heat flow anomalies need not be the result of fluid flow. Coupled with P-wave delay data to determine alluvial thickness and basement structure, heat flow modeling was useful for discriminating between conductive and convective effects of the heat flow anomalies in Grass Valley.

5.3 Recommendations and Future Studies

It has been concluded that the seismological methods can be useful for both the exploration and monitoring of geothermal resources. The approach taken will depend upon the type and size of the resources (steam, steam-water, hot water), the complexity of geology, and the regional seismicity and tectonics. The following recommendations should not be applied in a cookbook fashion, they are techniques that have proven useful in two particular geothermal regions and may be inadequate in other environments.

5.3.1 Exploration

The desirable data for exploration purposes are: microearthquake locations, fault plane solutions, and magnitudes, the moments, corner frequencies, and high frequency roll-off of P- and S-wave spectra, and P- and S-wave velocity and amplitude information. To obtain the necessary detail station placement for microearth-

quake analysis should be dense enough to provide 360° azimuthal coverage with at least several stations in each quadrant. If possible, 3-component recording should be done at each station with sufficient bandwidth (10^2 Hz) and dynamic range (10^4). The recording times will vary, but should be long enough to provide meaningful statistical analyses. Array size and configuration will depend upon the target, background noise, geology, and number of stations; however, for microearthquake analysis maximum station separation should be no more than several kilometers. To minimize horizontal refraction effects in attenuation and velocity analysis, stations should be placed perpendicular to the major geologic trends. For reliable reference data at least several stations should be placed on opposite sides and outside of the target region. By "leap-froging", station equipment expenditures can be kept to a minimum. For most purposes a 10 to 12 element array of horizontal and vertical geophones placed 0.25 to 1.0 km apart would provide sufficient velocity and attenuation data. With these data, meaningful comparisons can then be made to normal structure and regional seismicity to infer on the presence of a geothermal resource. Depending on the number and size of seismological anomalies further detailing work may be warranted; however, the decision to drill an

exploratory well should also be based on other available geophysical, geological and geochemical information.

5.3.2 Reservoir Monitoring

Essentially the same data set is required for reservoir monitoring as for exploration. However, with the addition of confirmatory well data, the interpretation of anomalous seismological data and their relation to the size and potential of the resource may be more meaningful. Mapping velocity and attenuation anomalies, if present, may outline steam zones or regions of metamorphism associated with the heat source or hydrothermal alteration related to hot water or steam. The spatial and temporal occurrence of microearthquakes may indicate volume changes associated to fluid withdrawal or adjustment within the reservoir. Temporal variations of the spatial characteristics of microearthquake source parameters may be an indication of reservoir configuration. To obtain useful microearthquake data, array dimensions should be twice the suspected reservoir width, with 360° azimuthal coverage both in and out of the production region. Depending upon microearthquake activity, sample lengths will vary, but should be no less than several weeks. Because of slowly occurring processes, monitoring should not be necessary more than once a year. Other array components and specifications are similar to exploration parameters. P- and S-wave

sources should be from local, regional and teleseismic distances to discriminate reliably between fine and broad structural effects as well as deep and shallow effects. Used wisely, seismological techniques, particularly microearthquake analysis, may provide economical answers to the question of reservoir volume, boundaries, and potential.

5.3.3 Future Studies and Development

Future work should be directed toward the compilation of detailed comprehensive case histories, as prospects are drilled. Stronger emphasis in seismic geothermal exploration should be placed on simultaneously utilizing the properties of P- and S-waves. The recent development of digital event recorders with adequate dynamic range and sampling rates make it possible to record the necessary volume and quality of data to resolve questions associated with microearthquake peculiarities in geothermal regions. Joint inversion of P- and S-wave data, from local earthquakes as well as regional sources, for velocity and Q structure may provide a more reliable exploration tool than spatial studies of individual parameters. Source properties of microearthquakes in geothermal regions may be differentiated from those in other areas by examining details of higher order moments of the source moment tensor.

Relatively elementary seismological techniques were used in this study. Still, it has been demonstrated that these methods are useful for detecting anomalous subsurface properties presumably associated with potential geothermal resources. With the refinement of the field procedure and the development of economical new techniques of in-field data acquisition and processing, seismological methods promise to become a significant element in geothermal exploration.

REFERENCES

Bakun, W.H., and C.G. Bufe, 1975. Shear Wave Attenuation Along the San Andreas Fault Zone in Central California. Bulletin Seism. Soc. Amer., v. 65, p 439.

Bakun, W.H., and A.G. Lindh, 1977. Local Magnitudes, Seismic Moments, and Coda Durations for Earthquakes Near Oroville, California. Bulletin Seism. Soc. Amer., v. 67, p 615.

Beyer, H., A. Dey, A. Liaw, E. Majer, T.V. McEvilly, H.F. Morrison, and H. Wollenberg, 1976. Preliminary Open File Report, Geological and Geophysical Studies in Grass Valley, Nevada. Lawrence Berkeley Laboratory Report, LBL-5262.

Birch, F., 1957. Contributions in Geophysics, Pergamon Press, London, 158 p.

Brace, W.F., and J.D. Byerlee, 1966. Stick-slip as a Mechanism for Earthquakes. Science, v. 153, p 990.

Brune, J.N., 1970. Tectonic Stress and the Spectra of Seismic Shear Waves From Earthquakes. J. Geophys. Res., v. 75, p 4997.

Brune, J.N., 1971. Correction (to Brune 1970). J. Geophys. Res., v. 76, p 5002.

Butler, D., 1974. Seismicity Report on Black Rock Desert Project, Northwest Nevada, Microgeophysics Corp., Golden, Colorado.

Cathles, L.M., 1977. An Analysis of the Cooling of Intrusives by Ground-water Convection Which Includes Boiling. Economic Geology, v. 72, p 804.

Combs. J., 1976. Microearthquake Studies Before and During Fluid Withdrawal and Reinjection Test, East Mesa Geothermal Field, Imperial County, California. Contribution #7-77, Center for Energy Studies, University of Texas at Dallas.

Combs, J. and Y. Rostein, 1975. Microearthquake Studies at the Coso Geothermal Area, China Lake, California. 2nd U.N. Symp. on the Dev. and Use of Geothermal Resources, San Francisco, p 909.

Conant, D.A., 1973. A Microearthquake Survey of Geothermal Areas in Iceland. Earthquake Notes, v. 43, p 19.

Dieterich, J.H., 1974. Earthquake Mechanisms and Modeling. Annual Rev. of Earth and Planetary Sci., v. 2, p 275.

Donnelly, J.M., 1977. Geochronology and Evolution of the Clear Lake Volcanic Field. Ph.D. Thesis, University of California, Berkeley.

Douglas, B.M. and A. Ryall, 1972. Spectral Characteristics and Stress Drop for Microearthquakes Near Fairview Peak, Nevada. J. Geophys. Res., v. 77, p 351.

Douglas , B.M., A. Ryall, and R. Williams, 1970. Spectral Characteristics of Central Nevada Microearthquakes. Bulletin Seism. Soc., Amer., v. 60, p 1547.

Eaton, G.P., R.L. Christiansen, H.M. Iyer, A.M. Pitt, D.R. Mabey, H.R. Blank, I. Zietz and M.E. Gettings, 1975. Magma Beneath the Yellowstone National Park. Science, v. 188, p 787.

Eaton, J.P., 1963. Crustal Structure from San Francisco, California to Eureka, Nevada, From Seismic Refraction Measurements. Geophs. Res., v. 68, p 5789.

Gardner, G.H.F., M.R.J. Wyllie, and D.M. Droschak, 1964. Effects of Pressure and Fluid Saturation on the Attenuation of Elastic Waves in Sands. J. Petroleum Tech., v. 16, p 189.

Goldstein, N.E. and B. Paulsson, 1977. Interpretation of Gravity Surveys in Grass and Buena Vista Valleys, Nevada. LBL Report 7013. Lawrence Berkeley Laboratory, Berkeley, California.

Goff, F.E., J.M. Donnelly, and B.C. Hearn, 1977. Geothermal Prospecting in The Geysers - Clear Lake Area, Northern California. Geology, v. 5, p 509.

Griggs, D.T., 1967. Hydrolytic Weakening of Quartz and Other Silicates. Geophys. J. Royal Astron. Soc., v. 14, p 19.

Griggs, D.T., F.J. Turner, and H.C. Heard, 1960. Deformation of Rocks at 500° to 800°C. Geological Soc. Am. Mem. 79, p 39.

Hamilton, R.M., and L.J.P. Muffler, 1972. Microearthquakes at The Geysers Geothermal Area, California. J. Geophys. Res., v. 77, p 2081.

Handin, J., 1966. Strength and Ductility, in Handbook of Physical Constants, S.P. Clark, Jr., (ed.). Geol. Soc. Amer. Memoir, 97, p 238.

Herrin, E., 1972. A Comparative Study of Upper Mantle Models: Canadian Shield and Basin and Range Province. In the Nature of the Solid Earth, ed. E. Robertson, McGraw-Hill, New York, p 677.

Hill, D.P., and L.C. Pakiser, 1966. Crustal Structure Between the Nevada Test Site and Boise, Idaho, From Seismic Refraction Measurements. American Geophysical Union Geophysical Monograph 10, p 391.

Hochstein, M.P., and T.M. Hunt, 1970. Seismic Gravity and Magnetic Studies, Broadlands Geothermal Field, New Zealand. Geothermics, v. 2, part I, p 333.

Hubbert, M.K., and W.W. Rubey, 1959. Role of Fluid Pressure in Mechanics of Overthrust Faulting . Bulletin, Geo. Soc. Amer., v. 70, p 115.

Iyer, H.M., and T. Hitchcock, 1975. Teleseismic Residuals at The Geysers Geothermal Area. Amer. Geophys. Union Trans., v. 56, p 1020.

James, R., 1968. Wairakei and Lardarello: Geothermal Power Systems Compared. New Zealand Journal of Science, v. 11, p 706.

Johnson, L.R. and T.V. McEvilly, 1974. Near-field Observations and Source Parameters of Central California Earthquakes. Bulletin Seism. Soc. Amer., v. 64, p 1855.

Johnson, D.H., M.N. Toksoz, and A. Timur, 1977. Attenuation of Seismic Waves in Dry and Saturated Rocks. II: Mechanisms. in Press.

Jones, C.J., 1915. The Pleasant Valley, Nevada, Earthquake of October 2, 1915. Bulletin Seism. Soc. Amer., v. 5, no. 4, p 190.

Knapp, R.B., and J.E. Knight, 1977. Differential Thermal Expansion of Pore Fields: Fracture Propagation and Microearthquake Production in Hot Pluton Environments. J. Geophys. Res., v. 82, p 2515.

Lachenbruch, A.H., and J.H. Sass, 1977. Geothermal Setting of the Battle Mountain High. Trans. Am. Geophys. Union, v. 58, no. 12, p 1237.

Lachenbruch, A.H., and J.H. Sass, 1978. Models of an Extending Lithosphere and Heat Flow in the Basin and Range Province. in Press.

Landisman, M., and W. Chaipayungpan, 1977. First Results from Electrical and Seismic Studies of Low Resistivity, Low Velocity Material Beneath Eastern Colorado. Geophysics, v. 42, no. 4, p 804.

Lange, A.L., and W.H. Westphal, 1969. Microearthquakes Near The Geysers, Sonoma County, California. J. Geophys. Res., v. 74, p 4377.

Liaw, A.L., 1977. Microseisms in Geothermal Exploration: Studies in Grass Valley, Nevada. Ph.D. Thesis, University of California, Berkeley.

Lin, W., 1977. Velocities of Compressional Wave in Rocks of Central California at High Pressure and High Temperature and Applications to the Study of the Crustal Structure of California Coast Ranges. Ph.D. Thesis, University of California, Berkeley.

Lippmann , M.J., C.F. Tsang, and P.A. Witherspoon, 1977. Analysis of the Response of Geothermal Reservoirs Under Injection and Production Procedures. J. of Petroleum Technology. in Press.

Matumoto, T., 1971. Seismic Body Waves Observed in the Vicinity of Mount Katmai, Alaska, and Evidence for the Existence of Molten Chambers. Bulletin, Geo. Soc. of Amer., v. 82, p 2905.

Matumoto, T., and P.L. Ward, 1967. Microearthquake Study of Mount Katmai and Vicinity, Alaska. J. Geophys. Res., v. 72, p 2557.

McGarr, A., 1976. Seismic Moments and Volume Change. J. Geophys. Res., v. 81, p 1487.

McLaughlin, R.J., 1977. The Franciscan Assemblage and Great Valley Sequence in The Geysers-Clear Lake Region of Northern California. In Field Trip Guide to The Geysers-Clear Lake Area. Geol. Soc. of Am. p 56.

McNally, K.C., 1976. Spatial, Temporal, and Mechanistic Character in Earthquake Occurrence, A Segment of the San Andreas Fault in Central California. Ph.D. Thesis, University of California, Berkeley.

Mogi, K., 1962. Magnitude-frequency Relation for Elastic Shocks Accompanying Fractures of Various Materials and Some Related Problems in Earthquakes. Bulletin Earthquake Res. Inst., v. 40, p 831.

Muffler, L.J.P., and D.E. White, 1969. Active Metamorphism of Upper Cenozoic Sediments in the Salton Sea Geothermal Field and the Salton Trough, Southeastern California. Bulletin, Geo. Soc. of Amer., v. 80, p 157.

Murase, T., and A.R. McBirney, 1973. Properties of Some Common Igneous Rocks andTheir Melts at High Temperatures. Bulletin, Geo. Soc. of Amer., v. 84, p 3563.

Nur, A., 1973. Role of Pore Fluids in Faulting. Phil. Trans. Royal Soc. Lond., v. 274, p 297.

Nur, A., and G. Simmons, 1969. The Effect of Saturation on Velocity in Low Porosity Rocks. Earth and Planetary Sci. Letters, v. 7, p 183.

Oliver, J., A. Ryall, J.N. Brune, D.B. Slemmons, 1966. Microearthquake Activity Recorded by Portable Seismographs of High Sensitivity. Bulletin of Seism. Soc. of Amer., v. 56, no. 4, p 899.

Parkhomenko, E.I., 1967. Electrical Properties of Rocks. Monographs in Geoscience., ed., R. Fairbridge. Plenum Press, New York, 314 pp.

Prodehl, C., 1970. Seismic Refraction Study of Crustal Structure in the Western United States. Bulletin, Geo. Soc. of Amer., v. 81, p 2629.

Raleigh, C.B., and M.S. Paterson, 1965. Experimental Deformation of Serpentinite and Its Tectonic Implications. J. Geophys. Res., v. 70, p 3965.

Ryall, A., 1977. Earthquake Hazard in The Nevada Region. Bulletin Seism. Soc., Amer., v. 67, p 517.

Ryall, A., K. Priestley, 1975. Seismicity, Secular Strain and Maximum Magnitude in the Excelsior Mountains Area. Western Nevada and Eastern California. Bulletin, Geo. Soc. of Amer., v. 86, p 1585.

Russell, I.C., 1896. U.S.G.S., Monograph II. Plate 44, p 274.

Sass, J.H., J.P. Ziagos, H.A. Wollenberg, R.J. Munroe, D.E. diSomma and A.H. Lachenbruch, 1977. Application of Heat-Flow Techniques to Geothermal Energy Exploration, Leach Hot Springs Area, Grass Valley, Nevada. U.S. Geological Survey, Open File Report 77-762.

Scholz, C.H., 1968. The Frequency-Magnitude Relation of Microfracturing in Rock and Its Relation to Earthquakes. Bulletin Seism. Soc. Amer., v. 58, p 399.

Smith, W.D., 1975. A Finite Element Study of the Effects of Structural Irregularities on Body Wave Propagation. Ph.D. Thesis, University of California, Berkeley.

Sorey, M.L., 1975. Numerical Modeling of Liquid Geothermal Systems. Ph.D. Thesis, University of California, Berkeley.

Spencer, E.W., 1969. Introduction to the Structure of the Earth. New York, McGraw-Hill.

Stanley, W.D., J.E. Boehl, F.X. Bostick and H.W. Smith, 1977. Geothermal Significance of Magnetotellaric Soundings in the Eastern Snake River Plain-Yellowstone Region. J. Geophys. Res., v. 82, p 2501.

Stauder, W., and A. Ryall, 1967. Spatial Distribution and Source Mechanism of Microearthquakes in Central Nevada. Bulletin Seism. Soc. Amer., v. 57, no. 6, p 1317.

Stesky, R.M., 1977. Rock Friction - Effect of Confining Pressure. Proc. of Conference II, Experimental Studies of Rock Friction With Application to Earthquake Prediction. U.S. Geological Survey, p 331.

Stuart, D.J., J.C. Roller, W.H. Jackson and G.B. Mangan, 1964. Seismic Propagation Paths, Regional Traveltimes and Crustal Structure in the Western United States. Geophysics, v. 29, no. 2, p 178.

Suppe, J.C., C. Powell, and R. Berry, 1975. Regional Topography, Seismicity, Quaternary Volcanism and the Present-day Tectonics of the Western United States. Amer. J. Sci., v. 275-A, p 397.

Teng, T., 1968. Attenuation of Body Waves and the Q Structure of the Mantle: J. Geophys. Res., v. 73, p 2195.

Thatcher, W. and T.C. Hanks, 1973. Source Parameters of Southern California Earthquakes. J. Geophys. Res., v. 77, p 1549.

Thompson, G.A., 1959. Gravity Measurements Between Hazen and Austin, Nevada: A Study of Basin and Range Structure. J. Geophys. Res., v. 64, p 217.

Thompson, G.A., D.B. Burke, 1974. Regional Geophysics of the Basin and Range Province. Annual Review of Earth and Planetary Sciences, v. 2, p 213.

Toksoz, M.N., C.H. Cheng and A. Timur, 1976. Velocities of Seismic Waves in Porous Rocks. Geophysics, v. 41 p 621.

Utsu, T., 1969. Aftershocks and Earthquake Statistics (I). J. of the Faculty of Science, Hokkaido University Series VII, v. 3, no. 3, p 129.

Walsh, J.B., 1968. Attenuation in Partially Melted Material. J. Geophys. Res., v. 73, p 2209.

Ward, P.L., 1972. Microearthquakes: Prospecting Tool and Possible Hazard in the Development of Geothermal Resources. Geothermics, v. 1, p 3.

Ward, P.L. and S. Bjornsson, 1971. Microearthquakes, Swarms and the Geothermal Areas of Iceland. J. of Geophys. Res., v. 76, p 3953.

Weres, O., K. Tsao and B. Wood, 1977. Resource Technology and Environment at The Geysers. Lawrence Berkeley Laboratory, LBL-5231.

Westphal, W.H., and A.L. Lange, 1967. Local Seismic Monitoring - Fairview Peak Area, Nevada. Bulletin Seism. Soc. Amer., v. 57, p 1279.

White, D.E., L.J.P. Muffler and A.H. Truesdell, 1971. Vapor-dominated Hydrothermal Systems Compared with Hot-water Systems. Economic Geology, v. 66, p 75.

White, J.E., 1975. Computed Seismic Speeds and Attenuation in Rocks with Partial Gas Saturation. Geophysics, v. 40, p 224.

Wilson, R.V., and R.R. Paul, 1965. Nevada Bureau of Mines Map 30. MacKay School of Mines, University of Nevada.

Woollard, G.P., and Joesting, 1964. Bouguer Gravity Map of the United States. Amer. Geophys. Union Special Committee for the Geophysical and Geological Study of the Continent.

Wyss, M., 1973. Towards a Physical Understanding of the Earthquake Frequency Distribution. Geophys. J. Royal Astron. Soc., v. 31, p 341.

Wyss, M., and J.N. Brune, 1968. Seismic Moment, Stress and Source Dimensions for Earthquakes in the California-Nevada Region. J. Geophys. Res., v. 73, p 4681.

TECHNICAL INFORMATION DEPARTMENT
LAWRENCE BERKELEY LABORATORY
UNIVERSITY OF CALIFORNIA
BERKELEY, CALIFORNIA 94720